



---

Publicly Accessible Penn Dissertations

---


1-1-2015

# The Identification of Novel Mechanisms in Neuronal Development and Degeneration

Angela Marie Jablonski

*University of Pennsylvania*, [angela.m.jablonski@gmail.com](mailto:angela.m.jablonski@gmail.com)

Follow this and additional works at: <http://repository.upenn.edu/edissertations>

 Part of the [Biology Commons](#), [Molecular Biology Commons](#), and the [Neuroscience and Neurobiology Commons](#)

---

## Recommended Citation

Jablonski, Angela Marie, "The Identification of Novel Mechanisms in Neuronal Development and Degeneration" (2015). *Publicly Accessible Penn Dissertations*. 1067.

<http://repository.upenn.edu/edissertations/1067>

This paper is posted at Scholarly Commons. <http://repository.upenn.edu/edissertations/1067>

For more information, please contact [libraryrepository@pobox.upenn.edu](mailto:libraryrepository@pobox.upenn.edu).

---

# The Identification of Novel Mechanisms in Neuronal Development and Degeneration

## **Abstract**

The goal of this dissertation is to further understand two key, broad processes which occur over the course of a neuron's lifetime: its development and possible degeneration in disease. We identify novel components in both of these processes and attempt to understand the functional significance as well as the mechanism each component uses to exert its effects.

We begin with work done focusing on how the neuron's dendritic tree develops. The development of neurons has two phases: (1) a first phase relying on a genetic program and (2) a second phase that uses synaptic activity to guide the fine tuning of connections. We are primarily interested in understanding how neurons develop within the motor system using cues from synaptic activity. One type of activity-dependent development in the motor system is driven by AMPA receptors assembled with the GluA1 subunit using the scaffolding protein, SAP97. In Chapter 2, we describe our finding that the small protein, CRIPT, functions in the development of the neuron's dendritic tree within the motor system. We show that CRIPT is expressed during the time in development when activity-dependent remodeling is occurring in the spinal cord. Additionally, we show that CRIPT binds to the PDZ3 domain of SAP97 using its C-terminus. Finally, we show that CRIPT is necessary for proper dendritic growth of the motor system and normal motor system responses *in vivo*.

There are a number of diseases that specifically target motor neurons. One adult-onset disease is Amyotrophic Lateral Sclerosis (ALS). Like many neurodegenerative diseases, it is a multifactorial disease and a contributing factor is the lack of proper protein quality control and the formation of large protein aggregates within motor neurons. In Chapter 3, we focus on how endoplasmic reticulum-associated degradation (ERAD) components might affect mutant proteins in ALS and their toxicity. ERAD is responsible for maintaining the proper folding of proteins that are to be trafficked to the cell surface or secreted from the cell. Although many proteins associated with ALS are not ERAD substrates, a number of ERAD components have been found to interact with ALS-causing mutant proteins and have been found to be mutated in forms of familial ALS. We identify new modifiers within the ERAD pathway of the toxicity of two ALS-linked proteins, mutant TDP-43 and mutant SOD1. We focus on the mechanism of one suppressor of ALS-linked proteotoxicity, the loss of RAD-23. The levels of RAD23 are increased in ALS models and reducing RAD-23 levels can suppress phenotypes in ALS models, as well as suppress motor neuron toxicity of the mutant proteins. We further show that reduced RAD-23 is able to accelerate the turnover of mutant proteins associated with ALS. Finally, we show that there is a mislocalization of RAD-23 protein and increased RAD-23 protein expression in post mortem spinal cord tissue of ALS patients, suggesting that RAD-23 may be a new novel target in the treatment of ALS.

Collectively, this work identifies and describes novel proteins and mechanisms involved in the development and pathobiology of motor neurons.

## **Degree Type**

Dissertation

---

**Degree Name**

Doctor of Philosophy (PhD)

**Graduate Group**

Neuroscience

**First Advisor**

Robert G. Kalb

**Keywords**

ALS, CRIPT, dendrite, development, neurodegeneration, RAD-23

**Subject Categories**

Biology | Molecular Biology | Neuroscience and Neurobiology

**THE IDENTIFICATION OF NOVEL MECHANISMS IN NEURONAL DEVELOPMENT  
AND DEGENERATION**

Angela Marie Jablonski

A DISSERTATION

in

Neuroscience

Presented to the Faculties of the University of Pennsylvania

in

Partial Fulfillment of the Requirements for the

Degree of Doctor of Philosophy

2015

Supervisor of Dissertation

*Signature* \_\_\_\_\_

Dr. Robert G. Kalb, M.D.

Professor of Neurology, Perelman School of Medicine at the University of Pennsylvania

Graduate Group Chairperson

*Signature* \_\_\_\_\_

Dr. Joshua Gold, Ph.D.

Professor of Neuroscience, Perelman School of Medicine at the University of Pennsylvania

Dissertation Committee

Dr. Todd Lamitina, Ph.D. – Visiting Associate Professor of Pediatrics and Cell Biology

Dr. Harry Ischiropoulos, Ph.D - Research Professor of Pediatrics and Systems Pharmacology and  
Translational Therapeutics

Dr. Kelly Jordan-Sciutto, Ph.D. - Chair and Professor of Pathology

Dr. Richard Morimoto, Ph.D. – Bill and Gayle Cook Professor of Biology

THE IDENTIFICATION OF NOVEL MECHANISMS IN NEURONAL DEVELOPMENT  
AND DEGENERATION

COPYRIGHT

2015

ANGELA MARIE JABLONSKI

This work is licensed under the  
Creative Commons Attribution-  
NonCommercial-ShareAlike 3.0  
License

To view a copy of this license, visit

<http://creativecommons.org/licenses/by-nc-sa/2.0/>

## DEDICATION

This dissertation is dedicated to the memory of my parents, Frank and Margaret Jablonski. I would have not reached this point without them. They are and will continue to be missed every single day.

“What though the radiance which was once so bright  
Be now for ever taken from my sight,  
Though nothing can bring back the hour  
Of splendor in the grass, of glory in the flower  
We will grieve not, rather find  
Strength in what remains behind;  
In the primal sympathy  
Which having been must ever be;  
In the soothing thoughts that spring  
Out of human suffering;  
In the faith that looks through death,  
In years that bring the philosophic mind.”

-William Wordsworth, “Splendor in the Grass”

## ACKNOWLEDGMENT

First and foremost, I would like to thank my advisor, Robert Kalb, for his guidance, training, and words of wisdom throughout my time here. He knew how to provide me with the right amount of guidance, while also giving me the needed independence to develop as a scientist. I am grateful for the countless number of hours he has spent filling my head with new information. His inspiring enthusiasm for science has helped me many times throughout my time as a graduate student. Bob, thank you for helping me develop as a scientist, listening to my crazy ideas (and letting me listen to yours), and for being so supportive and pushing me to always be better. I am also grateful to all of the previous and current members of the Kalb lab for providing a wonderful environment to work in every day.

The projects described in this dissertation would have not been possible without many collaborators. I would like to specifically acknowledge Brian Kraemer, Jiou Wang, Hannes Lans, and Lyle Ostow for not only the work that they contributed, but also for useful conversations. Thank you for making this work so much stronger than it would have been without you.

I'd also like to thank all of the members of my thesis committee including Todd Lamitina, Harry Ischiropoulos, Kelly Jordan-Sciutto, and Rick Morimoto for their time and support. I appreciate the hours that they spent with me in meetings – not only helping the scientific aspect of my work, but also helping me progress and grow into an independent researcher and developing further as a person. Thank you for always answering my questions, meeting with me whenever I needed it, helping me to focus, and finally telling me when it was time to let it go and be done.

I am also grateful to the outstanding Neuroscience Graduate Group at the University of Pennsylvania. This includes the administrators, faculty, and students. I want to specifically thank Mikey Nusbaum, Rita Balice-Gordon, Josh Gold, and Jane Hoshi who always seem to create the time necessary to keep the program running and be tremendously supportive. Thank you to all of you for creating such a fantastic, challenging, and supportive graduate program. I would also like to acknowledge the excellent Neuroscience program at Muhlenberg College where I completed my undergraduate studies. I would like to especially thank my undergraduate advisor, Jeremy Teissere, who did not only introduce me to neuroscience, research, and take me to my first Society of Neuroscience conference, but also has remained as an advisor to me throughout my time as a graduate student. Despite having an increasing number of students every year, he has always found the time to be tremendously supportive. Jeremy, accept this tremendous thank you from the bottom of my heart. I still remember when you wrote "Ph.D." down when I told you about my interests and declared Neuroscience as a major. Who knew we would eventually be here?

I also want to thank all of my friends and family, the people I've known for decades and all of the new lifelong friends I made throughout this process. Thank you for keeping me grounded, making me laugh, and commiserating with me as needed. There are just too many to name, you all know who you are. Thank you for the G-chats, listening to me over many happy hours and dinners, and always being there for me.

Unfortunately, there are so many people who have gotten me to this point, but cannot be physically here to see the final product and celebration. I am extremely grateful to the family members who supported me, but could not be here to see this milestone. I want to specifically acknowledge my mom, Peggy Jablonski. I could not have asked for a better role model of hard work and dedication than her. Thank you,



mom, for teaching me that anything is possible with a little bit of hard work and sacrificing every day for me. I know how happy you were to hear I was done, and you will still be here for the big day in your own way. I also am grateful to my father, Frank Jablonski. Dad, I can still hear you saying: “if you end up at a place like Penn, you better be ready to work hard.” I have never stopped hearing your voice say that since you’ve been gone, and it has kept me going. I’m also grateful to my grandmothers – Lottie Jablonski and Tushie Burns – two more women who modeled how to remain strong in times of adversity. You will all always be in my heart, and so will home and Shenandoah.

Last, but not least, I wish to thank my husband, David. I don’t know how I would have done the past five years without him. I appreciate the support he gave me throughout my training and the sacrifices he made over the past five years. He has been the one to keep our lives running when I was unable (literally). He has unconditionally supported me when I needed someone there. He was always there for the good and the bad (not just the bad, the absolute worst), and was always there to listen to me. I will never be able to repay him for how much he truly helped me throughout my time in graduate school. David, you have accepted me completely as a person since the day we met. I am so grateful I found someone I could always be my crazy self with. It’s a privilege to stand beside you in this journey and in life. I love you, always.

*Throughout my training, I was supported by the NIH Systems Integrative Biology (SIB) Training Grant and an NIH NRSA Pre-Doctoral Fellowship (5F31NS077726).*

## **ABSTRACT**

### **THE IDENTIFICATION OF NOVEL MECHANISMS IN NEURONAL DEVELOPMENT AND DEGENERATION**

Angela Marie Jablonski

Dr. Robert Gordon Kalb, M.D.

The goal of this dissertation is to further understand two key, broad processes which occur over the course of a neuron's lifetime: its development and possible degeneration in disease. We identify novel components in both of these processes and attempt to understand the functional significance as well as the mechanism each component uses to exert its effects.

We begin with work done focusing on how the neuron's dendritic tree develops. The development of neurons has two phases: (1) a first phase relying on a genetic program and (2) a second phase that uses synaptic activity to guide the fine tuning of connections. We are primarily interested in understanding how neurons develop within the motor system using cues from synaptic activity. One type of activity-dependent development in the motor system is driven by AMPA receptors assembled with the GluA1 subunit using the scaffolding protein, SAP97. In Chapter 2, we describe our finding that the small protein, CRIPT, functions in the development of the neuron's dendritic tree within the motor system. We show that CRIPT is expressed during the time in development when activity-dependent remodeling is occurring in the spinal cord. Additionally, we show that CRIPT binds to the PDZ3 domain of SAP97 using its C-

terminus. Finally, we show that CRIPT is necessary for proper dendritic growth of the motor system and normal motor system responses *in vivo*.

There are a number of diseases that specifically target motor neurons. One adult-onset disease is Amyotrophic Lateral Sclerosis (ALS). Like many neurodegenerative diseases, it is a multifactorial disease and a contributing factor is the lack of proper protein quality control and the formation of large protein aggregates within motor neurons. In Chapter 3, we focus on how endoplasmic reticulum-associated degradation (ERAD) components might affect mutant proteins in ALS and their toxicity. ERAD is responsible for maintaining the proper folding of proteins that are to be trafficked to the cell surface or secreted from the cell. Although many proteins associated with ALS are not ERAD substrates, a number of ERAD components have been found to interact with ALS-causing mutant proteins and have been found to be mutated in forms of familial ALS. We identify new modifiers within the ERAD pathway of the toxicity of two ALS-linked proteins, mutant TDP-43 and mutant SOD1. We focus on the mechanism of one suppressor of ALS-linked proteotoxicity, the loss of RAD-23. The levels of RAD23 are increased in ALS models and reducing RAD-23 levels can suppress phenotypes in ALS models, as well as suppress motor neuron toxicity of the mutant proteins. We further show that reduced RAD-23 is able to accelerate the turnover of mutant proteins associated with ALS. Finally, we show that there is a mislocalization of RAD-23 protein and increased RAD-23 protein expression in post mortem spinal cord tissue of ALS patients, suggesting that RAD-23 may be a new novel target in the treatment of ALS.

Collectively, this work identifies and describes novel proteins and mechanisms involved in the development and pathobiology of motor neurons.

## TABLE OF CONTENTS

<b>DEDICATION .....</b>	<b>III</b>
<b>ACKNOWLEDGMENT .....</b>	<b>IV</b>
<b>ABSTRACT.....</b>	<b>VII</b>
<b>LIST OF TABLES .....</b>	<b>XII</b>
<b>LIST OF FIGURES.....</b>	<b>XIII</b>
<b>CHAPTER 1: INTRODUCTION.....</b>	<b>1</b>
<b>NEURONAL DEVELOPMENT .....</b>	<b>1</b>
<b>ACTIVITY-DEPENDENT DEVELOPMENT.....</b>	<b>1</b>
<b>GLUR1 AND SAP97 PROMOTE DENDRITE GROWTH .....</b>	<b>5</b>
<b>CRIP1: A CANDIDATE EFFECTOR FOR GLUR1-DEPENDENT DENDRITE GROWTH .....</b>	<b>9</b>
<b>MOTOR NEURON DISEASE: AMYOTROPHIC LATERAL SCLEROSIS .....</b>	<b>10</b>
<b>GENETIC MODELS OF MOTOR NEURON DISEASE.....</b>	<b>12</b>
<b>ENDOPLASMIC REICULUM-ASSOCIATED DEGRADATION AND ALS .....</b>	<b>15</b>
<b>RAD-23: A MULTI-FUNCTIONAL PROTEIN.....</b>	<b>18</b>
<b>STATEMENT OF MOTIVATION AND HYPOTHESES.....</b>	<b>21</b>
<b>CHAPTER 2: IDENTIFYING THE DOWNSTREAM MACHINERY OF GLUR1 AND SAP97 IN DENDRITE DEVELOPMENT .....</b>	<b>23</b>
<b>SUMMARY.....</b>	<b>23</b>
<b>INTRODUCTION.....</b>	<b>24</b>
<b>MATERIALS AND METHODS .....</b>	<b>26</b>
<b>RESULTS .....</b>	<b>35</b>
<b>DISCUSSION.....</b>	<b>44</b>

FIGURE LEGENDS .....	47
<b>CHAPTER 3: LOSS OF RAD-23 PROTECTS AGAINST MODELS OF MOTOR NEURON DISEASE BY ENHANCING MUTANT PROTEIN DEGRADATION ..</b>	<b>59</b>
SUMMARY .....	59
INTRODUCTION.....	60
MATERIALS AND METHODS .....	62
RESULTS .....	74
DISCUSSION.....	88
TABLE LEGENDS.....	91
FIGURE LEGENDS .....	93
<b>CHAPTER 4: GENERAL CONCLUSIONS AND FUTURE DIRECTIONS .....</b>	<b>121</b>
ACTIVITY-DEPENDENT DEVELOPMENT.....	121
THE IDENTIFICATION OF OTHER MEDIATORS OF GLUA1-MEDIATED DENDRITE GROWTH .....	123
UNRESOLVED QUESTIONS REGARDING CRIPT'S ROLE IN DENDRITE GROWTH.....	124
THE IMPORTANCE OF ERAD COMPONENTS IN ALS.....	125
TARGETING RAD-23 IN NEURODEGENERATIVE DISEASE.....	128
HOW REDUCED RAD-23 ACCELERATES MUTANT PROTEIN TURNOVER AND MITIGATES TOXICITY.....	131
LOSS OF RAD-23 AS A PROTECTOR AGAINST PROTEOTOXICITY.....	133
A LINK BETWEEN NUCLEOTIDIE EXCISION REPAIR AND NEURODEGENERATIVE DISEASE .....	135
FINAL REMARKS .....	137
<b>APPENDIX 1: OTHER COMPONENTS IN THE GLUA1/SAP97/CRIPIT COMPLEX TO PROMOTE DENDRITE GROWTH .....</b>	<b>138</b>
SUMMARY .....	138
INTRODUCTION.....	138
MATERIALS AND METHODS .....	140

<b>RESULTS .....</b>	<b>143</b>
<b>DISCUSSION .....</b>	<b>145</b>
<b>FIGURE LEGENDS .....</b>	<b>147</b>
<b>APPENDIX 2: OTHER MODIFIERS OF MOTOR NEURON DISEASE MODELS .....</b>	<b>151</b>
<b>SUMMARY .....</b>	<b>151</b>
<b>INTRODUCTION.....</b>	<b>151</b>
<b>MATERIALS AND METHODS .....</b>	<b>154</b>
<b>RESULTS .....</b>	<b>157</b>
<b>FIGURE LEGENDS .....</b>	<b>160</b>
<b>BIBLIOGRAPHY .....</b>	<b>168</b>

## LIST OF TABLES

<b>Table 3.1. Mammalian ERAD genes and their predicted orthologs in <i>C. elegans</i>.</b>	<b>102</b>
<b>Table 3.2. List of primers used in genotyping <i>C. elegans</i> strains.</b>	<b>103</b>
<b>Table 3.3. A list of the <i>C. elegans</i> strains used in this study.</b>	<b>104</b>
<b>Table 3.4. Description of human ALS cases used for staining and expression analysis.</b>	<b>118</b>
<b>Table 3.5. Description of control cases used for staining and expression analysis.</b>	<b>119</b>
<b>Table 3.6. RAD-23 has opposing roles on substrate stabilization.</b>	<b>120</b>

## LIST OF FIGURES

Figure 2.1. CRIPT is <i>bona fide</i> PDZ3 and SAP97 interacting protein.....	51
Figure 2.2. CRIPT is necessary for the dendritic growth of spinal cord neurons. .	52
Figure 2.3. CRIPT is not sufficient to promote dendritic growth of spinal cord neurons. ....	53
Figure 2.4. CRIPT functions downstream of SAP97 in promoting dendrite growth. ....	54
Figure 2.5. CRIPT knockdown increases the number of excitatory and inhibitory synapses, but does not change synapse size.....	55
Figure 2.6. CRIPT's function in dendritic growth is independent from synaptic activity.....	56
Figure 2.7. Loss of <i>cript</i> decrease dendrite branch number <i>in vivo</i> . ....	57
Figure 2.8. Loss of <i>cript</i> results in a mechanosensory defect <i>in vivo</i> in young adults.....	58
Figure 3.1. Locomotor defects of <i>C. elegans</i> models of ALS and their modification by the loss of ERAD and UPS genes.....	106
Figure 3.2. Loss of <i>rad-23</i> in <i>C. elegans</i> protects against models of ALS via an effect in the nervous system. ....	107
Figure 3.3. Loss of <i>rad-23</i> in <i>C. elegans</i> protects against neurodegeneration following expression of mutTDP-43 <i>in vivo</i> .....	108
Figure 3.4. RAD-23 protein is expressed throughout the worm, including the worm nervous system. ....	109
Figure 3.5. Loss of <i>RAD-23</i> in <i>C. elegans</i> protects against aging decline and proteotoxicity.....	110
Figure 3.6. Loss of <i>rad-23</i> does not suppress the <i>C. elegans</i> mutTDP-43 locomotor deficit via known pathways. ....	111
Figure 3.7. Knockdown of RAD-23 orthologs in mammalian motor neurons protects against toxicity of mutSOD1 or mutTDP-43.....	112
Figure 3.8. hR23A expression is increased in the spinal cord of mutSOD1 mice at P90 and P120. ....	113
Figure 3.9. Manipulations of RAD-23 expression change TDP-43 and SOD1 abundance and solubility.....	114



<b>Figure 3.10. Loss of RAD-23 accelerates turnover through the proteasome and autophagy by increasing ubiquitination. ....</b>	<b>115</b>
<b>Figure 3.11. Loss of <i>rad-23</i> reduces TDP-43 and SOD1 insolubility. ....</b>	<b>116</b>
<b>Figure 3.12. hR23A and hR23B are aberrantly expressed in human ALS tissue. .</b>	<b>117</b>
<b>Figure A1.1. Association of GluA1 with SAP97 is activity-dependent. ....</b>	<b>149</b>
<b>Figure A1.2. Successful tool development to identify new SAP97 PDZ3 domain binding partners in neurons. ....</b>	<b>150</b>
<b>Figure A2.1. Overexpression of wild type (wt-) and mutant (mut-) TDP-43 (M337V) in the nervous system causes an accumulation of normally degraded ubiquitinated substrates in a non-cell autonomous manner. ....</b>	<b>162</b>
<b>Figure A2.2. Knockdown of <i>ufd-3</i>, but not <i>rad-23</i>, in <i>C. elegans</i> reduces ubiquitinated GFP abundance in mutTDP-43 background. ....</b>	<b>163</b>
<b>Figure A2.3. Expression of constitutively spliced XBP1 in the nervous system enhances toxicity of ER stress. ....</b>	<b>164</b>
<b>Figure A2.4. Stabilization of p53 by treatment with tenovin-1 protects motor neurons from toxicity caused by mutSOD1 (G85R). ....</b>	<b>165</b>
<b>Figure A2.5. Only ubiquitous knockdown of <i>ubql-1</i> enhances the mutSOD locomotor deficit. ....</b>	<b>166</b>
<b>Figure A2.6. Constitutively ‘on’ HIF1<math>\alpha</math> in the nervous sytem alone protects against mutSOD toxicity in <i>C. elegans</i>. ....</b>	<b>167</b>

## **CHAPTER 1: INTRODUCTION**

This thesis attempts to understand two major events in the life of the nervous system: the development of the nervous system and its possible degeneration, with a key emphases on the motor system. Here, I will outline the critical information needed to understand the progress made in these two areas.

### **NEURONAL DEVELOPMENT**

The development of the nervous system is roughly divided into two parts: (1) an activity-independent phase outlined by a genetic program and (2) an activity-dependent phase. Together, these phases produce the adult nervous system with the correct connectivity and physiology to produce meaningful behavior. This work primarily focuses on the second phase and the role of activity-dependent development.

### **ACTIVITY-DEPENDENT DEVELOPMENT**

Activity-dependent development during pre- and postnatal life is an important mechanism for the specification of synaptic phenotype and connectivity. Here, we will review some of the key experiments undertaken in the visual system that highlight the cell biological processes underlying activity-dependent development. These introductory remarks provide the context for thinking about the role of activity-dependent processes in motor system development.

In the mammalian visual system, retinal ganglion cells (RGC) project to the lateral geniculate nucleus (LGN) of the thalamus. Thalamocortical (TC) connections from the LGN project to the visual cortex. In mature animals, right and left eye afferents are

segregated from each other in both the LGN and visual cortex (Katz and Shatz, 1996; Mooney et al., 1996). For example, in adult cats and primates, TC afferents projecting to layer four of the visual cortex are organized into discrete right and left eye patches, referred to as ocular dominance columns (OCD) (Shatz, 1996). This circuitry arrangement subserves high acuity vision (Butts et al., 2007).

In their classic work, Hubel and Weisel showed that this pattern of visual cortex innervation is not present at birth, as right and left eye afferents demonstrate extensive overlap (Hubel et al., 1977). Most remarkably, they showed that the segregation of right and left eye afferents is driven by visual experience (Hubel et al., 1977). Monocular deprivation of one eye (by suturing the eyelid shut) during a discrete period in early postnatal life leads to a dramatic shift in TC innervation of the visual cortex (Hubel et al., 1977). The afferents from the nondeprived eye innervate a larger territory of the visual cortex, while those from the deprived eye innervate a smaller territory (Hubel et al., 1977). This experience-dependent shift in ocular dominance leaves a permanent imprint on visual system organization (Hubel et al., 1977).

How does environmentally evoked synaptic activity lead to changes in synaptic strength and connectivity? Substantial evidence supports the view that synapses will undergo strengthening and stabilization when the activity of pre- and postsynaptic elements is coincident. This model of synaptic plasticity was originally suggested in theoretical work by Daniel Hebb and has been most rigorously tested in long-term potentiation (LTP) paradigms (Hebb, 1949). Many forms of LTP depend upon the activation of *N*-methyl-d-aspartate receptors (NMDA-Rs). NMDA-Rs are believed to be the coincidence detectors responsible for detecting the simultaneous activity of pre- and

postsynaptic elements (Seeburg et al., 1995). The ionic mechanism underlying this process has been linked to the voltage-dependent block of NMDA-Rs by  $Mg^{2+}$  (Shaywitz and Greenberg, 1999). Patterned afferent input, sufficient to remove the  $Mg^{2+}$  block, allows NMDA-Rs to conduct  $Ca^{2+}$  influx, which inactivates several protein kinases, including  $Ca^{2+}$ /calmodulin-dependent protein kinase II (CamKII) (Seeburg et al., 1995). CamKII is necessary for the maintenance of LTP and phosphorylation of 2-amino-3-(3-hydroxy-5-methyl-isoxazol-4-yl) propanoic acid receptor (AMPA-R) subunits to increase their conductance (Shaywitz and Greenberg, 1999). These and other calcium-activated processes drive the observed synaptic plasticity (Shaywtiz and Greenberg, 1999; Luthi et al., 2004).

In the visual system, activity-dependent processes drive large-scale alterations in the architecture of axons and dendrites. How do activity-dependent changes in synapses control the growth and distribution of axons and dendrites? Vaughn proposed the synaptotropic hypothesis: dendritic branches are formed near active synapses and synapse stabilization consequently stabilizes dendrites (Vaughn, 1989). Original *in vivo* work from the Haas lab implicates beta-neurexin (NRX) and neuroligin-1 (NLG1) in this process, in which NMDA-R-dependent synapse maturation was required for persistent NRX-NLG1 function in dendritogenesis (Chen et al., 2010). Blocking synaptogenesis thereby blocks dendrite outgrowth stabilization. The linkage of synaptic plasticity to neurite architecture is a fundamental principle in developmental neuroscience and provides an explanation for earlier observations that the size and complexity of the dendrite tree controls the qualitative and quantitative nature of the afferent input (Oswald, 1989). In studies of rabbit ciliary ganglia, the number of ganglion cell primary dendrites is highly correlated with the number of innervating axons (Hume and Purves,

1981). This is not true of some of the cells in the neonate, where the initial set of inputs is confined to the cell body, allowing only one axon to survive (Hume and Purves, 1981). It is hypothesized that the complexity of some cells allows for a higher number of afferents to innervate the ganglion cell (Hume and Purves, 1981). Thus, a competition-based model of synapse formation holds for dendrite growth.

While many studies implicate AMPA-Rs in the control of dendrite growth, a consistent picture has yet to emerge. Blocking AMPAergic transmission in retinotectal neurons decreases synapse stabilization, and subsequent dendrite growth and stabilization (Haas et al., 2006). Conversely, Casticas et al. (2011) showed that enhanced conductance of Ca<sup>2+</sup>-permeable AMPA-Rs inhibited neurite outgrowth in dissociated chick retinal neurons (Casticas et al., 2001). Outside of the visual system, blockade of AMPA-Rs in chick motoneurons has also been seen to increase dendritic outgrowth in chick motoneurons, but only at certain time points in embryonic development (Ni and Maratin-Caraballo, 2010). It is unclear what role NMDA-Rs played in these processes because blocking AMPA-Rs will prevent NMDA-R activation.

In the central nervous system (CNS), it is understood that activation of AMPA-Rs, sufficient to relieve the voltage-dependent magnesium block of NMDA-Rs, drives activity-dependent plasticity, synaptic stabilization, and patterned innervation (Peng et al., 2009). Less understood is the extent to which NMDA-R-independent mechanisms can drive activity-dependent developmental processes. Next, we describe work in the spinal cord showing how AMPA-Rs assembled with the GluA1 subunit can promote activity-dependent development by an NMDA-R-independent process.

## GLUR1 AND SAP97 PROMOTE DENDRITE GROWTH

Neonatal motor neurons express a very high level of GluA1 (both mRNA and protein). GluA1's properties can be modified by alternative splicing and editing at the glutamine/arginine "Q/R" site. The GluA1 expressed during this developmental period contains the "flip" alternatively spliced exon and is unedited in the Q/R site (Jakowec et al., 1995a; Jakowec et al., 1995b). Previous work has shown that neonatal motor neurons express Ca<sup>2+</sup> permeable AMPA receptors (as one would expect if they were enriched with GluA1(Q)) (Jakowec et al., 1995b). Taken together with the electrophysiological data, it suggests that many AMPA-R are assembled of GluA1 homomers at this point in development in motor neurons.

The unusually high level of GluA1 expression by neonatal motor neurons raises the possibility that AMPA receptors assembled with GluA1 play a special role in activity-dependent motor system development. To examine this notion, we began by asking whether manipulation of GluA1 influenced spinal neuron dendritic architecture. Several approaches were taken. First, we found that knockdown of GluA1 expression inhibited dendrite growth. Conversely, overexpression of GluA1 in spinal neurons *in vitro* stimulated dendritic growth; this growth effect was blocked by the AMPA-R antagonist, CNQX (6-cyano-7-nitroquinoxaline-2, 3-dione) (Zhang et al., 2008). Second, we compared the effects of two types of overexpressed GluA1 in motor neurons *in vivo*. We used a version that robustly passes current (GluA1(Q)) and compared that with a version that passes very little current (GluA1(R)). Only overexpressed GluA1(Q) stimulated dendritic branching (Jeong et al., 2006). These results suggest: 1) that the activity of AMPA-R assembled with GluA1 is a crucial step for dendrite growth and 2) that this effect is Ca<sup>2+</sup>-dependent. Subsequent *in vitro* work indicates that the degree of calcium

permeability of AMPA-R assembled with GluA1 controls the dendritic growth process (Jeong et al., 2006).

One interpretation of the above results is that overexpression of GluA1 enhances neuronal depolarization, thereby promoting NMDA-R mediated events. We think this is not true for a number of reasons. First, our *in vivo* observations were made in juvenile rodents at a time when motor neurons do not express NMDA-R (Steganga and Kalb, 2001). It is possible that prior *in situ* hybridization and immunohistological studies were insufficiently sensitive to detect NMDA-R in juvenile motor neurons. To address this possibility, we expressed GluA1(Q) in juvenile animals and simultaneously treated them with the NMDA-R antagonist, MK-801 (Inglis et al., 2002). We know that MK-801 was administered in an effective dose because LTP could not be evoked in these animals (Inglis et al., 2002). Nonetheless, MK-801 did not block the pro-dendrite growth actions of overexpressed GluA1(Q) (Inglis et al., 2002). Second, we undertook *in vitro* pharmacological studies. Administration of MK-801 did not block the dendrite growth promoting actions of GluA1(Q). In contrast, administration of the L-type calcium channel blocker, nifedipine, did block the GluA1(Q) effect (Kalb et al., 2013). Taken together, all of these results suggest that GluA1 is sufficient to promote dendrite growth in an NMDA-R-independent manner.

The work described above primarily focuses on the effects of GluA1 on dendrite architecture *in vitro*. What about *in vivo*? To address this question, studies of the GluA1<sup>-/-</sup> mouse have been informative (Zhang et al., 2008). Analysis of the dendritic tree revealed that motor neurons from GluA1<sup>-/-</sup> animals are smaller and less branched at P10 and P23 (Zhang et al., 2008). This suggests that GluA1<sup>-/-</sup> motor neurons develop over a different trajectory than wild type (WT) motor neurons. How does this decrease in the

size and complexity of the motor neuron dendrite tree effect motor circuitry and behavior of the animal? To study the innervation of motor neurons within the segmental spinal cord, a recombinant Pseudorabies virus engineered to express green fluorescence protein (PRV-GFP) was employed. PRV-GFP labeling experiments revealed a distinct pattern of interneuronal connectivity in the spinal cord of GluA1<sup>-/-</sup> mice in comparison to WT mice. The greatest difference between genotypes was found in the number of contralaterally located interneurons, especially in Rexed's lamina VIII (Zhang et al., 2008). The stunted dendrite tree and change in interneuron connectivity correlate with a locomotor defect in the GluA1<sup>-/-</sup> animals. In comparison to WT counterparts, GluA1<sup>-/-</sup> mice showed poorer performance in grip strength, treadmill, and rotarod at P23 and adulthood (Zhang et al., 2008). This suggests that GluA1 is not only important for dendrite growth, but also for patterning segmental spinal cord circuitry and motor behavior. Furthermore, changes in development during the postnatal period lead to deficits throughout adulthood (Zhang et al., 2008).

By what molecular mechanism does the activity of AMPA-R assembled with GluA1 control the morphology of motor neuron dendritic architecture? A series of experiments have indicated that the multi-domain scaffolding protein, synapse-associated protein of 97 kDa molecular weight (SAP97), interacts with GluA1 and plays a key role in this process (Zhou et al., 2008). The C-terminal seven amino acids of GluA1 physically interact with the second PDZ domain of SAP97.

AMPA-R physiology and synaptic plasticity is entirely normal when the physical interaction between GluA1 and SAP97 is disrupted (Kim et al., 2005). This was demonstrated using mice in which the wild type allele of GluA1 was replaced by a version of GluA1 lacking the C-terminal seven amino acids of the protein known to bind



SAP97 (GluA1 $\Delta$ 7 mice) (Kim et al., 2005). Contrary to expectations, GluA1 also traffics normally to the cell surface in these mice, suggesting GluA1 chaperones SAP97 to synapses – not the vice versa. This was demonstrated further using biochemical and imaging methodologies (Kim et al., 2005). However, normal elaboration of motor neuron dendrites requires SAP97. This was demonstrated *in vitro*: knockdown of SAP97 decreases the total size of the dendritic tree and prevents the pro-dendrite growth effect of GluA1 overexpression (Kim et al., 2005) This was further confirmed *in vivo* – a smaller dendritic tree was found in the GluA1 $\Delta$ 7 mice (where SAP97 does not traffic to the cell surface) as well as in mice with a conditional deletion of SAP97 from motor neurons (Kim et al., 2005). Finally, co-overexpression of GluA1 and SAP97 *in vitro* has a synergistic pro-dendrite growth effect; this only depends on their co-localization at the plasma membrane, not their physical association (Kim et al., 2005). This was demonstrated using a membrane-targeted version of SAP97 in conjunction with GluA1 $\Delta$ 7 or a membrane-targeted version of SAP97 with mutations in its PDZ2 domain that make it incapable of binding GluA1 (Kim et al., 2005).

Together, these experiments suggest that the endogenous GluA1 and SAP97 complex is the necessary platform upon which GluA1-containing AMPA-R activity is translated into a signal(s) that stimulates dendritic growth and branching in the spinal cord.

How do GluA1 and SAP97 work together to promote dendrite growth? One hypothesis is that GluA1 and SAP97 help form the assembly of a multi-protein complex during GluA1-containing AMPA-R activity to activate downstream effectors capable of stimulating dendritic growth. At this time, the molecular mechanism by which SAP97 and GluA1 promote dendritic growth and branching is unknown. We do, however, have

evidence that the PDZ3 domain of SAP97 is crucial for these pro-growth effects by SAP97 and GluA1 (unpublished observations). Overexpression of SAP97 with a mutation in the PDZ3 domain no longer increases dendrite growth. Thus, it is logical to ask whether proteins that bind to the PDZ3 domain of SAP97 are part of the machinery to translate activity into growth. This is one current avenue for research and key downstream players in the GluA1-mediated process are beginning to be identified. One protein identified in this thesis work is CRIPT.

### **CRIPT: A CANDIDATE EFFECTOR FOR GLUA1-DEPENDENT DENDRITE GROWTH**

CRIPT (cysteine-rich-interactor-of-pDZ-three) was originally identified as a small 12 kDa protein that was localized to excitatory synapses. It is believed to be a crosslinking proteins between proteins in the post-synaptic density (i.e. PSD-95) and microtubules because it could be co-immunoprecipitated with tubulin and PSD-95 (Niethammer et al., 1998; Passafaro et al., 1999). It could also be co-immunoprecipitated with NR2B and Chapsyn-110 from synaptosomal preparations (Niethammer et al., 1998). Furthermore, overexpression of CRIPT in heterologous cells was shown to cause a redistribution of PSD-95 to microtubules (Niethammer et al., 1998).

We chose to focus on CRIPT as a possible mediator of GluA1- and SAP97-driven dendrite growth because it was found to selectively bind to the third PDZ domain (PDZ3) of PSD-95 previously. CRIPT contains a canonical PDZ-binding sequence at its terminus (-QTSV). Furthermore, CRIPT is conserved from mammals to plants (i.e. human and *Arabidopsis thaliana* CRIPT share 78% similarity in their amino acid sequences), suggesting an important functionality (Niethammer et al., 1998). CRIPT was also previously shown to be expressed throughout the rat nervous system in known sites

of plasticity, such as the hippocampus (Niethammer et al., 1998). Furthermore, it is likely that a protein involved in dendritic remodeling would interact with the cytoskeleton, such as microtubules, which CRIPT has been found to do (Niethammer et al., 1998).

Up until now, no definitive function of CRIPT has been established. For example, although interference of CRIPT's interaction with PSD-95 disrupts PSD-95's localization with microtubules (Passafaro et al., 1999), it had no effect on the clustering or number of NMDA-R. This work, therefore, proposes a novel function for CRIPT in the dendrite growth of spinal cord neurons. This work can be found in Chapter 2.

## **MOTOR NEURON DISEASE: AMYOTROPHIC LATERAL SCLEROSIS**

A number of neurodegenerative diseases are known to selectively target the upper motor neurons in the cortex and lower motor neurons in the brainstem and spinal cord. These diseases are known as motor neuron diseases (MND), but it is still not completely understood why these diseases target this subset of neurons.

The disease we focused on in this work is Amyotrophic Lateral Sclerosis (ALS), popularly referred to in the United States as Lou Gehrig's disease. ALS is commonly classified into two subtypes: (1) familial (fALS) and (2) sporadic (sALS), depending respectively on if the disease is or is not caused by a single genetic and inherited mutation. Familial ALS accounts for roughly 5-10% of cases and has been linked to a number of gene mutations. The most prevalent of these is the C9ORF72 mutation, although new mutations continue to be found. The disease tends to present itself earlier than some other neurodegenerative diseases, anywhere between 50 to 75 years of age, and disease progression lasts for three years on average. The disease has a worldwide incidence of two in every 100,000 individuals and men tend to present more often with

the disease than women (1.2-1.5:1 ratio) (Cronin et al., 2007). The disease can sometimes be associated with non-motor systems in a form of frontotemporal dementia (FTD). Postmortem tissue from both ALS and FTD patients reveals the presence of protein aggregates, strongly supporting the existence of a pathophysiological continuum between these two disorders (Forman et al., 2004). In fact, it is estimated that 15% of FTD patients meet the criteria to be diagnosed with ALS (Ringholz et al., 2005). The prevalence of protein aggregates within motor neurons in both sporadic and familial ALS tissue also points to a lack of protein quality control in the disorder, which is a major focus of the work discussed in this dissertation.

Patients with ALS exhibit progressive neuromuscular weakness, atrophy, and eventual death. Most patients will die from respiratory failure. The biggest motivation for studying the disease is that it has no known cure. The only drug known to modify the course of ALS is Riluzole, a drug that is thought to act by reducing the burden of glutamate excitotoxicity, but only achieves a modest improvement in survival (Miller et al, 2007). The lack of treatment is in part due to the multifactorial nature of the disease. Contributing pathogenic processes include glutamate excitotoxicity, protein misfolding, inflammation, oxidative stress, endoplasmic reticulum (ER) stress, mitochondrial dysfunction, impaired axonal transport, impaired endosomal trafficking, as well as dysregulated transcription and RNA processing (Ferraiuolo et al., 2011; Rothstein, 2009).

Due to the lack of promising treatment, there is an urgent need for ALS research. One of the obstacles in studying the disease is that most of the cases are sporadic and most research done in the laboratory to model and study the disease utilizes genetic models.

## GENETIC MODELS OF MOTOR NEURON DISEASE

In order to identify new modifiers of motor neuron disease, we utilized several models of motor neuron disease in the small genetically tractable nematode, *Caenorhabditis elegans* (*C. elegans*). Some of the mutations found in fALS include mutations in copper-zinc superoxide dismutase 1 (SOD1), TAR DNA-binding protein of 43 kDa molecular weight (TDP-43), fused in sarcoma (FUS), vesicle-associated membrane protein-associated protein B (VAPB), ubiquilin-2 (UBQLN2), and many more (Ferraiuolo et al., 2011). Here, we focused on models based on mutations commonly found in familial forms of ALS, mutant SOD1 (G85R), which counts for 20% of fALS cases (or 2% of total cases) (Wang et al, 2009) and mutant TDP-43 (M337V) (Liachko et al., 2010). Mutations in TDP-43 account for roughly 5% of fALS cases (Kabashi et al., 2008; Sreedharan et al., 2008; van Deerlin et al., 2008). It is important to note, however, that TDP-43 inclusions can be found in the tissue of both fALS and sALS patients (Baralle et al., 2013).

SOD1 was the first gene for which a causative mutation for ALS was found (Deng et al., 1993; Rosen et al., 1993). SOD1 is a ubiquitously-expressed cytosolic enzyme highly conserved across species involved in dismutating superoxide by binding copper and zinc ions and this property suggests that SOD1 helps to prevent oxidative stress (Ratovitski et al., 1999). Other functions for SOD1 have recently been identified and include roles in metabolism (Reddi and Culotta, 2013), copper buffering (Wei et al., 2001), the nitration of proteins (Beckman et al., 1993), and zinc homeostasis (Wei et al., 2001). Over 100 different mutations have been identified in SOD1 in fALS, and research has demonstrated that mutant SOD1 induces disease through a toxic gain-of-function mechanism. Over 150 mutations in SOD1 have been associated with human ALS cases

and there appears to be no correlation between the level of SOD1 dismutase activity and severity of the disease (Ratovitski et al., 1999). In addition, SOD1-null animals lack any overt ALS symptoms (Flood et al., 1999; Fischer et al., 2012). Meanwhile, mutant (G85R) SOD1 transgenic mice have the same survival times on both wild type (two copies of the SOD1 gene) and SOD1-null backgrounds (Brujin et al., 1998). Furthermore, mutant SOD1 that is enzymatically inactive due to depletion of copper loading was shown to be still capable of causing motor neuron degeneration (Subramaniam et al., 2002).

SOD1 is believed to induce its toxic effects in a both cell autonomous and non-cell autonomous manners (Ilieva et al., 2009). For example, expression of mutant SOD1 in astrocytes is sufficient to induce motor neuron death (Marchetto et al., 2008) and overexpression of mutSOD1 (G85R) in the nervous system of *C. elegans* is sufficient to cause a profound locomotor deficit (Wang et al., 2009). Certain studies have also found that overexpression of wild type SOD1 at high levels can also induce neurodegenerative symptoms including mitochondrial damage in the axons within the spinal cord, axonal degeneration itself, and eventually a moderate loss of spinal motoneurons at 2 years of age (Jaarsma et al., 2000). This suggests that the concentration of SOD1 must normally be controlled to prevent its toxicity

TDP-43 is a 414 amino acid protein encoded by the TARDP gene on chromosome 1. TDP-43 has been found to participate in many functions including transcription, mRNA processing, mRNA splicing, RNA transport, and stress granule formation (Ling et al., 2013). It has not been established yet whether loss or corruption of any of these functions has a link to TDP-43's role in ALS. TDP-43 has two RNA binding domains, a glycine rich domain, and nuclear export and import signals. In pathological

models of ALS, TDP-43 is found in the cytoplasm, where it is often found as an insoluble species. These insoluble species of TDP-43 contain a hyperphosphorylated form of TDP-43 and a C-terminus cleaved fragment (Neumann et al., 2006). At least 40 mutations in TDP-43 have been found in ALS and expression of different mutations in mutant TDP-43 (mutTDP-43) in the nervous system have had conflicting results on neuronal viability. For example, in one model, expressing mutant TDP-43 (Q331K) or mutant TDP-43 (M337V) in the mouse central nervous system showed large scale motor neuron degeneration (Arnold et al., 2013). Meanwhile, overexpressing other forms of mutant TDP-43 (G348C or A315T) displayed only mild neuronal loss (Swarup and Julien, 2011; Verbeeck et al., 2012). Recently, it has been found the expressing mutTDP-43 in astrocytes is sufficient to induce motor neuron death and ALS-like symptoms in rats (Tong et al., 2013). It is still unclear as to what the pathogenic effect of the mutant protein is and if it is a gain of function, loss of function, or both (Ling et al., 2013). However, overexpression of wild type TDP-43 in mouse and *C. elegans* models has also been shown to be toxic. Therefore, like SOD1, it appears TDP-43 levels need to be controlled and lack of the autoregulation of TDP-43 expression levels can lead to neurodegeneration (Igaz et al., 2011). Therefore, it has been proposed that perhaps what the mutations in TDP-43 do is increase the stability and thereby the abundance of the protein, which itself is toxic.

Both the mutTDP-43 and mutSOD1 models of ALS in *C. elegans* show severe locomotor deficits and the mutTDP-43 model also shows death of the GABAergic motor neurons (Wang et al., 2009; Liachko et al., 2010). Furthermore, both of these proteins have been shown to aggregate and form detergent insoluble proteins. Therefore, a high concentration of either SOD1 or TDP-43 appears to be toxic in itself. Therefore, one

common theme in both models is a lack of protein quality control. In addition, both models also show an increase in the ER unfolded protein response. Because ER stress and proteostasis have been a recurrent theme in ALS research (Matsus et al., 2013; Musaro, 2013), we chose to focus on the ER-resident process, ERAD (endoplasmic reticulum-associated degradation). ERAD and the unfolded protein response (UPR) are also known to be tightly linked; for example, ERAD requires an intact UPR and UPR induction leads to increased ERAD capacity (Travers et al., 2000).

### **ENDOPLASMIC REICULUM-ASSOCIATED DEGRADATION AND ALS**

ERAD (endoplasmic reticulum-associated degradation) is a conserved biological process used in the quality control of proteins that are destined to be trafficked to the cell surface or to be secreted from the cell. One cause of ER stress is the accumulation of misfolded proteins within the ER. In order to ensure this does not happen, ERAD is employed. This process can be roughly divided into a series of steps including: (1) recognition of the misfolded substrate; (2) retrotranslocation of the substrate from the ER lumen, (3) ubiquitination, and (4) degradation. If a lesion or misfolding is identified, that substrate is eventually targeted for ERAD after a number of opportunities to fold correctly by a number of recognition factors, such as YOS-9. From there, the protein is pumped out of the ER through the retrotranslocon channel, believed to mostly be comprised of DERLIN-1. This process requires energy and is driven by the AAA ATP-ase pump, CDC-48 (also known as VCP). Once the substrate is pumped through the ER, it is ubiquitinated and destined for the proteasome. Ubiquitination requires a number of steps and the action of several classes of proteins, including an E1 ubiquitin-activating enzyme, an E2 ubiquitin-conjugating enzyme, and an E3 ubiquitin-ligase. A number of ubiquitin receptors, such as UFD-2, UFD-3, and RAD-23 interact with CDC-48. From



there, the substrate is shuttled to the proteasome where it is ultimately degraded (Vembar and Brodsky, 2008).

Both sporadic and familial ALS cases have been found to have an abnormal ER stress response (Ilieva et al., 2007; Atkin et al., 2008; Hetz et al., 2009; Ito et al., 2009). There have been a number of links made between ERAD and ALS in the past couple of decades. For example, the ERAD component, VCP, has recently been found to be mutated in forms of fALS (González-Pérez et al., 2012). In addition, ERAD components have been found to erroneously interact with non-ERAD ALS-causing proteins. For example, DERLIN-1, believed to be the major constituent of the retrotranslocon channel used to pump misfolded substrates from ER (Lilley and Ploegh, 2004; Ye et al., 2004), has been shown to interact with mutant SOD1 (Nishitoh et al., 2008).

There have been conflicting studies regarding the role of ERAD and the UPR in ALS. In past work, mutSOD1 has been shown to accumulate within the ER and cause activation of the unfolded protein response (UPR) (Urushitani, et al., 2008). Inactivation of the PERK pathway within the UPR has been previously found to dramatically hasten the onset of disease in mutSOD1 (G85R) mice and mutSOD1 aggregation (Wang et al., 2011). This suggested that the UPR might be important to reduce proteotoxic burden by inhibiting the synthesis of more protein and more mutSOD1 which would continue to accumulate and aggregate (Wang et al., 2011). Activation of ER stress and thereby the UPR could go on to inhibit future protein synthesis until the current load of misfolded proteins could be cleared from the cell.

However, more recent research suggests that this might not be the case. For example, pharmacological reduction of ER stress was found to protect against TDP-43

neuronal toxicity *in vivo* in *C. elegans* (Vaccaro et al., 2013). This has also been translated into mammalian systems where XBP1-deficiency in the nervous system has been found to extend the lifespan of mutSOD1 mice (Hetz et al., 2009). Surprisingly, this appears to be a consequence of accelerated mutSOD1 turnover through accelerated autophagy (Matsus et al., 2009). Not only was this seen with knockdown of XBP1, but also by knockdown of a critical ERAD component, EDEM, in a cell culture system (Hetz et al., 2009). The major output of the ER stress response pathway is to inhibit further protein synthesis and this is regulated by phosphorylated-eIF2 $\alpha$ . Recently, it was shown that inhibitors of phosphorylated-eIF2 $\alpha$  could actually attenuate toxicity due to the aggregation of mutTDP-43 (Kim et al., 2014).

Therefore, one possible way to reduce toxicity of mutant proteins linked to ALS might be to accelerate their clearance or the clearance of other misfolded proteins. It is not intuitive that this can be done by the reducing activation of the ER stress and UPR pathways. Up until now, clearance of these large protein aggregates from neurons has been challenging. Forced expression of ubiquitin-proteasome components has not been sufficient to clear misfolded proteins from the cell in several experiments. For example, overexpression of ubiquilin-1 bound to ubiquitinated forms of mutTDP-43 and actually recruited TDP-43 to detergent-resistant cytoplasmic aggregates and no evidence is present that these aggregates went on to be destroyed (Kim et al., 2009). Therefore, overexpressing UPS components do not simply act in the destruction of misfolded proteins, and may have other functions in the cell.

Taken together, all of these reports suggest that ERAD and the UPR has a significant influence on ALS, although the meaning of that influence is still unresolved. Although one might predict that blocking the output of ER stress and the functioning of

ERAD components should be detrimental in models of motor neuron disease, there are clear examples where this is not the case. This suggests that there is still much insight to be gained into how to target ERAD and the UPR in ALS and neurodegenerative disease. It also warrants our investigation into the contribution of the ERAD pathway in ALS. This is further discussed in Chapter 3. The studies we performed in Chapter 3 describe a loss of function approach, although much of what we know to date has come from overexpression and *in vitro* studies. This is one unique advantage to the work described in this dissertation.

### **RAD-23: A MULTI-FUNCTIONAL PROTEIN**

In this thesis work, we specifically focused on one suppressor that was identified in our candidate gene screen approach, RAD-23. It is noteworthy that the CDC-48 interactors, UFD-2 and UFD-3 (Rumpf and Jentsch, 2006), were also identified as suppressors in our candidate gene approach in Chapter 3 and are known to interact with RAD-23 (Kim et al., 2004).

RAD-23 is a medium-sized multifunctional protein containing 400 amino acids with no enzymatic activity. It contains two UBA domains, one UBL domain, and one XPC domain (Chen et al., 2001). It is conserved from mammals to yeast (where it has been most extensively studied). In mammals, there are two genes that are homologous to the yeast and *C. elegans* RAD-23. These mammalian orthologs include hR23A and hR23B and are highly similar to one another. RAD-23 is able to bind to the ubiquitin chain on substrates through its ubiquitin-associated domains (UBA) (Bertolaet et al., 2001; Wilkinson et al., 2001) and to the proteasome through its ubiquitin-like element domain (UBL) (Schauber et al., 1998). Therefore, RAD-23 is part of a larger class of putative

ubiquitin-proteasome adaptors in ubiquitin (Ub)-mediated proteolysis. Other proteins in this class include DSK2, DDI1, and UBIQUILIN. RAD-23 is also sometimes considered a scaffolding protein due to the large number of protein-protein interactions capable of each of its domains. RAD23's function in the delivery of ubiquitinated substrates to the proteasome make it an essential component of ERAD, although RAD-23 has also been shown to interact with the protein glycanase, PNG-1, which deglycosylates substrates to help allow for their ultimate degradation (Kim et al., 2006; Habibi-Badabi et al., 2010). Unlike its substrates, it is also accepted that RAD-23 is a very stable protein that is not degraded by the canonical proteasomal pathway because it lacks any effective initiation region (Fishbain et al., 2011) and because its C-terminal UBA domain acts as *cis*-acting stabilization signal (Heinen et al., 2011).

Mice that are null for either hR23A or hR23B are viable, although the double knock-out mouse is embryonic lethal (Ng et al., 2003). As mentioned, RAD-23 has been previously shown to have an important role in protein turnover, although this role has been recently found to be more complex than initially anticipated. In some studies, loss of RAD-23 has been found to inhibit the turnover of a subset of proteins, such as glycoproteins (Chen et al., 2001). Meanwhile, other studies have found that RAD-23 might act to stabilize other substrates, namely p53 (Brignone et al., 2003) and XPC-1 (also known as RAD-4) (Ortolan et al., 2004). For example, hR23A and hR23B physically interact with XPC-1 and this interaction allows for stabilization of XPC-1 following the detection of DNA damage (Ortolan et al., 2004). Initial studies into the function of RAD-23 in yeast suggested that RAD-23 inhibited the formation of Lys48-linked polyubiquitin chains and this inhibition was counteracted by the ubiquitin chain-elongation factor, UFD-2 (Ortolan, et al., 2000; Chen, et al., 2001; Raasi, et al., 2003;

Varadan, et al., 2005). Furthermore, studies suggest that RAD-23 binding to the ubiquitin chain acts to protect the ubiquitinated substrate from ubiquitin chain elongation and deubiquitination (Raasi et al., 2003). However, studies in yeast also suggested that RAD-23 could promote the binding of ubiquitylated substrates to the proteasome (Chen et al., 2002). This controversy in the literature is still unresolved, although it suggests that RAD-23 may be both a facilitator and inhibitor of proteasomal degradation. This property of RAD-23 may provide efficient and selective proteasomal degradation within the proteome of the cell (Dantuma et al., 2009). Regardless, it is clear that RAD-23 has opposing effects on different client substrates and there must be some logic or evolutionary advantage as to why some clients of RAD-23 are degraded and others are given stability.

Unlike many other ubiquitin receptors, RAD-23 also has a separate function in nucleotide excision repair (NER). DNA damage is repaired by two separate pathways within NER: 1) global genomic NER (GGR) and (2) transcription-coupled NER (TC-NER) (Zhang et al., 2009; Le May et al., 2010). Both GGR and TC-NER are similar, although TC-NER refers to an incidence where DNA damage is not recognized until the stalling of RNA polymerase II at the site of a lesion during transcription (Marteijn et al., 2014). NER is a process by which lesioned DNA is excised by a complex and removed so that it can be repaired, allowing cells to cope with damage of their genomic content caused by intrinsic and extrinsic factors. The distinguishing feature of NER is that it senses structural distortions in the double helix, rather than specific base modifications like other forms of DNA repair (Dip et al., 2004). For example, one extrinsic factor that NER protects against is damage caused by ultraviolet (UV) light which can inflict helix-distorting DNA lesions in the genome (Madabhushi et al., 2014).

NER can be broadly separated into a series of steps: 1) lesion recognition; 2) unwinding of the DNA, 3) dual incision and excision of stretches of the damaged DNA; and 4) repair synthesis of the removed strand by DNA polymerase and ligation. RAD-23's role in NER is reliant upon its binding partner, XPC-1 (also known as RAD-4) where both proteins are responsible for the recognition of photolesions of DNA. XPC-1 and RAD-23 together bind damaged DNA and induces bending of the double helix so incision can take place and the lesioned DNA can be subsequently removed (Marteiijn et al., 2014).

Given the progress made in this work in establishing a link between RAD-23 and ALS, this work also highlights a sometimes overlooked, but intimate, link between the ubiquitin/proteasome system (UPS) and DNA repair. It also establishes a never before identified and novel role for RAD-23 in the stabilization of disease-causing mutant proteins.

## **STATEMENT OF MOTIVATION AND HYPOTHESES**

This thesis focuses on two separate processes affecting motor neurons: development and degeneration. In Chapter 2, we aim to identify how GluA1 and SAP97 translate synaptic activity of GluA1-containing AMPA receptors into dendrite growth. Up until now, the mechanisms by which plasticity governed in non-NMDA receptor settings is grossly under studied. Furthermore, by understanding the molecular components that promote dendrite growth, we might gain insight into how to manipulate them to promote regeneration following damage. We hypothesized that the small protein, CRIPT, interacts with SAP97 to promote dendrite growth because of its C-terminal PDZ3-interacting motif and known interaction with the microtubules of the cytoskeleton.

In the Chapter 3, we aim to understand the involvement of ERAD components in genetic models of ALS. Given the state of the literature within regards to whether loss of components are beneficial or detrimental, we hoped to bring insight into this topic. We also hoped to identify new targets in the treatment of ALS. Given the documented increase of ER stress levels in ALS found in the literature and number of ERAD components found to be mutated in fALS, we hypothesized that there may be an overload of involvement by ERAD and UPR components in neurodegeneration. Therefore, we utilized a loss of function approach using mutated ERAD and UPR components to test that hypothesis. We successfully found that loss of several ERAD components could suppress toxicity of ALS-causing proteins and focused on the loss of one suppressor, RAD-23. We found that there are increased levels of RAD-23 in ALS and these levels inhibit the ubiquitination and clearance of misfolded proteins that cause ALS. Future work will be required to determine if these findings are ALS-specific or may apply to other neurodegenerative diseases associated with proteotoxicity.

## CHAPTER 2: IDENTIFYING THE DOWNSTREAM MACHINERY OF GLUA1 AND SAP97 IN DENDRITE DEVELOPMENT

### SUMMARY

The dendritic tree is a key determinant of how neuronal information is processed. In the motor system, the dendritic tree of spinal cord neurons undergoes dramatic remodeling in an activity-dependent manner during early postnatal life. This leads to the proper segmental spinal cord connectivity that subserves normal locomotor behavior. This mechanism for establishing dendrite architecture in mammalian motor neurons relies on AMPA receptors assembled with the GluA1 subunit and is independent of NMDA receptors. The dendrite growth promoting activity of GluA1-containing AMPA receptors depends on its intracellular binding partner, SAP97, and SAP97's PDZ3 domain. We show here that CRIPT is a *bona fide* SAP97 PDZ3-domain binding partner and is necessary for the dendritic growth of mammalian spinal cord neurons. We further show that CRIPT has a well conserved ortholog in the nematode, *Caenorhabditis elegans*, and two loss of function alleles of CRIPT result in decreased branching of the well-studied PVD neuron *in vivo*. Loss-of-function *cript* in *C. elegans* leads to a functional consequence rendering *cript* mutants touch defective. Finally, we show that the mechanism by which CRIPT promotes dendritic growth is independent of synapse destabilization. Understanding the mechanisms that drive dendritic growth might be useful for enhancing recovery following insult to the central nervous system.



## INTRODUCTION

Activity-dependent development occurs throughout the neuroaxis, including the spinal cord during early postnatal life (Inglis et al., 2002; Haas et al., 2006; Ni and Martin-Caraballo, 2010). During early postnatal life, motor neurons express a very high level of GluA1 and this coincides with the period of extensive dendrite growth and remodeling (Jakowec et al., 1995; Jeong et al., 2006). These alterations in dendritic architecture are confined to a critical period and occur independent of NMDA (N-methyl-D-aspartic acid) receptors (Jakowec et al., 1995; Inglis et al., 2002; Jeong et al., 2006).

Activity-dependent growth of the dendritic tree in spinal cord neurons is driven by the GluA1 subunit of AMPA (2-amino-3-(3-hydroxy-5-methyl-isoxazol-4-yl)propanoic acid) receptors and its intracellular binding partner, synapse associated protein of 97 kDa (SAP97) (Zhang et al., 2008; Zhou et al., 2008). Animals lacking the GluA1 subunit or SAP97 in motor neurons have a stunted dendritic tree and suffer locomotor impairments that persist throughout life (Zhang et al., 2008; Zhou et al., 2008). All of the dendrite promoting actions of GluA1 are mediated by SAP97 (Zhou et al., 2008). Trafficking of SAP97 to the cell surface is dependent on the interaction of SAP97 with GluA1, but GluA1 is trafficked to the cell surface independently of GluA1's interaction with SAP97 (Zhang et al., 2006). SAP97 is a scaffolding protein with several protein-protein interacting modules, including SH3, L27, GUK, and 3 PDZ domains. Preliminary studies indicate that the PDZ3 domain of SAP97 is responsible for promoting dendritic growth (unpublished observations; Jablonski and Kalb, 2013).

To understand the molecular mechanism by which GluA1 and SAP97 promote activity-dependent dendrite growth, we asked: 1) what proteins bind to the PDZ3 domain

of SAP97? and 2) are such proteins able to modify the architecture of the dendritic tree?

Here we focus on cysteine-rich-interactor-of-PDZ-three (CRIPT), a 12 kDa protein that localizes to excitatory synapses and links proteins such as postsynaptic-density protein of molecular weight 95 kDa (PSD95) to microtubules (Niethammer et al., 1998; Passafaro et al., 1999). Given CRIPT's described interaction to PSD95's PDZ3 domain and its localization pattern, we investigated a potential role for CRIPT in GluA1 and SAP97-dependent dendrite growth.

## **MATERIALS AND METHODS**

### **Antibodies**

The following antibodies were used: immunoprecipitation of SAP97 (1:50; Thermo Pierce); immunoblotting and immunoprecipitation of CRIPT (1:500; Protein Tech Group); immunoprecipitation and immunoblotting of HA-tag (1:50 for IP and 1:1000 for IB; Convance); immunoblotting of SAP97 (1:1000; NeuroMab); immunoprecipitation and immunoblotting of the myc-tag (1:50 for IP and 1:1000 for IB; Cell Signaling); immunostaining of GFP (1:250; Sigma); immunostaining secondary antibody against GFP (1:500; Alexa Fluor 594). The following primary antibodies were used in quantitative inhibitory synapse studies: pre-synaptic marker GAD 65/67 (Rabbit anti-glutamate decarboxylase 65 & 67, Millipore # AB1511), and postsynaptic marker Alpha1 GABA-A receptor (Rabbit anti-Alpha1 GABA-A receptor, Clone N95/35 antibody NeuroMab #75-136). Secondary antibodies were Alexa Fluor 633 Goat Anti-Mouse IgG (H+L) (Invitrogen # A-21050) and Alexa Fluor 568 Goat Anti-Rabbit IgG (H+L) Antibody (Invitrogen # A-11011). GFP green fluorescence was sufficiently strong that enhancement with additional anti-GFP staining was unnecessary.

### **Mixed spinal cultures**

Mixed spinal cord neuron cultures were prepared as previously described (Jeong et al., 2006). They were maintained in glia-conditioned medium supplemented with trophic factors (Alomone Labs at 1.0ng/mL): human neurotrophin-3, human neurotrophin-4, human brain-derived neurotrophic factor, human cardiotrophin-1, human glial-derived neurotrophic factor, and rat ciliary neurotrophic factor. One half of the medium was replaced three times per week.

## **Heterologous cells and transfection**

HEK293 cells were maintained in Dulbecco's Modified Eagle's medium (DMEM) (Invitrogen) supplemented with 10% fetal bovine serum (FBS), 1% penicillin, and 1% streptomycin. Cells were transfected (Lipofectamine 2000; Invitrogen) per manufacturer's protocol when they were ~75% confluent and maintained in DMEM with 10% FBS until lysed 48 hours post transfection.

## **Immunoprecipitation experiments**

For immunoprecipitation experiments, lysates were made in 1% NP-40 lysis buffer (25mM Tris-HCl pH 7.4, 150mM NaCl, 1mM EDTA, 1% NP-40, 5% glycerol; 150 $\mu$ L per 60mm dish) supplemented with fresh protease inhibitor cocktail (Sigma). After 2 washes in ice-cold 1X phosphate-buffered saline (PBS), cells were lysed in lysis buffer, sonicated (20% strength, 10 seconds), and centrifuged at 14,000 rpm for 10 minutes (4°C) to remove cellular debris. 5% of the lysate was saved for input, and the remaining lysate was used for immunoprecipitation. For immunoprecipitation, DynaBeads Protein G (Invitrogen) were pre-cleared in PBS/1% Tween and were bound to the antibodies (4  $\mu$ g of antibody) (30' at room temperature (RT)). Lysate was then added, incubated for 1 hour at RT, and the lysate and bead mixture was washed in lysis buffer. Proteins were then boiled in 1% BME and SDS loading buffer. Proteins were immunoblotted following standard western blotting technique using 4-12% Bis-Tris gels (Invitrogen).

## **Surface plasmon resonance preparation**

The PDZ3 domain of SAP97 was amplified by PCR and the PCR product was ligated into the pGEX vector (GE) and transformed into BL21 strain. GST-fused PDZ3

was then extracted and purified from isopropyl  $\beta$ -D-1-thiogalactopyranoside (IPTG)-induced *E. coli* cultures with glutathione sepharose 4B matrix (GE) and eluted with 10 mM glutathione. Purified GST-PDZ3 fusion protein was further dialyzed to eliminate glutathione before plasmon resonance studies.

### **Surface Plasmon Resonance (SPR) Measurements and Affinity Analysis of Sensorgrams.**

Association and dissociations reactions of peptides CHRK1 (C-terminal amino acids of CRIPT) or CHRK2 (C-terminal amino acids of CRIPT V101A) (as analytes) and recombinant GST fusion protein GST-PDZ3 and GST (as ligands) were performed using a Biacore3000 instrument. Anti-GST antibody was immobilized on flow cell 3 and 4 according to the manufacturer's instructions. GST and GST-PDZ3 were then captured on flow cell 3 and flow cell 4 separately, where GST served for on-line reference subtraction. Both the analytes and the ligands were dissolved in the HBS running buffer (0.01M Hepes, 0.15M NaCl, 3mM EDTA, 0.005% v/v Surfactant P20) and their concentrations were determined at UV280nm using extinction coefficients calculated from the amino acid composition. The ligands were bound as densities between 1200RU and 1700RU. The analytes of CHRK1 and CHRK2 in 45uL volume each with various concentrations (62.5nM, 250nM, 4 $\mu$ M, 8 $\mu$ M, 10.24 $\mu$ M and 12.8 $\mu$ M) were injected over both GST and GST-PDZ3 surfaces at flow rate of 30 $\mu$ L/min. Dissociation time was monitored for 3min. A 40 second pulse of glycine-HCl pH2.2 was applied to regenerate the GST surface. For GST-PDZ3 surface regeneration, an additional 40 s pulse of glycine-HCl was applied. Analysis of steady-state affinity was performed using BIAevaluation software selecting reference-subtracted curves with a 1:1 interaction model. Affinity constant  $K_d$  was derived from Req vs. C (response unit at equilibrium vs.

peptide concentration) plot with the steady-state affinity model fit. Data for GST capture was subtracted from GST-PDZ3 values.

### **Neuronal transfection and neuron tracings**

At 5 days *in vitro* (DIV), mixed spinal cultures were transfected (Lipofectamine 2000; Invitrogen) with the overexpression plasmid or microRNA (miRNA) being tested in a 3:1 ratio with GFP to ensure all GFP-positive cells also expressed the desired construct. 5 days after transfection, cells were fixed in 4% paraformaldehyde (PFA) and immunostained with rabbit anti GFP antibody and secondary antibody. After immunostaining, the coverslip with the cells was mounted on the slide and viewed using fluorescent microscopy. Neuronal tracings were performed with the NeuroLucida program (MicroBrightField) and analyzed with the Neuroexplorer program (MicroBrightField). As previously described (Zhang et al., 2008), the minimum inclusion criteria for this study were: dendrites radially distributed ( $>180^\circ$ ) and no more than one primary dendrite is truncated (less than three times the cell body diameter). Quantitative descriptors of the dendrites were as follows: “1° dendrites,” the number of primary dendrites leaving the cell body, “branches, #”, the number of dendritic bifurcations, “length,” the sum of the lengths of all dendritic shafts from a single neuron divided by the number of primary dendrites, and “longest dendrite,” the length of the longest dendrite from the cell body to the most distal tip.

### **miRNA RNAi design**

miRNA was transfected (Lipofectamine 2000; Invitrogen) to knock down the expression of CRIPT in mixed spinal cultures. MiRNA was constructed by annealing two oligomers together of 21 base pairs homologous to the CRIPT sequence and adding

BspE1 and FseI restriction sites to the 5' and 3' ends respectively. Annealed oligomers were subsequently cloned into the p1006+ HSV vector using the BspEI and FseI restriction sites. MiRNA was designed against the rat CRIPT sequence corresponding to the ORF: 5'- CTCCACTTGCGAGAATTT-3'. We generated an RNAi-resistant CRIPT cDNA containing three silent mutations in the miRNA target sequence of CRIPT by using the QuikChange Site-Directed Mutagenesis Kit (Agilent). The miRNA target sequence was mutated to: 5'-CTCIACCTGTIAGAATTT-3'. Mutated nucleotides are underlined.

### **Membrane protein preparations**

Cells were washed twice using ice-cold PBS and suspended in hypotonic lysis buffer (10 mM KCl, 1.5 mM MgCl<sub>2</sub>, and 10 mM Tris-Cl, pH 7.4; 1.5 mL/60 mm plate). After incubation on ice for 10 minutes, cell lysis was finalized using a homogenizer (Dounce). The cell lysate was centrifuged at 2000 × g for 2 min to remove nuclei and cellular debris and the supernatant was centrifuged a second time at 100,000 × g for 30 min at 4°C to pellet cell membranes. The supernatant was saved as the 'cytoplasmic' fraction and the pellet ('membrane' fraction) was resuspended in RIPA buffer (50mM Tris-HCl pH 7.5, 150mM NaCl, 1mM EDTA, 1mM EGTA, 1% NP-40, 1% sodium deoxycholate) supplemented fresh with protease inhibitor cocktail (Sigma). Lysates were boiled for 5 minutes in 1% BME and loading buffer prior to standard western blotting technique using 4-12% Bis-Tris gels (Invitrogen).

### **Yeast-two-hybrid**

The flanked PDZ3 domain of SAP97 was amplified by PCR and cloned into the yeast bait phagemid pBD-GAL4. Full-length CRIPT was engineered into the yeast prey phagemid pAD-UAS. YRG-2 yeast were transformed (Clontech) according to the

manufacturer's instructions with phagemids or appropriate empty vector controls and grown under restrictive conditions (SD media lacking leucine, tryptophan, and/or histidine) and single colonies were subsequently streaked onto restrictive plates. The plasmid, pGBT9, was used as a positive control.

### **Quantitative analysis of excitatory and inhibitory synapses by imaging**

Cultures were prepared as described above, fixed at DIV21 with 4% PFA in 5% sucrose for 15 minutes, blocked with 5% FBS in minimal essential media (MEM), and primary antibodies for pre- and postsynaptic markers were applied together in 5% FBS in MEM overnight at 4°C. The next day, after washing 3 times in PBS, secondary antibodies were separately applied in PBS (one hour for each, then washed with PBS) at RT. Cover slips were dried and placed on slides with Fluorogel (Electron Microscopy Sciences). In the same experiment, 3-4 cover slips were stained for inhibitory synapses and the same numbers of cover slips were stained for excitatory synapses.

The methods for quantitative synaptic analysis have been described (Hughes et al., 2010a; Hughes et al., 2010b). Briefly, imaging data was collected from 20-30 randomly selected neurons (from 3-5 independent experiments) using an Olympus confocal microscope and all images were acquired at the same non-saturating laser power settings, photomultiplier voltage, gain and offset. Fluorescence was captured serially with an oil immersion 60X (1.4 numerical aperture) objective using lasers for green (488 Multi-line Argon Laser), red (559 Diode Laser) and far red (635 Diode Laser). The number and area of individual clusters were determined using interactive software (MetaMorph, Molecular Devices, Downingtown, PA; or custom-written ImageJ macros). Clusters with pixel overlap of pre- and postsynaptic markers were considered co-localized and thus synaptic (Krivosheya et al., 2008).



### **C. *elegans* maintenance**

All *C. elegans* strains were maintained using standard methodology (Brenner, 1974). Animals were maintained at 20°C on nematode growth medium (NGM) agar plates with live OP50 bacteria. Two strains used in this study containing deletions within the *C. elegans* ortholog of CRIPT, *tm427* and *tm430*, were received from National Bioresource Project in Japan and backcrossed three generations to ancestral N2 before being crossed into the  $P_{PVD}::GFP$  line (received from David M. Miller). We also utilized the *mec-4 (tu253)* and *mec-3* (CB1338) strains which were received from the Caenorhabditis Genetics Center (CGC). The *mec-4 (tu253)* strain was backcrossed 3 generations to ancestral N2 before being analyzed and crossed into the *tm430* strain.

### **C. *elegans* rescue cloning and lines**

Human CRIPT (hCRIPT) cDNA was amplified using PCR. Gateway cloning (Invitrogen) was employed and the BP reaction was used to construct the pDonR221-hCRIPT (pEntry hCRIPT) construct. The LR reaction was then performed using the following constructs for the 1<sup>st</sup>, 2<sup>nd</sup>, and 3<sup>rd</sup> positions respectively: *unc-119* promoter, pEntry hCRIPT, and the *unc-54* 3'UTR alongside the pCFJ150 destination plasmid for *C. elegans* expression. Sanger sequencing was used to confirm the correctness of the final construct,  $P_{unc-119}::hCRIPT::unc-54$  3'UTR ( $P_{neuron}::hCRIPT$ ) to drive expression of hCRIPT in the *C. elegans* nervous system when expressed. To create transgenic extrachromosomal arrays,  $P_{neuron}::hCRIPT$  was injected at a final concentration of 50ng/μL alongside a co-injection marker pCFJ150 ( $P_{myo-2}::mCherry$ ) at a final concentration of 5ng/μL which labeled the body wall muscle red. The final DNA concentration of the injection mix was 100ng/μL using a sonicated LacZ construct to

bring up the total DNA concentration. At least 3 independent transgenic lines were created for each and all were tested in corresponding assays.

### **C. *elegans* imaging**

All lines were synchronized before imaging to visualize the PVD neuron using GFP. Briefly, young adult hermaphrodites were allowed to lay eggs for 4-6 hours. At the L4 stage, worms were synchronized by the presence of the clear vulva. At the young adult stage (1 day post L4) worms were processed for imaging. Briefly, worms were immobilized using levamisole (10mM; Sigma) on fresh 4% agar pads and imaged using confocal microscopy. Z-stacks were taken and merged, and the compressed image was analyzed by counting the number of dendrites present on the PVD neuron dendritic tree (Smith, 2010; Smith, 2013) from the cell body to the posterior end of the animal. Analyst was blind to group during analysis.

### **Statistics**

Statistical analysis was performed using GraphPad Prism Version 6.00 for Windows, GraphPad Software, La Jolla, CA, USA ([www.graphpad.com](http://www.graphpad.com)). Unpaired t-test was used for all two-group comparisons. For data containing more than three groups, a one-way ANOVA with Dunnett's multiple comparisons test was used. For survival analysis, a log-rank (Mantel-Cox) test was used. The threshold for significance was always set to  $p < 0.05$ . For data concerning dendritic drawings, a Shapiro-Wilk test was run to test normality of the data. If the data were normally distributed, the data were analyzed with one-way ANOVA. Post-hoc analysis was performed with Tukey test. If the data did not distribute normally, a non-parametric Kruskal-Wallis test was used to

analyze data. Post-hoc analysis was performed with Dunn's test. The threshold for significance was set at  $p < 0.05$  for all tests.

## RESULTS

### CRIPT interacts with SAP97's PDZ3 domain

Preliminary studies to be discussed elsewhere identified the PDZ3 domain of SAP97 as important for the pro-dendrite-growth activity of SAP97. Since CRIPT binds to the PDZ3 domain of PSD-95 (Niethammer et al., 1998), a close relative of SAP97, we tested CRIPT binding to the PDZ3 domain of SAP97. Three sets of experiments were performed in a heterologous expression system (HEK293 cells). First, we established that full-length (FL) CRIPT and FL SAP97 co-immunoprecipitate together when the proteins are overexpressed in HEK293 cells (Figure 1A). To ask if the PDZ3 domain of SAP97 mediated this interaction, we attempted to co-immunoprecipitate CRIPT with versions of FL SAP97 containing ligand-binding-disabling mutations in the PDZ2 or PDZ3 domain. We found that mutations in PDZ3 (H469A, R470A), but not in PDZ2 (K323A, K326A), disrupted binding of CRIPT to SAP97 in the co-immunoprecipitation experiment (Figure 1B). Next, we attempted to co-immunoprecipitate FL SAP97 with WT FL CRIPT or a point-mutant FL version (CRIPT V101A) of the PDZ3-binding motif of CRIPT (-QTSV), previously shown to be incompetent in binding PSD-95 (Passafaro et al., 1999). We found that the CRIPT V101A mutation completely abolished CRIPT's binding to SAP97 (Figure 1C). Taken together, these data suggest that CRIPT requires a functional PDZ3 domain to interact with SAP97 and this interaction relies on CRIPT's canonical PDZ-interaction motif on its C-terminus.

We complemented these observations with two further approaches. First, in a yeast-two-hybrid (Y2H) assay, we found that full-length CRIPT interacts with the flanked PDZ3 domain of SAP97. FL CRIPT neither interacted with an empty bait vector, nor did the SAP97 PDZ3 domain interact with an empty prey vector (Figure 1D). Finally,

surface plasmon resonance (SPR) studies (SPR) demonstrated that a peptide corresponding to the C-terminal 18 amino acids of CRIPT bound to the PDZ3 domain of SAP97 with a  $K_d$  of 6.57 $\mu$ M, while a mutant version of this peptide containing the V101A mutation did not bind the PDZ3 domain of SAP97 (Figure 1E).

One limitation of the experiments thus far is that they were only indicative of an interaction in overexpression and non-physiological settings. Furthermore, an interaction may be detected in non-neuronal settings, but we were primarily interested in if the proteins interacted within the nervous system. Therefore, we attempted to co-immunoprecipitate SAP97 and CRIPT from mixed spinal cord cultures to determine if there is an endogenous interaction. We were successful in co-immunoprecipitating CRIPT and SAP97 in this experiment using endogenous proteins from mixed spinal cord cultures (Figure 1G).

To ask if CRIPT was expressed during the first two weeks of postnatal life in the mouse, when activity-dependent remodeling of the dendrite tree occurs in spinal cord neurons, we looked for expression of the proposed “GluA1/SAP97/CRIPT” complex in the spinal cord, cortex, and hippocampus of young mice. We found that CRIPT, SAP97, and GluA1 were expressed in the spinal cord prepared from mouse at P7 (Figure 1E). In sum, these studies show that native CRIPT is a *bona fide* binding partner of the PDZ3 domain of SAP97 and merits further investigation as a candidate molecule that acts to promote dendrite growth.

### **CRIPT is necessary for proper dendrite growth**

To determine if CRIPT can influence dendrite growth, we knocked down CRIPT in spinal cord neurons *in vitro* and quantitatively analyzed dendritic architecture. We

were able to decrease the abundance of CRIPT protein in spinal cord neurons by infecting mixed spinal cord cultures with a recombinant herpes simplex virus to express the CRIPT miRNA in neurons (Figure 2A). We next compared the dendritic tree of three experimental groups: 1) GFP alone, 2) GFP + scrambled miRNA and 3) GFP + CRIPT miRNA. We made camera lucida drawings of the dendritic tree and assessed the effect of CRIPT knockdown by comparing the dendrite parameters among the groups of neurons. Parameters tested included: the soma size; the number of primary dendrites; the number of branches; the total length of the dendritic tree, the average dendrite length; and the length of the longest dendrite. The scrambled miRNA had no effect on any of these parameters compared to the GFP control. Meanwhile, we found that miRNA knockdown of CRIPT led to a ~30% reduction in the total number of dendrite compared to GFP alone ( $p < 0.05$ ) or scrambled miRNA ( $p < 0.01$ ) treated neurons (Figure 2B). In addition, we found that knockdown of CRIPT also led to a ~20% decrease in the total size of the dendritic tree compared to GFP alone ( $p < 0.0001$ ) or the scrambled miRNA ( $p < 0.05$ ). To confirm the effect of CRIPT knockdown was in fact due to the reduced levels of CRIPT, we created an RNAi-resistant CRIPT cDNA (CRIPT<sup>res</sup>) by introducing silent mutations in the target sequence of the miRNA on CRIPT. By Western blot, we confirmed that CRIPT<sup>res</sup> was resistant to knockdown by the CRIPT miRNA, compared to the wild type version of CRIPT (CRIPT<sup>wt</sup>) in HEK293 cells (Figure 2C). We next transfected spinal cord neurons with either the scrambled miRNA, the CRIPT miRNA, or the CRIPT miRNA with the CRIPT<sup>res</sup> construct and again quantified the same dendritic parameters. We again found that knockdown of CRIPT reduced the total number of branches ( $p < 0.05$ ), as well as the total size ( $p < 0.001$ ), of the dendritic tree compared to the scrambled miRNA (Figure 2D). Meanwhile, the dendritic tree of neurons co-transfected with the CRIPT<sup>res</sup> construct showed no difference in any of the dendritic

parameters tested compared to the scrambled miRNA, but did have a greater number of branches ( $p < 0.001$ ) and overall tree size ( $p < 0.05$ ) compared to the CRIPT miRNA group alone. In sum, these data suggest that CRIPT is necessary for the proper growth of the dendritic tree.

### **CRIPT is not sufficient to induce growth of the dendritic tree**

We next asked if increasing CRIPT expression influenced dendrite architecture. To study this, we overexpressed two different versions of CRIPT in spinal cord neurons: wild type (WT) CRIPT or a version that is palmitoylated at the N-terminus of CRIPT to allow CRIPT to traffic to the cell surface. This palmitoylated version of CRIPT (pal-CRIPT) allowed us to surpass a possible limited number of SAP97 PDZ3 binding sites at the cell surface where CRIPT may be needed to influence dendritic architecture. Furthermore, studies to be described elsewhere found that SAP97's localization to the cell surface, but not SAP97's interaction with GluA1, is required for overexpression of SAP97 to increase dendrite growth. Subcellular fractionation followed by Western blot confirmed that palmitoylated CRIPT prefers membranes, whereas CRIPT without the palmitoylation sequence does not (Figure 3A) Spinal cord neurons were transfected with GFP, WT CRIPT, or pal-CRIPT and the same parameters of the dendritic tree were studied as described above. We found that there was no difference in dendritic architecture of control neurons versus neurons overexpressing WT or pal-CRIPT. Taken together, these overexpression studies indicate that CRIPT is not sufficient to enhance dendrite growth on its own, even when CRIPT is shuttled to membranes (Figure 3B).

### **CRIPT functions downstream of SAP97 in promoting dendrite growth**

Extensive work has previously shown that SAP97 promotes dendritic growth of motor neurons *in vitro* and *in vivo* (Zhang et al., 2008; Zhou et al., 2008). We show here that CRIPT binds to SAP97 *in vitro* and *in vivo* and also promotes dendritic growth of spinal cord neurons. Therefore, we determined if CRIPT was downstream of the promotion of dendritic growth of spinal cord neurons by SAP97. To do this, spinal cord neurons were transfected with GFP or SAP97 in the presence of the scrambled or CRIPT miRNA. In the presence of the scrambled miRNA, overexpression of SAP97 led to a ~30% increase in the total length and branch number of the dendritic tree compared to transfection with GFP alone ( $p < 0.05$ ). This promotion of dendritic growth by overexpression of SAP97 was entirely blocked when CRIPT was knocked down in neurons (Figure 4).

#### **Knockdown of CRIPT causes a homeostatic increase in synapse number**

CRIPT was previously shown to be enriched at the sites of excitatory synapses and to allow for proper clustering of proteins in the postsynaptic density (Niethammer et al., 2008; Passafaro et al., 2009). Therefore, we asked if knockdown of CRIPT caused any change in the amount of excitatory or inhibitory synapses. We quantified synapses using validated imaging analysis approaches (Krivosheya et al., 2008; Hughes et al., 2010a; Hughes et al., 2010b). Neurons were transfected with either a scrambled miRNA or CRIPT miRNA, as well as the GFP reporter, and subsequently stained for excitatory synapses (using antibodies to synaptophysin and PSD-95) or inhibitory synapses (using antibodies to GAD 65/67 and the Alpha1 GABA-A receptor). Co-localized pre- and postsynaptic puncta with pixel overlap were considered to be synapses. We found that knockdown of CRIPT resulted in a significant ( $p < 0.05$ ) 3-fold increase in the number of excitatory (Figure 5A) and inhibitory synapses (5C). Meanwhile, there was no change in



the size of synapses among groups (Figures 5B, 5D). This suggests that the neuron may compensate for the decreased dendritic arbor to balance activity by increasing both excitatory and inhibitory input.

### **CRIPT's function in dendritic growth is not activity-dependent**

Much of postnatal development is driven by activity-dependent events. Because knockdown of CR IPT increased synapse number and was found here to promote SAP97-dependent dendritic growth, we wondered if this form of dendritic growth was activity-dependent. To test this, we chronically treated cultures for 72 hours with high K<sup>+</sup> to stimulate synaptic activity of neurons *in vitro* in the presence of the scrambled or CR IPT miRNA. We found that again knockdown of CR IPT caused a ~25% reduction ( $p < 0.05$ ) in dendrite branch number compared to a scrambled miRNA when cultures were only treated with vehicle. However, in the presence of high K<sup>+</sup>, the effect of CR IPT knockdown was blocked (Figure 6). This suggests that CR IPT's function in dendrite growth is in a pathway independent from synaptic activity.

### **CR IPT promotes dendritic growth in vivo**

To address whether or not CR IPT functions in dendritic growth *in vivo* as well, we utilized the small nematode, *Caenorhabditis elegans* (*C. elegans*). We used *C. elegans* with a transgene expressing GFP under the control of a promoter allowing for expression in the PVD mechanosensory neuron of the animal (Smith, 2010; Smith 2013). The *C. elegans* genome encodes a protein, C36B1.14, which retains 41% amino acid identity compared to the human CR IPT protein. We compared the branch number of wild type (N2 Bristol strain) animals to those with two different loss-of-function (LOF) alleles (*tm430* and *tm427*) of CR IPT. Both of these alleles contain large ~400bp deletions near

the C-terminal region of the protein, which would also contain CRIPT's PDZ-interaction motif. We found that both independent alleles caused a decrease in the branch number of secondary and tertiary dendrites of the PVD mechanosensory neuron (Figure 7A-7B). Along with the previously described *in vitro* data, this suggests that CRIPT also has an important role for dendritic growth and development *in vivo*. The *tm430* allele specifically caused a significant ~25% reduction in the branch number of secondary ( $p < 0.05$ ) and tertiary dendrites ( $p < 0.05$ ) (Figure 7C-7D).

To determine if the dendrite growth defect of the *cript* mutants was relevant to our mammalian studies, we overexpressed human CRIPT under the control of a nervous system specific promoter ( $P_{\text{neuron}}::\text{hCRIPT}$ ) in *cript (tm430)* mutants where the PVD neuron is labeled with GFP and quantified dendrite number. We found that overexpression of the human ortholog of CRIPT in the nervous system was sufficient to rescue the decrease in secondary and tertiary branches in the *cript (tm430)* mutants compared back to wild type. This was also sufficient to rescue the defect in two other independently generated lines (data not shown). This suggests that C36B1.14 is homologous to the mammalian CRIPT and was evolutionarily conserved to retain an important function in dendrite growth from the nematode to mammals.

### **Loss of *cript* causes a mechanosensory defect in vivo**

*C. elegans* utilize two neurons, MEC-4 and PVD, to respond to harsh touch. Therefore, the PVD neuron in *C. elegans* is responsible for response to harsh touch in *mec-4 (tu253)* mutants, rendering any response to harsh touch completely reliant on the PVD neuron (Liu et al., 2011). For example, it was previously shown that DMA-1 promotes dendritic growth of the PVD neuron and, therefore, in *dma-1; mec-4* double

mutants, there is a reduced response to harsh touch (Liu et al., 2011). However, the harsh touch response pathway is entirely reliant on the MEC-3 neuron and, therefore, *mec-3* mutants exhibit a touch defect on its own. We tested if the reduced dendritic arbors of the PVD neuron seen in *cript* mutants caused a mechanosensory deficit to the animal. We utilized the harsh touch response assay (Way and Chalfie, 1989) to ask if the reduced dendritic branching of the *cript* mutant caused a touch defect in *cript; mec-4* double mutants. In this assay, we compared the touch response of wild type animals as a negative control, *mec-3 (CB1338)* animals as a positive control, *cript (tm430)* single mutants, *mec-4 (tu253)* mutants, and finally the *cript (tm430); mec-4 (tu253)* double mutants. Using a one-way ANOVA amongst all of the groups ( $F_{(4,10)}=11.93$ ;  $p = 0.0008$ ), we confirmed that the *mec-3 (tu253)* mutants were ~40% defective to light touch ( $p < 0.05$ ), whereas less than 10% of wild type animals display a lack of response to light touch. Meanwhile, *cript; mec-4* double animals displayed a large and significant ( $p < 0.01$ ) defect to light touch in approximately ~50% of animals compared to wild type animals. This was not observed in *cript* or *mec-4* single mutants which only had a defect to touch in roughly 20% of animals and was not significant compared to wild type (Figure 8A). This suggests that the lack of dendrite branching observed in *cript* mutants has a functional and mechanical consequence.

To test if it was the PVD dendrite defect caused by the loss of *cript* responsible for the touch defect, we again overexpressed  $P_{\text{neuron}}::\text{hCRIPT}$  in the *cript (tm430); mec-4 (tu253)* animals. We found that overexpression of human CRIPT in the nervous system was sufficient to partially rescue the touch defect of the *cript (tm430); mec-4 (tu253)* animals. Approximately 50-60 percent of *cript (tm430); mec-4 (tu253)* animals showed a touch defect, and this was reduced to 20-30% when hCRIPT was overexpressed in the

nervous system ( $p < 0.01$ ). This effect was found in all 4 independently generated extrachromosomal array lines when non-transgenic animals were compared to their transgenic counterparts at the young adult stage (L4 + 1 day old) (Figure 8B).

## DISCUSSION

Using multiple techniques, we show that CRIPT is a *bona fide* binding partner of the pro-dendrite growth domain of SAP97, PDZ3. CRIPT has previously been shown to bridge microtubules to other proteins in the postsynaptic density, such as PSD-95 and SAP102 (Passafaro, et al., 1999). These observations point to the existence of a hetero-oligomeric protein complex at or near the postsynaptic density. The present work is the first to link CRIPT to a biological process. CRIPT is necessary, but not sufficient, for dendrite growth of spinal cord neurons. We furthermore are importantly able to rescue to the reduced dendritic branching and growth in knockdown of CRIPT using the RNAi-resistant CRIPT cDNA. This is noteworthy because many other MAGUK and postsynaptic density proteins have redundant roles (Elias, et al., 2007). We suggest that a multi-protein molecular “machine” – composed of GluA1, SAP-97, and CRIPT – work together to promote dendrite growth.

While overexpression of SAP-97 stimulates dendrite growth (Zhou et al, 2008), here we show that overexpression of CRIPT has no effect on the dendrite tree. These observations raise the possibility that the assembly of a multi-protein complex of correct stoichiometry is required for promotion of dendrite growth. In this formulation, CRIPT must associate with other SAP97 binding partners, presumably at the postsynaptic density, to effect changes in dendrites. An alternative possibility is that the PDZ3 domain of SAP97 is already saturated with endogenous CRIPT and thus exogenously provided CRIPT cannot localize to the postsynaptic density to stimulate dendrite growth. This seems less likely since forced localization of CRIPT to the plasma membrane, by addition of a palmitoylation sequence, did not confer dendrite growth promoting action. We are currently using a directed candidate gene approach with more than 25 known

SAP-97 binding partners to identify the missing factor(s) which SAP-97 utilizes in addition to CRIPT to promote dendrite growth.

It is likely that assembly of GluA1 and SAP97 uses CRIPT to promote dendritic growth via CRIPT's interaction with the cytoskeleton. Previously, blocking interactions to CRIPT's PDZ3 domain had no effect on the number of synapses or NMDA receptors (Passafaro et al., 1999). However, changes in the cytoskeleton have been previously shown to have large effects on the dendritic tree and overall plasticity of neuron architecture (Urbanska et al., 2012) and actin polymerization has been shown necessary for growth cone filopodia (Yamada et al., 2013).

Regardless of the mechanism of how CRIPT is able to promote dendritic growth, we here show that loss of CRIPT results in decreased dendritic growth both *in vitro* and *in vivo* in two well-used models. In addition, we show that defects of dendritic growth cause a mechanosensory deficit *in vivo* suggesting that proper dendritic growth during development is a critical step for proper motor movement in adulthood. This could be partially rescued by overexpressing the human ortholog of CRIPT in neurons alone. These data utilizing mammalian spinal neurons and the nematode further suggest that the mechanism of CRIPT action is conserved from the nematode to mammals. Our results suggest, however, that the mechanism by which CRIPT promotes dendritic growth is not via the hypothesized model of synapse stabilization. Instead, our data suggest the opposite. These data are in accordance with a number of model of homeostatic synaptic plasticity (Pozo and Godo, 2010). In this case, the neuron may be upregulating the number of synapses given the small dendritic tree to hold connections and incoming activity constant. This would suggest that synapse formation can also happen downstream of how dendritic architecture is set. This mechanism would allow

the neuron to offset the possibility of any excessive excitation or inhibition in the case of an increase in the dendritic tree.

Understanding how activity-dependent development of the dendritic tree is promoted may aid efforts to promote recovery following injury to the central nervous system. Repetitive activation of motor circuits has been shown to improve rehabilitation in patients following motor injury (Spooren, et al., 2008). This is consistent with our findings that activity promotes dendritic remodeling and this leads to the development of normal locomotor behavior (Inglis, et al., 2002; Zhang, et al., 2008; Zhou, et al., 2008).

## FIGURE LEGENDS

**Figure 2.1. CRIPT is *bona fide* PDZ3 and SAP97 interacting protein.** (A) Full-length (FL) myc-tagged SAP97 co-immunoprecipitates with FL HA-tagged CRIPT when they are overexpressed in HEK293 cells. Neither protein immunoprecipitates when a negative control IgG antibody is used in place of HA antibody. (B) Overexpressed HA-tagged CRIPT co-immunoprecipitates with SAP97 containing a mutation in the PDZ2 domain, (K323A, K326A), but mutation of the PDZ3 domain (H469A, R470A) disrupts this interaction. (C) Overexpression of myc-tagged full-length SAP97 and full-length WT CRIPT or full-length CRIPT V101A in HEK293 cells and immunoprecipitation of myc tag on SAP97. Mutating the PDZ3-interaction motif of CRIPT (CRIPT V101A) abolishes the interaction between SAP97 and CRIPT. (D) Full-length CRIPT interacts with the PDZ3 domain of SAP97 in a yeast-two-hybrid assay. (E) Surface plasmon resonance shows a specific, saturable interaction between the 18 C-terminal amino acids of CRIPT and the PDZ3 domain of SAP97 ( $K_d$  of 6.57 $\mu$ M), but no interaction when the CRIPT V101A mutation is present. (F) Endogenous CRIPT and endogenous SAP97 co-immunoprecipitate together in lysates prepared from mixed spinal cultures at DIV14. Western blot immunoblotting for endogenous SAP97 and CRIPT of input lysate and immunoprecipitations using a negative control IgG and CRIPT IgG. Blot was incubated with SAP97 and CRIPT antibody at the same time. (G) CRIPT, SAP97, and GluA1 are co-expressed in mouse spinal cord at P7 during the period dendritic remodeling occurs.

**Figure 2.2. CRIPT is necessary for the dendritic growth of spinal cord neurons.**

(A) Infection of HSV-CRIPT miRNA into mixed spinal cord culture is capable of knocking down CRIPT in neurons compared to a scrambled miRNA. (B) Knockdown of CRIPT results in a significant decrease in a decrease in the number of branches ( $p = 0.0018$ ; F



= 6.892) and total length ( $p = 0.0023$ ;  $F = 6.956$ ) of the dendritic tree according to a one-way ANOVA. \*Differs from +GFP group,  $p < 0.05$ ; †Differs from +scrambled miRNA group,  $p < 0.05$ . (C) Representative Western blot of knockdown using CRIPT miRNA. Wild type (WT) CRIPT (CRIPT<sup>WT</sup>) is knocked down by CRIPT miRNA compared to scrambled miRNA. RNAi-resistant CRIPT (CRIPT<sup>res</sup>) is not knocked down by CRIPT miRNA compared to scrambled miRNA (D) Co-transfection of RNAi-resistant CRIPT is sufficient to prevent decrease in the number of branches and total length of the dendritic tree by CRIPT miRNA. <sup>Δ</sup>Data shown as mean  $\pm$  SEM; \*Differs from +GFP group,  $p < 0.05$ ; †Differs from +CRIPT miRNA group,  $p < 0.05$ .

**Figure 2.3. CRIPT is not sufficient to promote dendritic growth of spinal cord neurons.** (A) pal-myc-CRIPT prefers the membrane fraction, but CRIPT without the palmitoylation sequence prefers the cytoplasmic fraction. (B) Overexpression of WT CRIPT or pal-myc CRIPT at the cell surface has no effect on the size or complexity of the dendritic tree.

**Figure 2.4. CRIPT functions downstream of SAP97 in promoting dendrite growth.** Knockdown of CRIPT prevents growth and branching caused by SAP97 overexpression in mixed spinal cord neurons. \*Differs from +GFP group,  $p < 0.05$ ; †Differs from +SAP97 + +scrambled miRNA group,  $p < 0.05$ .

**Figure 2.5. CRIPT knockdown increases the number of excitatory and inhibitory synapses, but does not change synapse size.** (A) Knockdown of CRIPT increases the number of excitatory synapses (\* $p < 0.05$ , Student's *t-test*). (B) Knockdown of CRIPT has no effect on the size of excitatory synapses. (C) CRIPT knockdown increases the number of inhibitory synapses (\*\*\*\* $p < 0.0001$ ; Student's *t-test*) compared to a

scrambled miRNA. (D) CRIPT knockdown has no effect on the size of inhibitory synapses. (n=20 per group).

**Figure 2.6. CRIPT's function in dendritic growth is independent from synaptic activity.** High K<sup>+</sup> is capable of promoting dendritic growth and branching in the presence of CRIPT miRNA. \*Differs from +scrambled miRNA group + vehicle,  $p < 0.05$ ; †Differs from +scrambled miRNA + high K<sup>+</sup> group,  $p < 0.05$ ; †Differs from CRIPT miRNA group,  $p < 0.05$ .

**Figure 2.7. Loss of *cript* (*tm430*) decreases dendrite branch number *in vivo*.** (A) Representative full body image of PVD neuron labeled with GFP in a N2 Bristol strain (wild type; “wt”) young adult (L4 stage + 1 day old). (B) Schematic of PVD neuron and its primary (1°), secondary (2°), and tertiary (3°) branches used for quantification. (C) Representative images of the PVD neuron labeled with GFP of indicated genotypes in the tail region used for quantification at the young adult stage (L4 stage + 1 day old). (D) Quantification of the number of primary (1°), secondary (2°), and tertiary (3°) branches in indicated strains (n ≥ 10 per genotype). Analyst was blinded to genotype during quantification. We found that *cript* (*tm430*) mutants have a significant decrease in secondary (\*\* $p < 0.01$ ; *post hoc* test following one-way ANOVA) ( $F_{(3,37)} = 6.781$ ;  $p = 0.0009$ ). and tertiary (\*\* $p < 0.01$ ; *post hoc* test following one-way ANOVA) ( $F_{(3,37)} = 6.365$ ;  $p = 0.0014$ ). branch number. This was completely rescued by overexpression of the human ortholog of CRIPT in the nervous system using the *unc-119* promoter ( $P_{\text{neuron}}$ ) which also increased the number of primary dendrites compared to N2 (WT) (\* $p < 0.05$ ; *post hoc* test following one-way ANOVA) ( $F_{(3,37)} = 3.569$ ;  $p = 0.0232$ ).

**Figure 2.8. Loss of *cript* results in a mechanosensory defect *in vivo* in young adults.** (A) WT (N2 Bristol strain), *cript (tm430)*, *mec-3* (CB1338), and *cript (tm430); mec-4 (tu253)* animals were scored for their response to harsh touch. Average of 3 independent experiments is shown. Experiments were all completed with analyst blinded to genotype. We found that *cript (tm430); mec-4 (tu253)* animals show a synthetic touch defect (\*\* $p < 0.01$  according to a *post hoc* test following a one-way ANOVA). We also confirmed that *mec-3* (CB1338) animals are touch defective compared to wild type (N2) (\*\* $p < 0.005$  according to a *post hoc* test following a one-way ANOVA) ( $F_{(4,10)} = 11.93$ ;  $p = 0.0008$ ). (B) Touch defect is suppressed in *cript (tm430); mec-4 (tu253)* animals by overexpression of the human ortholog of CRIPT in the nervous system using the unc-119 promoter ( $P_{\text{neuron}}$ ) in four independent extrachromosomal array lines (\*\* $p < 0.01$  according to a *post hoc* test following a one-way ANOVA when compared to non-transgenic counterparts). One strain (line 1) fully rescued the touch defect when compared to wild type (N2) in a *post hoc* test following a one-way ANOVA ( $F_{(8,18)} = 26.45$ ;  $p < 0.0001$ ).

Figure 2.1. CRIPT is *bona fide* PDZ3 and SAP97 interacting protein.

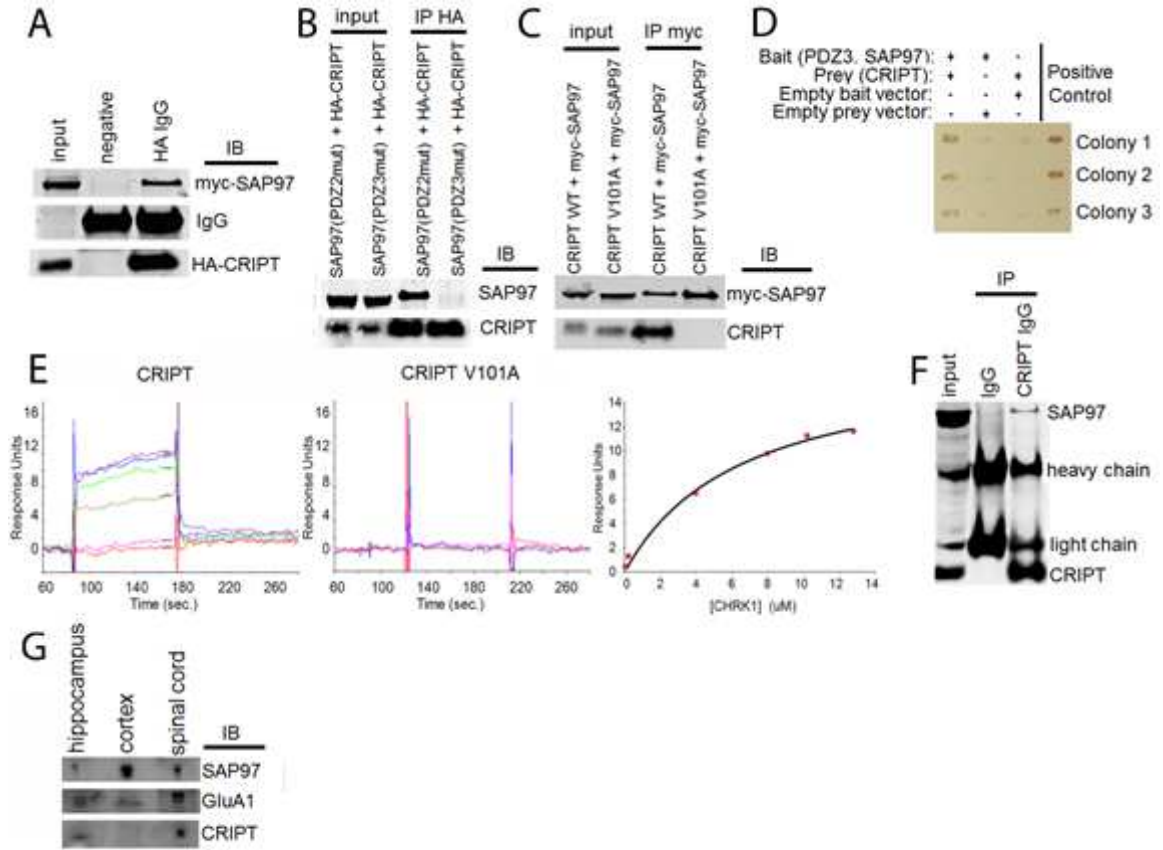


**Figure 2.2. CRIPT is necessary for the dendritic growth of spinal cord neurons.**

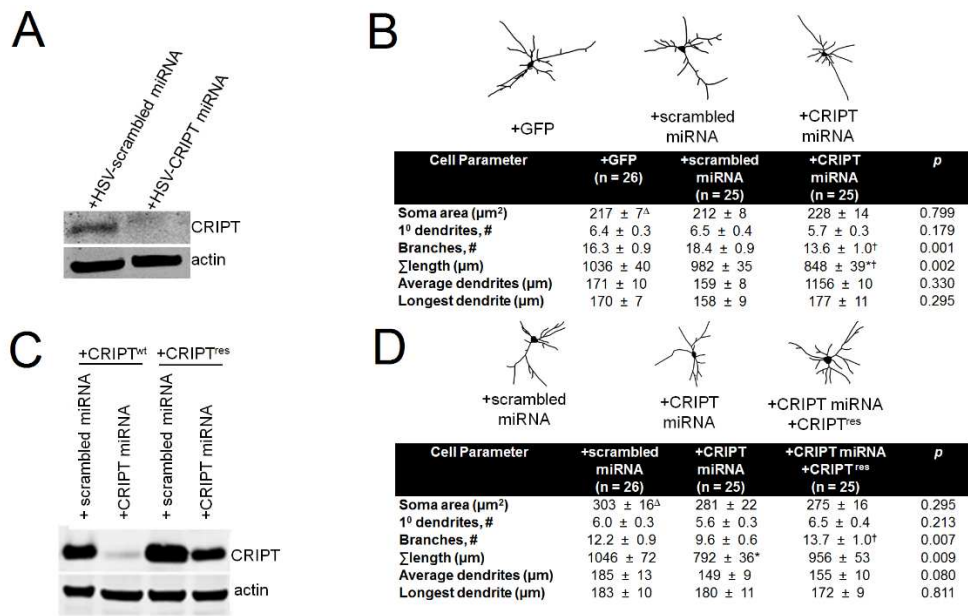


**Figure 2.3. CRIPT is not sufficient to promote dendritic growth of spinal cord neurons.**

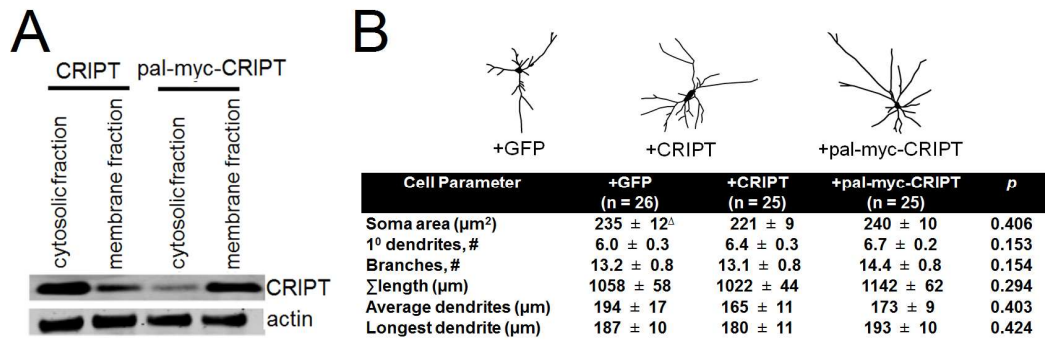
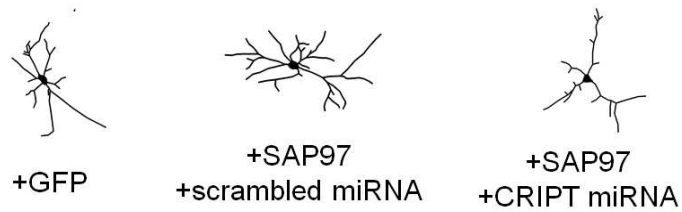


**Figure 2.4. CRIPT functions downstream of SAP97 in promoting dendrite growth.**



Cell Parameter	+GFP (n = 26)	+SAP97 +scrambled miRNA (n = 25)	+SAP97 +CRIPT miRNA (n = 25)	<i>p</i>
Soma area ( $\mu\text{m}^2$ )	278 $\pm$ 10 <sup>Δ</sup>	285 $\pm$ 17	257 $\pm$ 10	0.155
1 <sup>0</sup> dendrites, #	5.1 $\pm$ 0.3	5.0 $\pm$ 0.2	4.8 $\pm$ 0.2	0.530
Branches, #	10.0 $\pm$ 0.7	13.3 $\pm$ 1.1*	10.1 $\pm$ 0.6 <sup>†</sup>	0.016
$\Sigma$ length ( $\mu\text{m}$ )	1037 $\pm$ 47	1292 $\pm$ 87*	1009 $\pm$ 48 <sup>†</sup>	0.014
Average dendrites ( $\mu\text{m}$ )	217 $\pm$ 15	262 $\pm$ 18	219 $\pm$ 13	0.170
Longest dendrite ( $\mu\text{m}$ )	230 $\pm$ 11	251 $\pm$ 12	229 $\pm$ 11	0.310

Figure 2.5. CRIPT knockdown increases the number of excitatory and inhibitory synapses, but does not change synapse size.

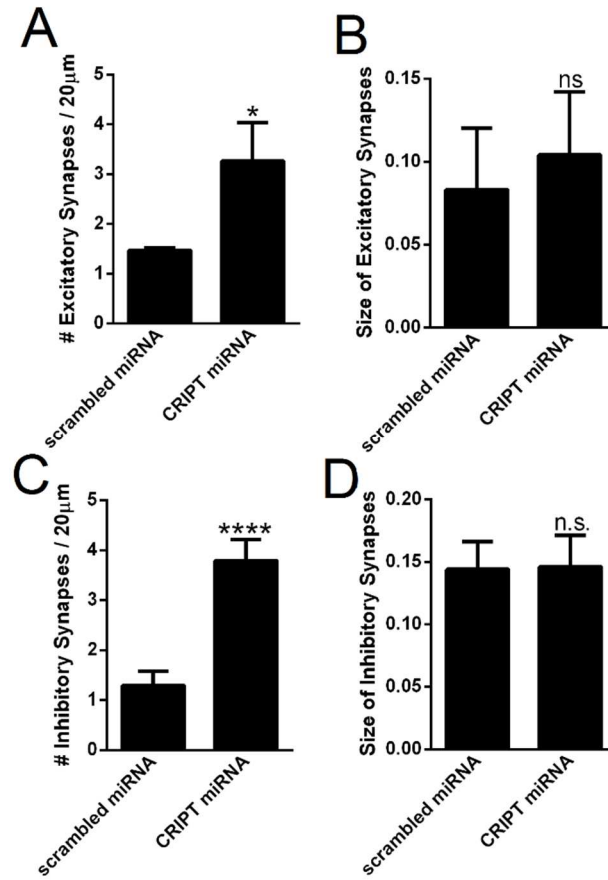




**Figure 2.6. CRIPT's function in dendritic growth is independent from synaptic activity.**

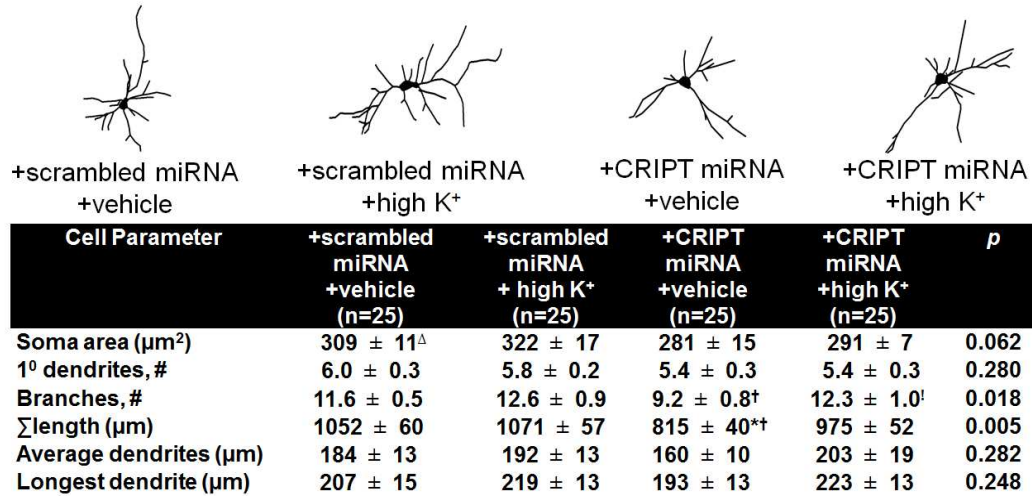
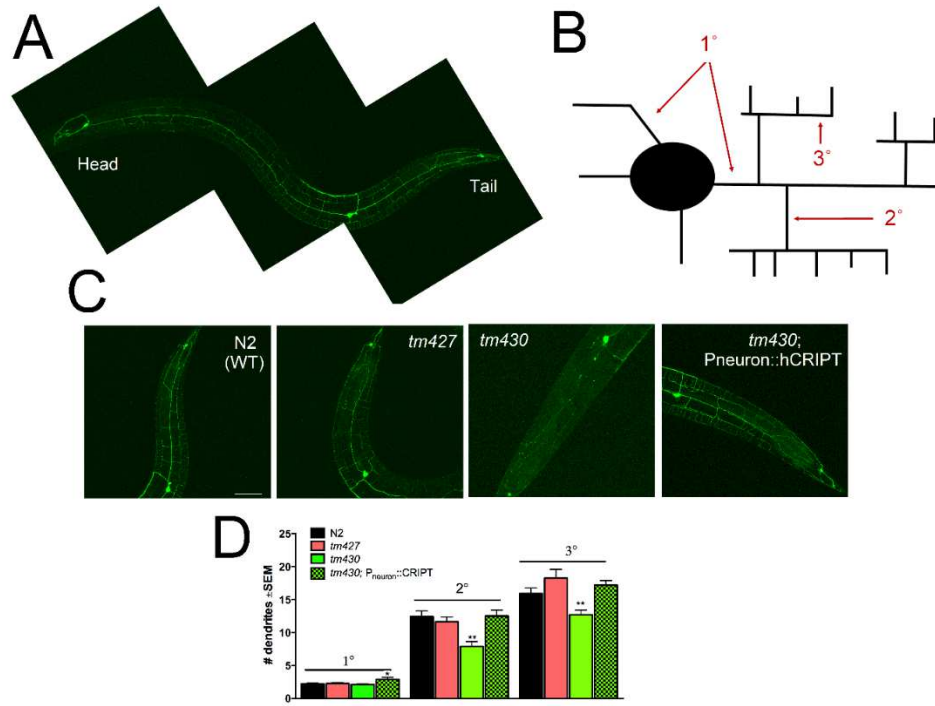
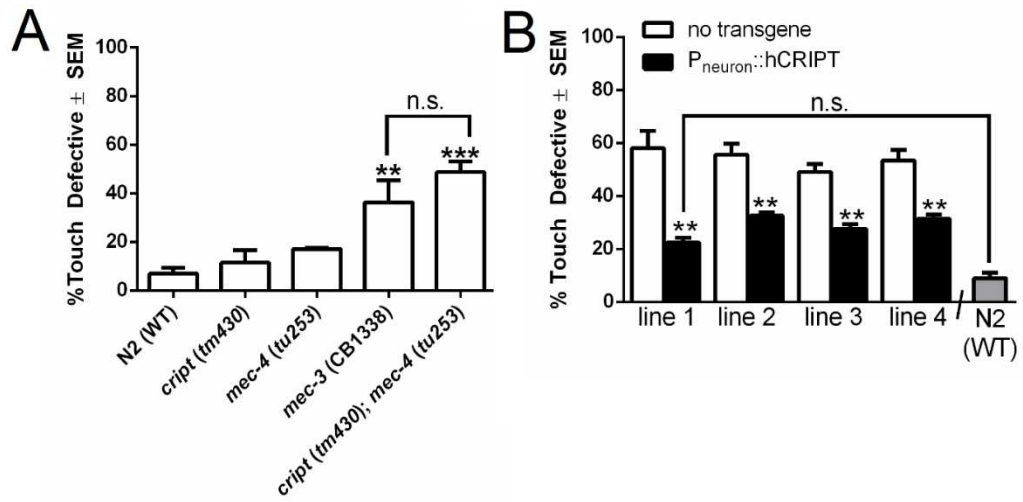


Figure 2.7. Loss of *cript* decrease dendrite branch number *in vivo*.



**Figure 2.8. Loss of *cript* results in a mechanosensory defect *in vivo* in young adults.**



## CHAPTER 3: LOSS OF RAD-23 PROTECTS AGAINST MODELS OF MOTOR NEURON DISEASE BY ENHANCING MUTANT PROTEIN DEGRADATION

### SUMMARY

Misfolded proteins accumulate and aggregate in neurodegenerative disease. The existence of these deposits reflects a derangement in the protein homeostasis machinery. Using a candidate gene screen, we report that loss of RAD-23 protects against the toxicity of proteins known to aggregate in ALS. Loss of RAD-23 suppresses the locomotor deficit of *C. elegans* engineered to express mutTDP-43 or mutSOD1 and also protects against aging and proteotoxic insults. Knockdown of RAD-23 is further neuroprotective against the toxicity of SOD1 and TDP-43 expression in mammalian neurons. Biochemical investigation indicates that RAD-23 modifies mutTDP-43 and mutSOD1 abundance, solubility, and turnover by altering the ubiquitination status of the substrate and accelerating its flux through the proteasome and autophagy pathways. In human ALS spinal cord, we find that RAD-23 abundance is increased and mislocalized within motor neurons. We propose a novel pathophysiological function for RAD-23 in the stabilization of disease proteins associated with neurodegeneration.

## INTRODUCTION

ALS (Amyotrophic Lateral Sclerosis) is a multifactorial, adult onset motor neuron disease that causes death of the upper and lower motor neurons leading to muscle denervation and eventual paralysis. Approximately ninety percent of cases of ALS are sporadic and the remaining cases are caused by single gene mutations (Rothstein, 2009). The pathophysiology of ALS has been linked to oxidative stress, excitotoxicity, impaired protein homeostasis, and defects in RNA biology (Ling et al., 2013).

The earliest events seen in the rodent ALS models include the accumulation of misfolded proteins, ER (endoplasmic reticulum) stress, and activation of the unfolded protein response (UPR) (Kikuchi et al., 2006; Saxena et al., 2009; Walker et al., 2013). Exacerbated ER stress has also been found in forms of sporadic ALS (Atkin et al., 2008). One way cells deal with ER stress, linked to the accumulation of misfolded proteins in the ER lumen, is by ERAD (ER-associated degradation). In this process, terminally misfolded ER lumen proteins are cleared from the ER through a multi-step process for degradation by the 26S proteasome (Vembar and Brodsky, 2008). Positive and negative regulators of this process are known to exist (Rumpf et al., 2006) and several components of the ERAD pathway have been identified as being mutated in forms of familial ALS (Johnson et al., 2010; Deng et al., 2011).

We hypothesized that components of ERAD might be modifiers of ALS. To test this, we undertook a candidate gene forward genetics approach (Table 1) to determine the effect of loss-of-function (LOF) alleles (mutants) of ERAD components in *C. elegans* models of ALS, modeled by expression of mutant (M337V) TDP-43 (mutTDP-43) in the nervous system. These animals show a strong locomotor deficit (Liachko et al., 2010).

Among the modifiers (Figure 2B), we found that a LOF mutation of *rad-23* suppressed the locomotor deficit of mutTDP-43.

RAD-23 has two known functions: (1) it can bind ubiquitinated substrates and the proteasome to aid in clearance of certain substrates (Chen and Madura, 2002) and (2) it assists in nucleotide excision repair (NER) initiation to correct distorted double helices resulting from DNA damage (Dantuma et al., 2009; Bergink et al., 2012). We show that loss of *rad-23* has a beneficial effect in *C. elegans* and mammalian models of ALS. This effect is linked to improved protein homeostasis and clearance of ALS-causing proteins by loss of RAD-23.

The pathophysiological relevance of our work to human disease is suggested by changes in RAD-23 abundance and cellular distribution in ALS spinal cord samples. We propose that native RAD-23 acts as an “anti-chaperone” to stabilize and prevent the turnover of misfolding-prone proteins that cause ALS. These data raise the possibility that targeted reduction of RAD-23 could have therapeutic utility in ALS.

## MATERIALS AND METHODS

### Antibodies

The following antibodies were used in this study: hR23A (Abcam ab55725), hR23B (Abcam ab88053), TDP-43 (Abcam ab57105 for IB; ThermoPierce PA5-17011 for IP), myc (Cell Signaling 2276), hSOD1 (Abcam ab52950), V5 (EMD Millipore ab3792), GFP (Sigma G1546), beta-actin (Sigma A2066), ubiquitin (Dako Z0458), SMI32 (Invitrogen), biotinylated goat anti-mouse IgG (Vector BA-9200), and anti-mouse and anti-rabbit AlexaFluor antibodies (Invitrogen). Goat anti-TDP-43 antibody was developed in the Petrucelli laboratory.

### C. elegans strains

All animals were grown on Nematode Growth Media (NGM) plates and seeded with *Escherichia coli* (*E. coli*) OP50 and maintained at 20°C (Brenner, 1974). The following *C. elegans* strains were obtained from the *C. elegans* Genetic Center and National Bioresource Project for the Nematode: the N2 Bristol strain, *rad-23* (*tm3690* and *tm2595*), *ufd-3* (*tm2915*), *cdc-48.1* (*tm544*), *cdc-48.2* (*tm659*), *ubxn-4* (*tm3247*), *ubql-1* (*tm1574*). All strains were backcrossed to ancestral N2 as indicated in Table S3. The hSOD-expressing lines P<sub>snb-1</sub>::WT SOD1-YFP and P<sub>snb-1</sub>::G85R SOD1-YFP and hTDP-43-expressing lines P<sub>snb-1</sub>::WT TDP-43 and P<sub>snb-1</sub>::TDP-43 (M337V) were generated as described previously (Wang et al., 2009 and Liachko et al., 2010 respectively). Compound mutant strains, consisting of the mutation/allele and the TDP-43 or SOD1 transgene were confirmed by fluorescence and the PCR using primers for the allele (see Table 2). The G85R; *sid-1* (*pk3321*); P<sub>unc-119</sub>::SID-1 worm was created as previously described (Calixto et al., 2010; Lim et al., 2012). The RAD-23 rescue lines

were created using Gateway Cloning (Invitrogen). Briefly, RAD-23 genomic DNA was amplified from DNA isolated from WT *C. elegans* and cloned into the pDonR221 entry vector. The LR reaction was then performed with P<sub>unc-119</sub> (nervous system expression) (first position), the RAD-23 entry clone (second position), and unc-54 3'UTR entry clone (third position). The resulting vector was confirmed by Sanger sequencing and injected into the gonads of either mutTDP-43 or mutTDP-43; *rad-23 (tm3690)* animals until 3 stable lines were created. The RAD-23 expression construct was co-injected with a P<sub>unc119::GFP</sub> co-injection marker. A list of all strains used in this study can be found in Table 3. All animals were grown on Nematode Growth Media (NGM) plates and seeded with *Escherichia coli* (*E. coli*) OP50. All animals were maintained at 20°C (Brenner, 1974).

### **Locomotor assays**

*C. elegans* locomotor assays were performed as a swimming assay in a drop of M9 buffer (22mM KH<sub>2</sub>PO<sub>4</sub>, 42mM Na<sub>2</sub>HPO<sub>4</sub>, 86mM NaCl) on the surface of an agar plate. For each assay, 15 to 25 worms were allowed to lay eggs for 4 hours. Behavior was blindly recorded at the young adult stage (24 hours after L4) for 30 seconds on a video camera attached to a Zeiss Stemi SV11 dissecting scope. Five replicates containing 7-10 animals per group were tested. Videos were tracked analyzed using the Parallel WormTracker (<http://wormsense.stanford.edu/tracker>; Miriam Goodman; Stanford University, Palo Alto, CA) script on MATLAB (MathWorks) to determine the average speed (millimeters (mm) per second). Each experiment was completed three independent times on different days. One representative experiment is shown unless otherwise indicated.



### **RNAi knockdown in *C. elegans***

Each RNAi (RNA Interference) colony was grown overnight in Luria broth (LB) containing ampicillin (50 $\mu$ g/mL), and 200 $\mu$ L was seeded onto NGM plates containing isopropylthiogalactoside (IPTG) (1mM) to induce dsRNA expression. The RNAi clone for *rad-23* was generated as described previously in the Ahringer library (Fraser *et al.*, 2000), and its correctness was confirmed by sequencing. For locomotor experiments, staged L4 animals were placed on RNAi plates overnight. On the next day, young adult *C. elegans* were transferred to a fresh RNAi plate and allowed to lay eggs for 4-6 hours. Progeny were subsequently tested at the young adult (L4+1 day) stage for locomotor activity as described above. For RNAi experiments, the average of three independent experiments is shown.

### **Tunicamycin lifespan assay**

Wild type (WT) (N2 Bristol strain) or *rad-23* (*tm3690*) *C. elegans* were allowed to lay eggs on NGM plates for 4-6 hours (“egg dropping”). At the young adult stage, 100 animals were placed on NGM plates supplemented with either vehicle (DMSO) or tunicamycin (Sigma T7765; 5 $\mu$ g/mL). NGM plates were all seeded with OP50 and the final concentration of DMSO in the plates did not exceed 0.2%. Animals were transferred to a fresh plate every day and scored for survival by response to light touch. Bagging worms or worms with a vulva explosion phenotype were excluded from the analysis. All assays were completed blind to genotype.

### **Heat shock lifespan assay**

For heat shock assay, wild type (WT; N2 Bristol strain) or *rad-23 (tm3690)* animals were allowed to lay eggs on NGM plates for 4-6 hours. At the L4 stage, ~50 animals per group were transferred to a fresh plate. At the young adult (L4+1 day) stage, NGM plates were fully submerged into a water bath in a plastic bag at 34°C. Plates were removed briefly every hour so that animals could be scored for survival by response to a light touch. Bagging worms or worms with a vulva explosion phenotype were excluded from the analysis. All analyses were performed blind to genotype.

### **Biomechanical profiling software**

We used a MATLAB-based image analysis program to quantify the biomechanics *C. elegans* swimming behavior as previously described (Sznitman et al., 2010; Krajacic et al., 2012). Wild type (WT; N2 Bristol strain) or *rad-23 (tm3690)* animals were allowed to lay eggs for 4-6 hours. Worms were staged at the L4 stage based on the transparency of the vulva mark. At L4 and for 5 days post L4, recordings were taken ( $\geq 10$ /group at each time point). Briefly, one to three animals were transferred into a 50 $\mu$ L drop of M9 buffer in the recording chamber and, after 2 minutes of acclimation, were covered with a cover slip. Recordings of 4-15 seconds of a single animal in the chamber were obtained using standard bright-field microscopy at 26 frames per second. For each recording of a single animal, worm curvature was captured and plotted over time. Worm speed, force, and power calculation were performed in MATLAB (MathWorks) (Schnitzman et al., 2010; Krajacic et al., 2012). All analyses were performed blind to genotype.

### **UV sensitivity assay**

UV survival experiments were performed as previously described (Lans *et al.*, 2010). For each genotype, 16-25 *C. elegans* young adults were irradiated at the

indicated UV-B dose and, following 24 hrs of recovery, transferred to 4-5 NGM plates to lay eggs for a 2-3 hour period. Survival of progeny was later assessed.

### **Fluorescence recovery after photobleaching (FRAP) assay**

Animals were immobilized with 10 mM levamisole and examined with a Leica DMI3000 B confocal microscope. Experiments were performed as described in Wang *et al.*, 2010.

### **Recombinant Herpes Simplex Virus (HSV) constructs**

*hR23A* and *hR23B* miRNA was designed against the target sequences, 5'-CCAGAACATGCGGCAAGTGAT-3' and 5'- TGGTAACTGAGATCATGTCAA -3', respectively. Primers were annealed and cloned into the p1006(+) vector backbone using the BspE1 and FseI restriction sites. The p1006(+) amplicon plasmids were then used to generate recombinant herpes simplex virus (HSV) as described previously (Neve *et al.*, 1997). The titer of virus used in these experiments was  $\sim 3 \times 10^7$  plaque-forming units/mL.

### **Cell culture**

Mixed spinal cord neuron cultures were prepared as described previously (Mojsilovic-Petrovic *et al.*, 2006). Briefly, an astrocyte feeder layer was prepared from the cortex of newborn Sprague Dawley rat pups (postnatal day 2 (P2)) and grown to  $\sim 80\%$  confluency. Subsequently, dissociated embryonic day 15 (E15) spinal cord neurons were added. One to two days later, AraC (5mM) (catalog #C6645; Sigma) was added for 24 hours to arrest astrocyte proliferation. Cultures were maintained in glia-conditioned medium supplemented with the following trophic factors (1.0ng/mL each):

human neurotrophin-3, human neurotrophin-4, human brain-derived neurotrophic factor, and rat ciliary neurotrophic factor (Alomone Labs). Half of the culture medium was replaced on a biweekly basis.

HEK293 (Human Embryonic Kidney 293) cells were grown in Dulbecco's modified eagle's medium (DMEM) (Invitrogen) supplemented with 10% FBS (Sigma) and 1% Pen-Strep (Sigma). Wild type (WT), hR23A<sup>-/-</sup>, and hR23B<sup>-/-</sup> mouse embryonic fibroblasts (MEFs) were maintained in DMEM with GlutaMax and high glutamine (Invitrogen) supplemented with 10% FBS (Sigma) and 1% Pen-Strep (Sigma). MEFs were created as previously described in Okuda et al., 2004.

### **Transfections**

Cells were transfected using Lipofectamine 2000 (Invitrogen) in antibiotic-free medium once cells reached ~75% confluency. Media was replaced after 24 hours. Experiments were carried out 48 hours post transfection unless otherwise indicated.

### **Cycloheximide assays**

When cells were 75% confluent, the HEK293 cells were co-transfected (Lipofectamine 2000; Invitrogen) with indicated TDP-43 or SOD1 expression constructs and a control or RAD-23 (hR23A or hR23B) miRNA using Lipofectamine 2000 (Invitrogen) in antibiotic-free media. MEFs were transfected (Lipofectamine 2000; Invitrogen) with TDP-43 expression construct and LacZ or respective hR23A or hR23B cDNA if indicated. After 24 hours, cells were re-plated in standard media at equal densities in duplicate or triplicate as needed. 24 hours later, the media was removed and replaced with standard media and cycloheximide (CHX; Sigma; final concentration of 100µg/mL) or vehicle (DMSO (Sigma)). At subsequent time points, cells were washed

twice in ice-cold PBS supplemented with cycloheximide (50µg/mL) and lysed in radioimmunoprecipitation (RIPA) buffer (1% NP-40, 0.1% SDS, 50mM Tris-HCl pH7.4, 150mM NaCl, 0.5% sodium deoxycholate, 1mM EDTA). All buffers used in this study were supplemented with complete protease inhibitor cocktail (Roche). Samples were then processed for Western blot. Samples were then processed for Western blot. In certain experiments, vehicle (DMSO), MG-132 (5µM), epoxomicin (100nM), or 3-methyladenine (3-MA) (10mM) (all from Sigma) was added thirty minutes following the addition of CHX.

### **RNA isolation and mRNA measurements**

RNA RNA was extracted from untransfected and transfected HEK293 cells using the RNeasy Mini Kit (Qiagen). Total RNAs from *C. elegans* were purified using TRIzol reagent (Invitrogen) followed by DNase I (Promega) digestion. One microgram (µg) of DNase-treated RNA was reverse transcribed using iScript cDNA synthesis kit (Bio-Rad) followed by the manufacturer protocol. The cDNAs were subjected to real-time qPCR in a total volume of 25 µl, containing 1x Power SYBR Green Master Mix (Life Technologies) and 200 nM primer. The qPCR reaction were amplified and analyzed in triplicate using StepOne™ RealTime PCR system (Life Technologies). To enable normalization of the input target cDNA added to each well, the endogenous controls, *alpha tubulin (tba-1)* for *C. elegans* experiments and *beta actin* for HEK293 cell experiments were amplified simultaneously in a separate reaction well but under identical thermal cycling condition. Amplification data were analyzed and relative quantification data were obtained using the StepOne™ software v2.2.2. All experiments were repeated three independent times. Primers for amplification of target mRNA were as follows: *hTDP-43*: 5'-ATGGAAAACAACCGAACAGG-3' and 5'-

AAAGCCAAACCCCTTTGAAT-3'; *beta-actin*: 5'-CTCTTCCAGCCTTCCTTCCT-3' and 5'-AGCACTGTGTTGGCGTACAG-3'; *tba-1*: 5'-AAGATGCCGCCAACAACTAC-3' and 5'-CCTCCTCCGAATGAATGAAA-3'.

### **Soluble versus insoluble preparations**

For all soluble/insoluble preparations, cells were lysed in RIPA buffer and sonicated (20% strength, 10sec). Lysates was then briefly centrifuged to remove cellular debris (5,000xg, 10', 4°C). Supernatant was then centrifuged (100,000xg, 30', 4°C) and the supernatant was considered the 'soluble' fraction. The pellet was washed in RIPA buffer and re-centrifuged (100,000xg, 30', 4°C). Supernatant was discarded. The pellet was resuspended in urea buffer (8M urea; 4% CHAPS; 50mM dithiothreitol (DTT); 40mM Tris pH 8.0; 2.5mM EDTA) and considered the 'insoluble' fraction. Samples were then processed for Western blot.

### **Sequential soluble and insoluble preparation from *C. elegans***

Sequential soluble and insoluble preparations were performed as previously described in Liachko et al., 2010. The total protein fraction was collected by homogenizing worms in RAB high salt buffer. The packed worm pellet was resuspended twice in low-salt buffer (LS) (10mM Tris, 5mM EDTA, 10% sucrose, pH 7.5) and was completely lysed by sonication. The homogenate was centrifuged at 25,000xg for 30 min and the supernatant was considered the LS fraction. The LS pellet extracted with nonionic detergent-containing buffer (TX) (10mM Tris, 5mM EDTA, 1% Triton X-100, 10% sucrose, pH 7.5) and centrifuged for 20' at 180,000xg. The supernatant was considered the TX fraction. The pellet was extracted with ionic detergent-containing buffer (SARK) (10mM Tris, 5mM EDTA, 1% Sarkosyl, 10% sucrose, pH 7.5) and

centrifuged at 180,000xg for 20min. The supernatant was considered the SARK fraction. The final detergent-resistant pellet was resuspended in UREA (30mM Tris, 7M Urea, 2M Thiourea, 4% CHAPS (3-[(3-cholamidopropyl)dimethylammonio]-1-propanesulfonate), pH 7.5). All buffers contained complete protease inhibitor cocktail (Roche) and 0.5mM PMSF (phenylmethylsulfonylfluoride).

### **RAD-23 expression manipulation and TDP-43 abundance**

HEK293 cells were co-transfected as outlined above in a 3:1 ratio of miRNA to TDP-43 expression construct. After 48 hours, cells were lysed in RIPA buffer and samples were processed for Western blot. For RNAi rescue experiment, 2µg of LacZ or appropriate hR23A or hR23B RNAi-resistant cDNA was co-transfected. To generate RNAi-resistant cDNA, three silent mutations were introduced into the miRNA target sequence using the QuikChange Lightning Multi-Site Mutagenesis kit (Agilent) per manufacturer protocol. Mutations introduced into hR23A or hR23B target sequence are outlined here (nucleotide mutations introduced are underlined): for hR23A: 5'-CCAAAATATGCGCCAGGTGAT-3'; for hR23B: 5'-TGGTGACCGAAATCATGTCAA-3'. Mutated cDNAs were sequenced for correctness prior to use.

### **Mouse strains**

Male heterozygote G93A mutSOD1 mice on the congenic C57BL/6 background (Strain 004435; Jackson Laboratory) were backcrossed with C57BL/6 mice. Non-transgenic (non-Tg) littermates served as control mice. Only male G93A mutSOD1 mice and control littermates were used for experimentation. Mice were fed a standard diet (Purina 5010) and were housed on a 12 h light/dark cycle. Genotypes were determined by PCR using tail snip DNA. Primer sequences were: 5'-cgcgactaacaatcaaagtga-3'; 5'-

catgagccctaatacctctga-3'; 5'-gtaggtggaaattctagcatcatcc-3'; and 5'-ctagggcacagaattgaaagatct-3'. All animals were treated in strict accordance with the National Institutes of Health Guide for the Care and Use of Laboratory Animals and were approved by the Children's Hospital of Philadelphia Institutional Animal Care and Use Committee.

### **Ubiquitination Assays**

Vehicle (DMSO) or MG-132 (5 $\mu$ M) was added twelve hours before cell lysis. Cells were lysed in RIPA buffer supplemented with 50mM N-ethylmaleimide to inhibit deubiquitinase activity and myc-TDP-43 was immunoprecipitated where relevant using the Immunoprecipitation Kit (Thermo) per manufacturer protocol. Samples were then processed for Western blot.

### **Immunohistochemistry**

Patient tissue was deparaffinized. Endogenous peroxidase was blocked with 3% hydrogen peroxide in methanol for 30 minutes. Sections were washed in water and immersed in 0.1M Tris buffer (pH 7.6) and 0.1M Tris/2% FBS (fetal bovine serum) for 5 minutes each. Sections were incubated with  $\alpha$ -hR23A and  $\alpha$ -hR23B mouse antibody (Abcam). After washing with 0.1M Tris buffer (pH 7.6) and 0.1M Tris/2% FBS, sections were incubated with biotinylated goat anti-mouse IgG (1:200; Vector Laboratories) for 30 minutes at room temperature. After washing with 0.1M Tris buffer (pH 7.6) and 0.1M Tris/2% FBS, sections were then incubated with Vectastain ABC (Vector Laboratories) for 45 minutes. After washing with 0.1% PBST followed by 0.1M Tris (pH 7.5) and 0.3M NaCl. Peroxidase activity was then detected with DAB (Dako). Slides were then dehydrated in ascending series of ethanol and coverslipped.



## **Meso Scale Discovery (MSD) assay**

First, the carbon surface wells on a 96-well MSD assay plate were coated with a rabbit anti-V5 or goat anti-TDP-43 capture antibody diluted 1:500 in Tris-buffered saline (TBS). Following an overnight incubation at 4°C, wells were washed once with TBS containing 0.2% Tween 20 (TBST), and blocking buffer (3% non-fat milk in TBST) was added to wells for 2 hours at room temperature to prevent non-specific binding. The plate was then washed four times, and lysate from hR23A/pcDNA transfected cells (background control wells), or cells transfected to overexpress hR23A/WT TDP-43 and hR23A/mutTDP-43 were added to wells, in triplicate, at a final concentration of 15 µg/well. The plate was incubated at room temp for 2 hours to allow capture of TDP-43 by anti-V5 or hR23A by the anti-TDP-43 antibody coated onto wells. Following washes to remove unbound proteins, wells were treated with specific primary antibody to detect captured protein (V5 or TDP-43) and secondary antibody (goat or rabbit polyclonal) labeled with an electrochemiluminescent compound, the SULFO-TAG (Meso Scale Discovery, 2 µg/ml), in blocking buffer. Plates were washed after a 2 hour incubation period, and a MSD Read Buffer that provides the appropriate chemical environment for electrochemiluminescence was added to wells prior to loading plates into the MSD Sector Imager 2400. Inside the instrument, a voltage was applied to the plate electrodes causing the SULFO-TAG bound to the electrode surface to emit light. The intensity of emitted light at 620nm was measured to provide a quantitative measurement of the amount of binding in each well. The binding signal was calculated by subtracting the average background signal from wells treated with lysate from control transfected cells, from the average signal from wells treated with lysate from cells expressing the different TDP-43 products.

## **Statistics**

Statistical analysis was performed using GraphPad Prism Version 6.00 for Windows, GraphPad Software, La Jolla, CA, USA ([www.graphpad.com](http://www.graphpad.com)). Unpaired t-test was used for all two-group comparisons. For data containing more than three groups, a one-way ANOVA with Dunnett's multiple comparisons test was used. For survival analysis, a log-rank (Mantel-Cox) test was used. The threshold for significance was always set to  $p < 0.05$ .

## RESULTS

### Loss of ERAD components modify ALS phenotypes in *C. elegans*

We asked whether mutant loss-of-function (LOF) versions of ERAD or UPR genes (Table 1) suppressed or enhanced the proteotoxic insults relevant to neurodegenerative disease. We used *C. elegans*, engineered to express wild type (WT) or mutSOD1 (Wang et al., 2009) and WT or mutTDP-43 (Liachko et al., 2010) in the nervous system. As previously reported, these ALS models display a severe locomotor deficit and swim at roughly ~10% the speed of wild type (WT) (N2 Bristol) animals (Figure 1A) (Lim et al., 2012). To identify modifiers of mutTDP-43, ERAD mutants were placed on the mutTDP-43 background and the effect on locomotion was determined. None of the ERAD mutants on their own showed any change compared to WT animals in a swimming assay at the young adult stage (L4 stage + 1 day) tested (data not shown).

Of the modifiers found using this approach (Figure 1B), we chose to focus on RAD-23 for multiple reasons. First, based on RAD-23's role as a shuttle between ubiquitinated substrates and the proteasome (Schauber *et al.*, 1998), we anticipated that loss of *rad-23* would worsen the mutTDP-43 phenotype and this is the opposite of what we found. Second, RAD-23 has an additional role in NER and NER defects have been linked to neurodegeneration (Jaarsma et al., 2011; Madabhushi, et al., 2014). Third, *rad-23* mutants showed the strongest suppression among the modifiers. Finally, the other identified suppressors of mutTDP-43 appeared to do so through independent pathways (Figure 1C-1D). The other identified suppressors, loss of *ufd-2* (Figure 1C) and loss of

*ufd-3* (Figure 1D), both resulted in an additive suppression of the locomotor deficit when placed on the mutTDP-43 background with loss of *rad-23*.

### **Loss of *rad-23* suppresses two models of ALS**

In addition to the first *rad-23* mutant used (*tm3690*), we found that a second mutant of *rad-23* (*tm2595*) (Figure 2A) also showed a two-fold suppression of the locomotion deficit caused by mutTDP-43 (Figures 2B-2C) and mutSOD1 (Figures 2D-2E) ( $p < 0.05$ ). The mutations used are deletions in different portions of RAD-23. In addition, neither *rad-23* mutant affected the locomotion of transgenic worms expressing wtSOD1 or wtTDP-43. *Rad-23* mutants alone were identical to WT in the swimming assay (Figure 2F).

To understand whether it was loss of *rad-23* in the nervous system or other tissue suppressing the locomotor deficit, we used RNAi and rescue approaches. We found that mutSOD1 fed *rad-23* RNAi showed no suppression of the locomotor deficit (Figure 2G). In contrast, mutSOD1 animals fed *rad-23* RNAi where the RNAi effect is reduced in peripheral tissues and boosted in the nervous system (mutSOD; *sid-1*;  $P_{\text{neuron}}::\text{SID-1}$ ) showed a ~2-fold suppression of the mutSOD1 locomotor deficit ( $p < 0.01$ ) (Calixto et al., 2010) (Figure 2G). These data suggest that loss of *rad-23* in the nervous system protects against mutSOD1.

Outcrossing the *rad-23* (*tm3690*) allele rescued mutTDP-43 toxicity, suggesting the suppression in the *rad-23* background is not due to loss of expression of the mutTDP-43 transgene (Figure 2H). We also generated several lines overexpressing the genomic *C. elegans* RAD-23 locus under the control of a nervous system-specific promoter. We found that overexpression of RAD-23 in the nervous system rescued the

beneficial effect of loss of *rad-23* in mutTDP-43; *rad-23* animals (Figure 2I), but overexpression of RAD-23 in the nervous system of mutTDP-43 alone had no effect on the average speed of mutTDP-43 (Figure 2J). In sum, these data indicate that loss of *rad-23* acts in a cell autonomous manner within the nervous system to suppress mutTDP-43 and mutSOD1 toxicity.

It has been previously described that mutTDP-43 leads to neurodegeneration of the GABAergic motor neurons in *C. elegans* causing motor neuron death, broadening of the axons, and gaps in the ventral nerve cord (Liachko et al., 2009). We examined GABAergic motor neurons in WT, mutTDP-43, and mutTDP-43; *rad-23* animals and found that loss of *rad-23* reduced the number of animals that displayed broadening of axons in the mutTDP-43 background (Figure 3A) and also reduced the number of gaps in the ventral nervous cord in the mutTDP-43 background (Figure 3B). In sum, we found that loss of *rad-23* suppressed the degeneration of GABAergic neurons caused by mutTDP-43 (Figure 3C). Thus, loss of *rad-23* suppresses both the locomotor deficit and neurodegenerative phenotype associated with mutTDP-43.

To date, the tissue expression pattern of *C. elegans* RAD-23 has not been defined. To address this, we created a worm expressing a RAD-23::GFP translational fusion expressed under the control of the endogenous RAD-23 genomic locus. We found RAD-23 expression throughout the animal at the young adult (L4 +1 day) stage (Figures 4A-4C), including neuronal cell bodies and processes (Figure 4D) and the nerve cord (Figure 4F).

### **Loss of *rad-23* protects against proteotoxicity at the cost of DNA damage**

Because loss of *rad-23* protected against two ALS-associated proteins, we wondered if loss of *rad-23* had broader beneficial actions. Because neurodegeneration is often age-related, we looked at age-related decline in motor function in *C. elegans* using multi-dimensional biomechanical profiling software (Krajacic et al., 2012). The average speeds of WT and *rad-23* mutants were identical at the L4 and young adult stage. However, *rad-23* mutants showed increased average speeds compared to WT in later ages at 4 ( $p < 0.05$ ) and 5 days ( $p < 0.05$ ) post L4 (Figure 5A). Loss of *rad-23* also resulted in increased force (Figure 5B), and power (Figure 5C) compared to WT at these ages ( $p < 0.05$ ). Moreover, *rad-23* had a more coordinated biomechanical profile than WT at 5 days post L4 (Figure 5D).

ALS and other forms of neurodegeneration show increased levels of ER stress and attenuation of ER stress has been shown to be beneficial (Vaccaro et al., 2013; Walker et al., 2013; Thompson et al., 2014). We investigated if loss of *rad-23* attenuated *C. elegans*' response to ER stress, induced by tunicamycin. The lifespans of WT and *rad-23* mutants exposed to vehicle are identical; in contrast, *rad-23* mutants show an extension of their lifespan by 22.2% compared to WT when grown on tunicamycin ( $p < 0.0001$ ) (Figure 5E). In a second stress assay, we found that loss of *rad-23* conferred a ~25% extension of lifespan at high heat (34°C) ( $p < 0.0001$ ) (Figure 5F).

Because *rad-23* was originally identified in yeast by having increased sensitivity to UV irradiation (Prakash et al., 1993), we examined UV sensitivity in loss of *rad-23* backgrounds (Lans et al., 2010). There was no difference in UV sensitivity between WT and animals overexpressing SOD1 or TDP-43. We confirmed both *rad-23* mutants (*tm2595* and *tm3690*) showed a hypersensitivity to UV stress compared to WT ( $p < 0.0001$ ). This result substantiates that the *rad-23* mutants used in this study are very

likely null for *rad-23*. Interestingly, overexpressing either SOD1 or TDP-43 in the loss of *rad-23* backgrounds causes a synthetic hypersensitivity on a UV sensitivity assay compared to loss of *rad-23* alone ( $p < 0.0001$ ) (Figure 5G). These data suggest that loss of *rad-23* confers a specific resistance to proteotoxic insults and age-related decline, but a deficit in DNA damage repair.

### **Loss of *rad-23* does not protect against mutTDP-43 toxicity via several known genetic pathways**

Given the link to DNA damage, we used *C. elegans* genetics to determine if genes known to function with *rad-23* in the NER pathway could modify the mutTDP-43 and mutSOD1 phenotypes. Strains harboring mutations in various NER components neither showed a baseline difference compared to WT in the swimming assay (data not shown) nor suppressed the mutTDP-43 phenotype (Figure 6A-6C). This suggests that loss of *rad-23* does not protect against mutTDP-43 via the NER pathway.

We also examined mutants in molecular components known to associate with RAD-23 in ERAD. PNG-1 physically and genetically interacts with RAD-23 in yeast and *C. elegans* (Habibi-Babadi, et al., 2010). We found no suppression of mutTDP-43 toxicity by *png-1* (*cy9*) (Figure 6D). UFD-3 mutants in yeast have reduced bulk ubiquitin levels (Johnson et al, 1995) and can antagonize UFD-2 (Rumpf et al., 2006), an interactor of RAD-23 (Kim et al., 2004) and CDC-48 (Bohm et al., 2011). We found that *ufd-2* (*tm1380*) and *ufd-3* (*tm2915*), but not *cdc-48.1* (*tm544*) or *cdc-48.2* (*tm659*), suppressed the locomotor deficit of mutTDP-43 (Figure 1B). We could not study the effect of loss of *cdc-48.1* and *cdc-48.2* together because loss of both genes results in a larval lethality. We therefore tested if suppression of mutTDP-43 by *rad-23*, *ufd-2*, and *ufd-3* was by the

same pathway. When either *ufd-2* or *ufd-3* was placed on the mutTDP-43; *rad-23* background, there was an additive suppression of the mutTDP-43 locomotor deficit. This observation suggests that the beneficial effect of loss of *rad-23* is not through a linear pathway with *ufd-2* or *ufd-3* (Figure 1C-1D).

### **Knockdown of RAD-23 in mammalian motor neurons protects against toxicity caused by TDP-43, SOD1, and ER stress**

Mammals contain 2 orthologs of the nematode RAD-23 which retain 40% amino acid identity, hR23A and hR23B. We investigated if knockdown of *hR23A* or *hR23B* protected against TDP-43 and SOD1 toxicity in mammalian motor neurons. We created miRNAs targeting endogenous *hR23A* and found specific knockdown of hR23A, but not hR23B or a co-transfected GFP plasmid (Figure 7A, 7B 7E). A specific *hR23B* miRNA was also generated (Figure 7C-7E). We engineered a herpes simplex virus (HSV) to express the designed miRNAs targeting *hR23A* and *hR23B*. Because HSV is a neurotropic virus, it will not knockdown *hR23A* or *hR23B* in glia. We found that *hR23A* and *hR23B* knockdown led to specific target knockdown in rat mixed spinal cord cultures (Figure 7F).

When recombinant HSV engineered to express wtSOD1 or wtTDP-43 is infected into mixed spinal cord cultures, there was a ~25% decrease in five day motor neuron survival. In contrast, when neurons were infected with a HSV engineered to express mutSOD1 or mutTDP-43, there was a ~50% decrease in five day motor neuron survival. We found that knockdown of hR23A protected against wt and mutSOD1 toxicity ( $p < 0.01$ ,  $p < 0.001$  respectively) (Figure 7G, Figure 7I), as well as wt and mutTDP-43 toxicity ( $p < 0.01$ ,  $p < 0.01$  respectively) (Figure 7H). We found that knockdown of hR23B



also protected against the toxicity of wtSOD1 ( $p < 0.005$ ), mutSOD1 ( $p < 0.001$ ), wtTDP-43 ( $p < 0.005$ ), and mutTDP-43 ( $p < 0.001$ ) toxicity (Figure 7G-7I). Thus, reducing the amount of endogenous hR23A or hR23B in mammalian spinal cord neurons protects against SOD- and TDP-43-induced motor neuron death.

To determine if knockdown of RAD-23 orthologs in mammalian neurons protected against ER stress, mixed spinal cord neurons were infected with HSV to express either a *hR23A*, *hR23B*, or control miRNA along with either LacZ to mimic a “non-ALS” condition or mutSOD1 to mimic an “ALS” condition. 24 hours later, neurons were treated with vehicle or tunicamycin (2.5  $\mu\text{g}/\text{mL}$ ) to induce ER stress. Motor neuron survival was assessed 48 hours later (Figure 7J). Under +LacZ conditions, we found that tunicamycin reduced motor neuron survival by ~40% compared to vehicle. This was suppressed entirely by hR23A ( $p < 0.01$ ) and hR23B ( $p < 0.05$ ) knockdown, although *hR23A* and *hR23B* knockdown had no effect on motor neuron survival on their own. In addition, under the mutSOD1 condition, we found that *hR23A* ( $p < 0.05$ ) and *hR23B* ( $p < 0.01$ ) knockdown reduced toxicity of mutSOD1. Tunicamycin exacerbated toxicity of mutSOD1 by ~10%, and this was suppressed by reducing hR23A ( $p < 0.001$ ) and hR23B ( $p < 0.005$ ). In sum, reducing RAD-23 abundance renders motor neurons resistant to invoked ER stress.

### **hR23A expression is increased in the spinal cord of mutSOD1 mice**

Given that reduced RAD-23 expression protected against the toxicity of two ALS models, we examined the abundance of hR23A and hR23B in the mouse ALS (mutSOD1 (G93A)) model compared to controls. At a pre-symptomatic time point (P60), we found no difference in hR23A or hR23B expression in the brain and spinal cord of

mutSOD1 mice compared to age- and sex-matched controls. At symptomatic and end-stage time points, we found a ~50% increase in hR23A (Figure 8A-8B) expression in the spinal cord of the mutSOD1 mice at P90 ( $p < 0.05$ ) and P120 ( $p < 0.01$ ). There was no change in hR23B expression in the spinal cord at P90 ( $p = 0.8419$ ) or P120 ( $p = 0.3592$ ) (Figure 8C-8D). We did not find any change in hR23A ( $p = 0.1208$ ) or hR23B ( $p = 0.4032$ ) expression in the total brain lysate at P120 from the same animals. We confirmed that there is an increase in p-eIF2 $\alpha$ , a marker of ER stress, at P60 in the spinal cord of mutSOD1 mice ( $p < 0.05$ ), as previously reported (Nagata et al., 2007; Wang et al., 2011) (Figure 8E-8F). Therefore, hR23A expression is increased in an ALS mouse model at time points associated with disease, and suggests this increase occurs after the onset of ER stress.

### **Loss of RAD-23 accelerates the degradation of mutTDP-43 and mutSOD1**

To identify the mechanism by which loss of *rad-23* confers protection against proteotoxicity, we examined the steady state levels of mutTDP-43 following overexpression and knockdown of RAD-23 in HEK293 cells. Co-transfection of the mutTDP-43 expression construct with a hR23A or hR23B expression construct led to a small increase in mutTDP-43 abundance (Figure 9A-9B). In contrast, when endogenous *hR23A* or *hR23B* was knocked down by co-transfection of the *hR23A*, *hR23B*, or control miRNA with the mutTDP-43 expression construct, we found a ~90% reduction ( $p < 0.005$ ) in the total amount of mutTDP-43 protein (Figure 9A-9B). We found no change in human TDP-43 mRNA levels after RAD-23 knockdown, compared to a control miRNA (Figure 9C), suggesting the changes in protein abundance are unlikely to be linked to transcription.

We examined the rate of TDP-43 and SOD1 degradation with or without knockdown of *hR23A* or *hR23B*. TDP-43 has been reported to have a half-life of ~50 hours and ALS-linked mutations in TDP-43 result in a more stable protein than WT (Ling et al., 2010; Austin et al., 2014; Barmada et al., 2014). HEK293 cells were transfected with the plasmid expressing TDP-43 or SOD1 along with a *hR23A*, *hR23B*, or control miRNA. 48 hours later, new protein synthesis was inhibited by the addition of cycloheximide (CHX) and lysates were probed for TDP-43 or SOD1 at time intervals thereafter. We found that knockdown of *hR23A* led to an accelerated loss of mutTDP-43 (Figure 9D-9E;  $p < 0.05$ ) and mutSOD1 (Figure 9F-9G;  $p < 0.01$ ) after 180 minutes of CHX; knockdown of *hR23A* or *hR23B* had no effect on the degradation of wtTDP-43 or wtSOD1 (data not shown). There was roughly 30% less mutTDP-43 and mutSOD1 protein remaining in *hR23A* knockdown compared to controls and a further ~40-50% ( $p < 0.05$ ) reduction after 270 minutes (Figure 9H-9I).

In order to confirm that it is reduced RAD-23 levels which accelerate mutTDP-43 turnover, we utilized a line of RAD-23-null mouse embryonic fibroblasts (MEFs) (Okuda et al., 2004). We compared mutTDP-43 degradation during CHX treatment in *hR23A*<sup>-/-</sup> and *hR23B*<sup>-/-</sup> MEFs to WT MEFs. After inhibiting protein synthesis for 180 minutes, we found a ~40% greater reduction in mutTDP43 abundance in *hR23A*<sup>-/-</sup> and *hR23B*<sup>-/-</sup> MEFs versus WT MEFs (Figure 9J). Restoring RAD-23 expression in the RAD-23-null MEFs blocked the accelerated degradation of RAD-23 (Figure 9K).

In contrast to the observed results for mutTDP-43 and mutSOD1, we found that knockdown of *hR23A* and *hR23B* inhibited the degradation of CPY\*, a canonical yeast ERAD substrate, after CHX (Figure 9L). This suggests the inhibition of ALS-linked protein clearance by RAD-23 is specific, and does not apply to all substrates.

We employed the same experimental paradigm in primary neurons from mixed spinal cord cultures and showed that knockdown of *hR23A* or *hR23B* accelerated the degradation of mutSOD1 (Figure 10A). To confirm that effects of RAD-23 knockdown on mutTDP-43 abundance were RAD-23 specific, we showed that we could rescue the reduced mutTDP-43 abundance in RAD-23 knockdown conditions by co-transfecting a RNAi-resistant RAD-23 cDNA (*hR23A<sup>res</sup>* or *hR23B<sup>res</sup>*) to restore RAD-23 in the HEK293 cells (Figure 10B-10D). Knockdown of *hR23A* or *hR23B* reduced mutTDP-43 abundance if cells were transfected with a LacZ control, but co-transfection with the RNAi-resistant RAD-23 cDNA prevented mutTDP-43 removal. These data show that the reduction of mutTDP-43 is RAD-23-dependent and reduced RAD-23 leads to accelerated mutTDP-43 and mutSOD-1 turnover in multiple cell lines, including primary neurons.

### **Loss of RAD-23 increases flux through the proteasome and autophagy by increasing polyubiquitination**

RAD-23 is known to interact with ubiquitinated substrates and the proteasome (Chen et al., 2002) and we found that *hR23A* associates with mutTDP-43 (Figure 10E). RAD-23 overexpression can inhibit proteasomal degradation by inhibiting ubiquitination (Ortolan et al., 2000; Raasi and Pickart, 2003), although the use of overexpression paradigms may lead to non-physiological activities. To determine if RAD-23 inhibits the turnover of mutTDP-43 through the proteasome and/or autophagy pathways in our loss of RAD-23 setting, we utilized several pharmacological inhibitors of the proteasome, the ubiquitin/proteasome system (UPS) more broadly, and autophagy. Briefly, HEK293 cells were transfected with the mutTDP-43 construct and the *hR23A*, *hR23B*, or control miRNA. Drugs targeting the UPS or autophagy pathways were added thirty minutes after CHX (Figure 10F). Lysates were collected at 0 and 270 minutes of CHX and the amount

of mutTDP-43 remaining was determined. We found that inhibition of the proteasome by MG-132, the UPS by epoxomicin “epox”, and autophagy by 3-MA blocked the accelerated turnover by RAD-23 knockdown (Figure 10F-10G). In the vehicle (DMSO) condition, *hR23A* knockdown ( $p < 0.05$ ) and *hR23B* knockdown ( $p < 0.01$ ) reduced the amount of mutTDP-43 remaining after 270 minutes of CHX by ~50% compared to control. These data suggest that the enhanced clearance of mutTDP-43 by reducing RAD-23 is mediated by the UPS and autophagy. This is in accordance with recent work showing that mutTDP-43 is degraded by both the UPS and autophagy (Scotter et al., 2014).

We reasoned that the lack of discrimination between the UPS and autophagy pathways might be because reduced RAD-23 is affecting the process in a step upstream from degradation, such as ubiquitination. We examined total ubiquitinated protein in *hR23A*- and *hR23B*-null MEFs and found no difference from WT MEFs. However, there was increased flux of ubiquitinated substrates through the proteasome in *hR23A*- and *hR23B*-null MEFs (Figure 10H) because inhibiting the proteasome with MG-132 led to a higher accumulation of non-degraded ubiquitinated substrates. We determined the ubiquitination status of mutTDP-43 following RAD-23 knockdown in HEK293 cells and found an increase in the ubiquitination of mutTDP-43 (Figure 10I). We also examined ubiquitination of mutTDP-43 +/- MG-132 to estimate flux of the ubiquitinated substrates through the proteasome. We found that the MG-132 induction ratio of polyubiquitinated TDP-43 was increased following RAD-23 knockdown by ~50% compared to WT (Figure 10J-10K). This suggests that the increased level of polyubiquitinated mutTDP-43 correlates with increased flux through the proteasome. In sum, these data suggest that

hR23A and hR23B normally inhibit the ubiquitination of mutTDP-43 and hinder its proteasomal degradation.

### **Loss of *rad-23* decreases mutTDP-43 and mutSOD1 insolubility**

Since TDP-43 inclusions are made up of insoluble TDP-43 aggregates, we investigated the effect of reducing RAD-23 on TDP-43 solubility *in vivo* and *in vitro*. In *C. elegans*, we found that loss of *rad-23* resulted in a decrease of total insoluble TDP-43 (Figure 11A). We detected a decrease in phospho-TDP-43 levels in *C. elegans* in the loss of *rad-23* background (Figure 11B) and phospho-TDP-43 has been implicated as the toxic species in ALS (Neumann et al., 2009). We overexpressed hR23A or hR23B in HEK293 cells and looked at the effect on mutTDP-43 solubility compared to a LacZ transfection control. We found that overexpression of hR23A increased the insolubility of mutTDP-43 (Figure 11C). We measured *hTDP43* mRNA abundance in hTDP43-expressing *C. elegans* in WT and loss of *rad-23* backgrounds. We found a significant increase in *hTDP-43* mRNA compared to WT in the loss of *rad-23* background (Figure 11D). These data are consistent with the known negative autoregulation of TDP-43 on its mRNA (Avendando-Vasquez et al., 2012; Polymenidou et al., 2011).

To test our hypothesis that the other suppressors identified in our candidate gene approach were via independent pathways, we examined the ability of loss of *ufd-2* (*tm1380*) to reduce mutTDP-43 abundance on its own and with loss of *rad-23*. We found that loss of *ufd-2* (*tm1380*) also reduced mutTDP-43 protein abundance and the abundance of phosphorylated mutTDP-43 in *C. elegans*, although the effect was smaller than loss of *rad-23* (*tm3690*). Meanwhile, when loss of *ufd-2* and loss of *rad-23* are both placed on the mutTDP-43 background, loss of *ufd-2* (*tm1380*) and *rad-23* (*tm3690*)

together caused an even greater effect (Figure 11E) than when either gene is mutated on its own.

The correctly folded conformation of a protein is in equilibrium with multiple misfolded conformations, and these later species are prone to aggregate into oligomers and higher order structures. The dwell time of misfolded conformations is a function of the free energy barriers between states and generally increases as aggregates form (Fawzi et al., 2008). This can be probed by examining the fluorescence recovery time after photobleaching (FRAP) of fluorescently tagged misfolding-prone proteins. Misfolded proteins become less mobile within cells and have a slower recovery time following photobleaching (Wang *et al.*, 2009; Scotter *et al.*, 2014). We examined the ability of mutSOD1 tagged with YFP in the *C. elegans* nervous system to recover following photobleaching in WT and loss of *rad-23* backgrounds *in vivo*. Loss of *rad-23* allowed for increased recovery of YFP-tagged mutSOD1 over WT (Figure 11F-11G;  $p < 0.05$ ). These data indicate that loss of *rad-23* leads to an increase in the pool of readily exchangeable and mobile mutSOD1. In sum, loss of *rad-23* leads to a decrease of soluble and insoluble species, as well as a reduction in the toxic phosphorylated TDP-43 species.

### **hR23A and hR23B are aberrantly expressed in human ALS spinal cord**

Changes in the abundance of RAD-23 could have pathophysiological relevance to human ALS. A single nucleotide polymorphism (SNP) was found to be correlated with changes in hR23A expression (Myers et al., 2007) and the same SNP was found to be associated with sporadic ALS (Cronin et al., 2007). In addition, a microarray study found that *hR23A* expression was increased in postmortem fALS spinal cord tissue compared

to controls (Dangond et al., 2004). To directly implicate our findings to the human condition, we compared hR23A and hR23B expression and localization in the spinal cords of sALS and fALS cases with spinal cords from non-neurodegenerative disease controls.

We found several alterations in the expression pattern of hR23A and hR23B in ALS tissue (Figure 12A-12C; Tables 4-5). hR23A and hR23B accumulated in deposits within the cytoplasm of motor neurons in both sALS and fALS cases (Figure 12B). In addition, hR23A and hR23B tended to accumulate in the nucleus more robustly in ALS cases than controls (Figure 12B). We also found substantially greater protein abundance of hR23A ( $p < 0.05$ ) and hR23B ( $p < 0.01$ ) in ALS spinal cord tissue (Figure 12C) compared to controls. Taken together, these data indicate that there is a mislocalization and accumulation of RAD-23 in human ALS pathology.



## DISCUSSION

We show that reducing RAD-23 abundance protects against the toxicity of two misfolding-prone proteins that cause ALS. Mechanistically, this is linked to increased mobility, accelerated degradation, and reduced steady-state levels of the toxic proteins (Figure 12D). This is likely to be directly relevant to the human condition because we detect increased levels of RAD23 in postmortem ALS spinal cord samples and RAD-23 is mislocalized in ALS motor neurons. Elevated RAD-23 levels lead to the accumulation of misfolded conformers by inhibiting their polyubiquitination and preventing their clearance through protein degradation pathways. These observations highlight the role of native proteins that modify the ubiquitination status of toxic proteins in human neurodegenerative disease.

RAD-23 was originally identified in yeast in a screen for genes that influence sensitivity to UV irradiation (Watkins et al., 1993). Subsequent work demonstrated that RAD-23 plays a critical role in protein homeostasis (Schauber et al., 1998). A unified picture of RAD-23 function in protein turnover has not emerged, however, due to: 1) the diversity of platforms employed to interrogate its function (purified proteasomes, yeast, mammalian cells including MEFs), 2) the variety of studied substrates (i.e. reporters such as ubiquitin fusion degradation substrates and various physiological clients), and 3) the recognition that the biological function of RAD-23 is exquisitely controlled by its expression level and the stoichiometry with other proteins in the UPS (Verma et al., 2004) (Table 6). Even when controlling for these factors, it is clear that endogenous RAD-23 accelerates the degradation of some substrates and stabilizes the abundance of other substrates. The features that distinguish these substrates is unknown.

The domain structure of RAD-23 implies a mechanism for its operation as a “shuttle factor.” The RAD-23 ubiquitin-associated domain (UBA) binds to ubiquitin chains of client proteins (Chen et al., 2001; Wilkinson et al., 2001; Chen and Madura, 2002) and brings them to the proteasome via the interaction of the RAD-23 ubiquitin-like domain (UBL) and RPN-10, a subunit of the 19S cap of the proteasome (Schauber et al., 1998; van Laar et al., 2002). In parallel with this activity, RAD-23 also acts as a protein stabilization factor by binding polyubiquitin chains of specific lengths and blocking further chain elongation and/or remodeling, events required for efficient client degradation (Raasi and Pickart, 2003). RAD-23 was shown to stabilize the NER factor, RAD-4, in yeast and mammals by inhibiting its ubiquitination (Lommel et al., 2002; Ng et al., 2003) and RAD-23 can also prevent the clearance of other disease-related proteins (Blount et al., 2014).

Overexpression of RAD-23 can inhibit ubiquitin chain elongation (Ortolan et al., 2000; Ortolan et al., 2004). We find increased steady-state levels of ubiquitinated mutTDP-43 in RAD-23 knockdown cells and this is associated with enhanced flux through the UPS. This agrees with studies following the degradation of the reporter substrate Ub<sup>V96</sup>-V-βgal in yeast lacking *rad-23* (Rao and Sastry, 2002). In addition, we find that ubiquitinated mutTDP-43 is also a target of the autophagic pathway and this is in line with work using other aggregation-prone proteins (Lu et al., 2014). We hypothesize that endogenous RAD-23 binds to a select population of ubiquitinated substrates and impedes their degradation by controlling the remodeling of ubiquitin chains. In the absence of RAD-23, ubiquitin chain maturation is unleashed and substrate flux is enhanced (Lambertson et al., 1999; Verma et al., 2004).

Past work has also identified RAD-23 proteins as forming inclusions in a handful of neurodegenerative diseases, including Huntington's disease, Parkinson's disease, and several forms of ataxia (Bergink et al., 2006). Taken together, interventions which reduce the abundance of RAD-23 or its association with specific substrates are predicted to be therapeutic for diseases caused by the accumulation of misfolded proteins.

## TABLE LEGENDS

### **Table 3.1. Mammalian ERAD genes and their predicted orthologs in *C. elegans*.**

There are ~25 ERAD genes predicted to be conserved in *C. elegans*. Of these, viable mutants are available in many and were used in a candidate gene approach to identify novel modifiers of mutTDP-43 toxicity in *C. elegans*. Components in bold have no available mutants.

**Table 3.2. List of primers used in genotyping *C. elegans* strains.** A table of all of the primers used in genotyping the *C. elegans* strains used in this study. Further information available upon request.

**Table 3.3. A list of the *C. elegans* strains used in this study.** A table of all of the *C. elegans* strains used in their study and their corresponding information.

**Table 3.4. Description of human ALS cases used for staining and expression analysis.** The 12 ALS cases from which postmortem spinal cord tissue was taken following autopsy. UE: upper extremities; LE: lower extremities; sALS = sporadic ALS; fALS = familial ALS (i.e. positive family history). ALS cases in Figure 12C were loaded in Western blot in this order: JH79, JH82, JH74, JH74, JH83.

**Table 3.5. Description of control cases used for staining and expression analysis.** The 9 control cases from which postmortem spinal cord tissue was taken following autopsy. Control Case #1 in Figure 12A was 78 and Control Case #2 in Figure 12 A was 23. Control cases in Figure 12C were loaded in Western blot in this order: 6, 23, 67, 31, 26.

**Table 3.6. RAD-23 has opposing roles on substrate stabilization.** Table summarizing past findings on RAD-23 manipulation and substrate turnover.

## FIGURE LEGENDS

**Figure 3.1. Locomotor defects of *C. elegans* models of ALS and their modification by the loss of ERAD and UPS genes.** (A) Pronounced defects in locomotion were seen in the animals overexpressing mutSOD1, wtTDP-43, and mutTDP-43 in the nervous system in comparison with N2 (WT) ( $F_{(4,20)} = 36.75$ ,  $p < 0.0001$ ) (\* $p < 0.05$ ; \*\*\*\* $p < 0.001$ , Dunnett's multiple comparison test). (B) Locomotion of mutTDP-43 animals in the background of mutant ERAD and UPS alleles. Average speed of animals of indicated genotypes in a 30 second forced swimming assay in M9. Both suppressors and enhancers were found. No change: there was no significant change in the locomotor deficit of that background ( $p > 0.05$ , Student's *t-test*); Enhancer: there was a significant decrease in the average speed of the animals ( $p < 0.05$ , Student's *t-test*). Suppressor: there was a significant increase in the average locomotor speed of those animals ( $p < 0.05$ , Student's *t-test*). Note: *cdc-48.1* (*tm544*); *cdc-48.2* (*tm659*) mutants are synthetic lethal and therefore the effect of both mutants together cannot be tested in this study. (C) Loss of *rad-23* and *ufd-2* suppress mutTDP-43 toxicity via independent pathways. Average speed of animals of indicated genotypes in a 30 second forced swimming assay in M9. A one-way ANOVA reveals group differences in the average speed of mutTDP-43, mutTDP-43; *rad-23* (*tm3690*), mutTDP-43; *ufd-2* (*tm1380*), and mutTDP-43; *rad-23* (*tm3690*); *ufd-2* (*tm1380*) ( $F_{(3,16)} = 13.41$ ;  $p = 0.0001$ ). \* $p < 0.05$ , \*\*\*\* $p < 0.001$ . (D) Loss of *rad-23* and *ufd-3* suppress mutTDP-43 toxicity via independent pathways. Average speed of animals of indicated genotypes in a 30 second forced swimming assay in M9. A one-way ANOVA reveals group differences in the average speed of mutTDP-43, mutTDP-43; *rad-23* (*tm3690*), mutTDP-43; *ufd-3* (*tm2915*), and mutTDP-43;

*rad-23 (tm3690); ufd-3 (tm2915)* ( $F_{(3,16)} = 60.55$ ;  $p < 0.0001$ ). \* $p < 0.05$ , \*\*  $p < 0.01$ ; \*\*\*\* $p < 0.001$ .

**Figure 3.2. Loss of *rad-23* in *C. elegans* protects against models of ALS via an effect in the nervous system.** (A) Schematic of *C. elegans* RAD-23 gene with predicted protein shown. Lines represent areas with insertions and/or deletions in the used mutants. (C-D) Loss of *rad-23 (tm2595)* (C) or *(tm3690)* (D) causes a two-fold suppression in the locomotor deficit of mutTDP-43, but has no effect on wtTDP-43 ( $p = 0.108$  for *tm2595* and  $p = 0.473$  for *tm3690*). (E-F) Loss of *rad-23 (tm2595)* (E) or *(tm3690)* (F) leads to a two-fold suppression in the locomotor deficit of mutSOD1 animals, but has no effect on the wtSOD1 animals ( $p = 0.615$  for *tm2595* and  $p = 0.274$  for *tm3690*). (F) Neither *rad-23* allele is different from WT speed in the swimming assay. ( $F_{(2,12)}=0.006579$ ;  $p = 0.9934$ ) (G) mutSOD1 fed *rad-23* RNAi for two generations shows no change ( $p = 0.7748$ ), but mutSOD1; *sid-1*;  $P_{\text{neuron}}::\text{SID-1}$  animals show a significant improvement. (H) Outcrossing the *rad-23 (tm3690)* allele from mutTDP-43; *tm3690* leads to a rescue of the mutTDP-43 locomotor deficit. (I) Overexpression of RAD-23 in the nervous system of mutTDP-43; *rad-23 (tm3690)* is sufficient to rescue the mutTDP-43 locomotor deficit. (J) There is no change in the average locomotor speed of the mutTDP43 animals when RAD-23 is overexpressed in the nervous system ( $F_{(5,24)}=1.112$ ;  $p = 0.3801$ ). \* $p < 0.05$ , \*\* $p < 0.01$ , \*\*\* $p < 0.005$ , Student's *t*-test.

**Figure 3.3. Loss of *rad-23* in *C. elegans* protects against neurodegeneration following expression of mutTDP-43 *in vivo*.** We generated animals with GABAergic motor neurons labeled with GFP using  $P_{\text{unc-25}}::\text{GFP}$  in WT (N2; "control"), mutTDP-43, and mutTDP-43; *rad-23 (tm3690)* backgrounds. (A) Loss of *rad-23* reduces the percentage of *C. elegans* with mutTDP-43 that display broadening of axons. (B)

mutTDP-43 causes an increase in the number of gaps within the ventral nerve cord of animals compared to control ( $***p < 0.005$ , Dunnett's multiple comparison test following one-way ANOVA). Loss of *rad-23* reduces the number of ventral nerve cord gaps in the mutTDP-43 animals to WT. There is no significant difference in the number of gaps in mutTDP-43; *rad-23* animals compared to controls. (C) Representative images of WT, mutTDP-43, and mutTDP-43; *rad-23 (tm3690)* animals labeled with  $P_{unc-25}::GFP$ .

**Figure 3.4. RAD-23 protein is expressed throughout the worm, including the worm nervous system.** (A-C) A RAD-23 protein translational fusion with GFP driven by the endogenous *rad-23* promoter ( $P_{RAD-23}::RAD-23::GFP$ ) is expressed throughout the worm in young adult animals. (D) RAD-23 protein is expressed in the cell body and processes of a mechanosensory neuron (arrowhead), (E) vulva of the worm, (F) nerve cord (arrowhead), and (G) the head.

**Figure 3.5. Loss of RAD-23 in *C. elegans* protects against aging decline and proteotoxicity.** (A-D) Biomechanical profiling of N2 (WT) and *rad-23 (tm3690)* animals ( $n \geq 10$ /group). There is no difference between WT and *rad-23 (tm3690)* in speed (A), force (B), and power (C) at L4 through 3 days post L4. At 4 and 5 days post L4, *rad-23* animals perform better in speed (A), force (B), and power (C) measurements than WT. (D) *Rad-23* animals show a more coordinated biomechanical profile at 5 days post L4 than WT. (E) The lifespan of *rad-23* animals is extended by 22.2% compared to WT on tunicamycin ( $p < 0.0001$ ), but the lifespans of WT and *rad-23* are identical on vehicle ( $p = 0.646$ ). (F) *Rad-23* animals show a ~25% lifespan extension during heat stress compared to WT ( $p < 0.0001$ ). (G) There are no group differences in survival among WT, wtTDP-43, mutTDP-43, wtSOD1, and mutSOD1 with increasing doses of UV ( $F_{(4,15)}=0.1285$ ;  $p = 0.9697$ ). There are group differences among WT, *rad-23 (tm2595)*



and *tm3690*), and mutTDP-43 and mutSOD1 in the *rad-23 (tm3690)* background ( $F_{(6,21)}=2.961, p < 0.05$ ). As predicted, loss of *rad-23 (tm2595 and tm3690)* causes a hypersensitivity to UV stress compared to wild type animals ( $p < 0.001$ ). mutTDP-43 and mutSOD1 in the loss of *rad-23* background show a synthetic hypersensitivity to UV stress ( $p < 0.001$ ). \* $p < 0.05$ , \*\* $p < 0.01$ , \*\*\* $p < 0.005$ , \*\*\*\* $p < 0.001$ ; Student's *t*-test.

**Figure 3.6. Loss of *rad-23* does not suppress the *C. elegans* mutTDP-43 locomotor deficit via known pathways.** Loss of (A), *xpa-1* (A), or *ercc-1* (B), or *csb-1* (C), or *png-1* (D) do not protect against the locomotor deficit caused by mutTDP-43 in the swimming assay ( $p > 0.05$ , Student's *t*-test). Experiments were all completed three times on independent days. One representative experiment is shown. Description of alleles: *ok698* - 913bp deletion; *tm2073* - 804bp deletion; *ok2335* - 1620bp deletion; and *cy9* - single nucleotide polymorphism.

**Figure 3.7. Knockdown of RAD-23 orthologs in mammalian motor neurons protects against toxicity of mutSOD1 or mutTDP-43.** (A-E) *hR23A* or *hR23B* miRNA knocks down endogenous target in HEK293 cells ( $n=3/\text{group}$ ), but does not knock down the expression of a co-transfected GFP plasmid. \* $p < 0.05$ , \*\* $p < 0.01$ . (F) HSV infection of miRNA to *hR23A* or *hR23B* in mixed spinal cord cultures leads to specific knock down of target protein compared to control. (G) Infection of mixed spinal cord cultures with LacZ or a *hR23A*, *hR23B*, or control miRNA has no effect on survival ( $F_{(3,12)}=0.8132, p = 0.3166$ ). Knockdown of *hR23A* or *hR23B* protects against motor neuron death caused by wtSOD1 ( $F_{(3,12)}=17.39, p = 0.0001$ ) and mutSOD1 ( $F_{(3,12)}=54.64, p < 0.0001$ ). (H) Infection of mixed spinal cord cultures with LacZ or a scrambled, *hR23A*, or *hR23B* miRNA has no effect on motor neuron survival ( $F_{(3,12)}= 0.8875, p = 0.2100$ ). Knockdown of *hR23A* or *hR23B* protects against motor neuron death caused by wtTDP-43

( $F_{(3,12)}=16.66$ ,  $p = 0.0001$ ) and mutTDP-43 ( $F_{(3,12)} = 48.07$ ;  $p < 0.0001$ ).  $**p < 0.01$ ,  $*** p < 0.005$ ,  $****p < 0.001$ . (I) Representative brightfield images of mixed spinal cord cultures infected as indicated stained for a SMI-32 motor neuron marker. Co-infection of mutSOD1 cultures with HSV-miRNA to *hR23A* or *hR23B* increases motor neuron survival. (J) Knockdown of *hR23A* or *hR23B* protects against motor neuron death caused by mutSOD1 ( $F_{(2,6)}=13.99$ ,  $p = 0.0055$ ), but has no effect on survival in motor neurons infected with LacZ ( $F_{(2,6)}=4.745$ ,  $p = 0.0581$ ) in cultures treated with vehicle. Knockdown of *hR23B* protects cultures infected with HSV-LacZ ( $F_{(2,6)}=11.82$ ,  $p = 0.0083$ ) or HSV-mutSOD1 ( $F_{(2,6)}=101.9$ ,  $p < 0.0001$ ) from toxicity of ER stress caused by tunicamycin.

**Figure 3.8. *hR23A* expression is increased in the spinal cord of mutSOD1 mice at P90 and P120.** (A-B) Representative Western blot (A) and quantification ( $n=3-5$ /group) (B) of *hR23A* expression in the spinal cord and brain of age-matched males. *hR23A* expression is increased in the spinal cord of mutSOD1 mice compared to WT (C57Bl6) at P90 and P120, but not at P60. (C-D) Representative Western blot (C) and quantification ( $n=3-5$ /group) (D) of *hR23B* expression in the spinal cord and brain of age-matched males. There is no change in *hR23B* expression in the spinal cord or brain at P60, P90, or P120. (E-F) (E) Representative Western blot and (F) quantification of phosphorylated eIF2 $\alpha$  (p-eIF2 $\alpha$ ) expression in the spinal cord and brain of age-matched animals ( $n=4$ /group). There is an increase in phosphorylated eIF2 $\alpha$  (p-eIF2 $\alpha$ ) expression in the spinal cord at P60 in G93A mice, but not in the brain.  $*p < 0.05$ ,  $**p < 0.01$ , Student's *t*-test.

**Figure 3.9. Manipulations of RAD-23 expression change TDP-43 and SOD1 abundance and solubility.** (A-B) Representative Western blot (A) and quantification

(B) of the amount of total mutTDP-43 following overexpression or knockdown of *hR23A* or *hR23B*. There is a ~90% decrease ( $p < 0.005$ ) in the abundance of mutTDP-43 following knockdown of *hR23A* or *hR23B*. (C) There is no change in the amount of *hTDP-43* mRNA normalized to *actin* in HEK293 cells following *hR23A* or *hR23B* knockdown (n=3/group). *hTDP-43* mRNA from untransfected cells was subtracted from all values. (D) Representative Western blot of mutTDP-43 expression for the indicated time points following cycloheximide (CHX) treatment with either a control or *hR23A* miRNA. ( $F_{(2,8)}=0.1380$ ;  $p = 0.8732$ ) (E) Quantification (n=4 independent experiments) of % of starting mutTDP-43 remaining. (F) Representative Western blot of mutSOD1 expression for the indicated time points following CHX with either a control or *hR23A* miRNA. (G) Quantification (n=3 independent experiments) of % of starting mutSOD1 remaining. (H-I) Knockdown of *hR23A* further reduces % of starting mutTDP-43 remaining after 270 minutes of CHX (n=3 independent experiments). ( $*p < 0.5$ ) (H) Representative Western blot and (I) quantification of mutTDP-43 remaining after 270 minutes of CHX in the presence of the indicated miRNA. (J) Amount of mutTDP-43 remaining is reduced after 180 minutes of CHX in *hR23A*- and *hR23B*-null mouse embryonic fibroblasts (MEFs) compared to WT. (K) WT or *hR23B*-null (*hR23B*<sup>-/-</sup>) were co-transfected with mutTDP-43 construct and LacZ or full length (FL) *hR23B* construct. Media was changed 24 hours later and cells were re-plated at equal densities another 24 hours later. Cycloheximide was then added 24 hours after re-plating for indicated periods of time. Samples were processed for Western blot and probed with myc and actin antibodies. (L) Representative Western blot of CPY\*-GFP expression for the indicated time points following CHX treatment with indicated miRNA  $*p < 0.05$ ,  $**p < 0.01$ , Student's *t*-test.

**Figure 3.10. Loss of RAD-23 accelerates turnover through the proteasome and autophagy by increasing ubiquitination.** (A) Representative Western blot of mutSOD1 turnover rate in neurons at 0' and 180' of cycloheximide (CHX). Mixed spinal cord culture neurons were infected with HSV to express mutSOD1 and *hR23A*, *hR23B*, or control miRNA. (B-D) Co-transfection of RNAi-resistant *hR23A* and *hR23B* cDNAs prevents reduced mutTDP-43 in *hR23A* and *hR23B* knockdown conditions. (B) Western blot image; *hR23A* miRNA knocks down endogenous *hR23A* compared to control miRNA, but does not knock down RNAi-resistant *hR23A* (*hR23A<sup>res</sup>*) cDNA. (C) Western blot image; *hR23B* miRNA knocks down endogenous *hR23B* compared to control miRNA, but does not knock down RNAi-resistant *hR23B* (*hR23B<sup>res</sup>*) cDNA. (D) Co-transfection of a *hR23A* or *hR23B* miRNA dramatically decreases total mutTDP-43 protein compared to control. This is blocked by co-transfection with *hR23A<sup>res</sup>* or *hR23B<sup>res</sup>* cDNA. (E) Meso Scale Discovery (MSD) assays to determine the binding of *hR23A* and TDP-43 in transfected HEK293 cells. All samples were normalized to *hR23A*/pcDNA binding signal lysates. Anti-V5 was used as a capture antibody for the binding of TDP-43 from transfected cell lysates and anti-TDP-43 was used to capture binding of *hR23A* from transfected cell lysates. Western blot analysis of protein expression levels in transfected cell lysates is also depicted. \* $p < 0.05$ , \*\* $p < 0.01$ , Student's *t*-test. (F) HEK293 cells were transfected with mutTDP-43 and *hR23A*, *hR23B*, or control miRNA. CHX was added for 4.5 hours and indicated drug was added 30' after CHX. Representative Western blots for indicated experiments are shown. (G) Quantification of Western blots. Treatment with MG-132, epoxomicin ("epox"), and 3-MA blocked the turnover of mut-TDP43 by ~25%. (n=5 independent experiments for +scrambled miRNA; n=3 independent experiments for +*hR23A* miRNA; n=3 independent experiments for +*hR23B* miRNA). ( $F_{(8,20)}=3.156$ ;  $p = .0176$ ) \* $p < 0.05$ ; \*\* $p < 0.01$ . (H) Total polyubiquitinated

(polyUb) substrate load in indicated MEF lines following –MG-132 (DMSO) or +MG-132 treatment for 12 hours. MG-132 Induction Ratio: +MG-132/-MG-132 (all normalized to actin). (I) Representative Western blot of polyUb-mutTDP-43 following immunoprecipitation (IP) of myc-mutTDP-43. (J) Input showing total polyUb-load in HEK293 cells transfected with mutTDP-43 and indicated miRNA. Cells were treated with DMSO (-MG-132) or MG-132 (+MG-132) 12 hours before cell lysis as indicated. Myc-mutTDP-43 was immunoprecipitated and immunoblotted for ubiquitin and myc. (K) Quantification (n=3 independent experiments) of Western blots shown in panel I. Data was normalized to average control miRNA condition. There is an increase in ubiquitinated mutTDP-43 and its flux through the proteasome following RAD-23 knockdown.

**Figure 3.11. Loss of *rad-23* reduces TDP-43 and SOD1 insolubility.** (A)

Representative Western blot of hTDP-43 protein abundance following a sequential detergent extraction of *C. elegans* overexpressing mutTDP-43 in WT or *rad-23* backgrounds. Loss of *rad-23* causes a shift of TDP-43 to a more soluble (TX) fraction over insoluble (SARK, UREA) fractions. (B) There is a decrease of phospho-TDP-43 in the loss of *rad-23* background in soluble and insoluble fractions in *C. elegans*. (C) Representative Western blot showing there is an increase in the abundance of insoluble mutTDP-43 in HEK293 cells following co-transfection with the hR23A cDNA. (D) qPCR (n=3/group) measuring *hTDP-43* mRNA abundance normalized to *tba-1* in indicated strains. # = undetected, \*\**p* < 0.01. (E) *rad-23* (*tm3690*) and *ufd-2* (*tm1380*) cause an additive effect on reduced mutTDP-43 and phosphorylated-TDP43 abundance in *C. elegans*. (F-G) FRAP on mutSOD1-YFP aggregates within the *C. elegans* nervous system. MutSOD1-YFP has a higher rebound with loss of *rad-23*

(*tm3690*). (F) Representative images of FRAP assay. (G) Quantification of FRAP (n=14/group). Data are normalized to starting fluorescence intensity. \* $p < 0.05$ .

**Figure 3.12. hR23A and hR23B are aberrantly expressed in human ALS tissue.** (A-B) There is mislocalization of hR23A and hR23B in motor neurons of the spinal cord in ALS cases. (A) Representative images of motor neurons within the gray matter of spinal cord from control and ALS cases. Insets within ALS Case #2 depict granular cytoplasmic and nuclear staining often found in ALS cases. (B) Distribution of hR23A and hR23B cytoplasm and nuclear staining found in control (n=9) and ALS cases (n=12). (C) There is an increase in hR23A and hR23B protein expression in ALS (n=5) spinal cord sections compared to controls (n=5) (\*\* $p < 0.01$ , Student's *t*-test). (E) Proposed model. Loss of *rad-23* destabilizes aggregates allowing for them to become more soluble and more easily degraded.

**Table 3.1. Mammalian ERAD genes and their predicted orthologs in *C. elegans*.**

Mammalian Gene	Worm Gene	Putative Function	Mutant Available	Mutation Description	Comment
EDEM1	C47E12.3	Glycosylhydrolase-47 family	ok2898	378bp deletion	
EDEM2	F10C2.5	Glycosylhydrolase-47 family	tm6057	563bp deletion	Affects >1 gene
OS9	Y105E8A.2	Inspects client proteins for terminal $\alpha$ 1,6 linked mannose	tm5511	517bp deletion	Another allele for this gene, <i>tm3941</i> , causes lethality and sterility
TEB4	F55A3.1	DOA10 ligase component	gk218188	Introduces stop codon mid-gene	
Erasin	ZK353.8	DOA10 ligase component	tm3247	323bp deletion	Tested
HRD1	F55A11.3	E3 ubiquitin ligase	tm1743	473bp deletion + 38bp insertion	
HRDL-1	F26E4.11	E3 ubiquitin ligase	gk28	1981bp deletion	RNAi results in embryonic lethality
Derlin-1	F25D7.1	HRD ligase component; retrotranslocon	tm2839	224bp deletion	Tested
Derlin-2/Derlin-3	R151.6	HRD ligase component	tm5861	499bp deletion	
RNF5	C16C10.7	RMA1 ligase	tm794	647bp deletion	
p97 (VCP)	C06A1.1	Extractor	tm544	688bp deletion	Tested
p97 (VCP)	C41C4.8	Extractor	tm659	639bp deletion	Tested
UFD-2	T05H10.5	p97 (VCP) co-factor	tm1380	915bp deletion	Tested
UFD-3	C05C10.6	p97 (VCP) co-factor	tm2915	747bp deletion	Tested
RAD-23	ZK20.3	Proteasome adaptor	tm3690; tm2595	432bp deletion; 677bp deletion + 28bp insertion	Tested
UBQLN-2	F15C11.2a	Proteasome adaptor	tm1574	755bp deletion	Tested
<b>UBC-14</b>	<b>Y87G2A.9</b>	<b>E2-ubiquitin conjugating enzyme</b>	<b>None</b>		
<b>UBE2K</b>	<b>F40G9.3</b>	<b>Ubiquitin-conjugating enzyme</b>	<b>None</b>		
<b>UBE2G</b>	<b>F58A4.10.1</b>	<b>E2-ubiquitin conjugating enzyme</b>	<b>None</b>		
<b>ERManI</b>	<b>T03G11.4</b>	<b>Glycosylhydrolase-47 family</b>	<b>None</b>		
<b>Npl4</b>	<b>F59E12.5</b>	<b>Proteasome adaptor</b>	<b>None</b>		
<b>UFD-1</b>	<b>F19B6.2a</b>	<b>p97 (VCP) co-factor</b>	<b>None</b>		
<b>UBE2J1, UBE2J2</b>	<b>D1022.1a</b>	<b>E2-ubiquitin conjugating enzyme</b>	<b>None</b>		
<b>UBE2G2</b>	<b>Y87G2A.9</b>	<b>E2-ubiquitin conjugating enzyme</b>	<b>None</b>		

Table 3.2. List of primers used in genotyping *C. elegans* strains.

Gene	Allele	Primers (5'-3') Upper/Lower
<i>rad-23</i>	<i>tm2595</i>	CAGGATGGTTTTGTCCGTTAC ACATGCGAAATAAGCCTCCAC
	<i>tm3690</i>	AAGGCGATGAATACACATTCTTGG ATCGATAACCTGGATGAGGGATGG
<i>ufd-3</i>	<i>tm2915</i>	TTTTGGGCAATAGATGGAGGC AAATGCCCGAGCTTCTGG
<i>ufd-2</i>	<i>tm1380</i>	TACTTGGAGAGCCAACTTCGC ACAAAATCCATAGAAGATGCC
<i>cdc-48.1</i>	<i>tm544</i>	TTCCACGTGGTGGCTTGATAC AACCCGCATTACGTGCTC
<i>cdc-48.2</i>	<i>tm659</i>	ATGGAGCTGATTGATTTGGAG AACTTCATTGCCTCCTCGAAGTG
<i>derlin-1</i>	<i>tm2909</i>	TTCCATCTTGACCGTGAATACC ATATCTACTTCCTTCTCGAACCG
<i>ubxn-4</i>	<i>tm3247</i>	ACATGTTTGTCCGGCCTCTG AACTTTCAACACCTAGTCC
<i>ubql-1</i>	<i>tm1574</i>	GCATATTGAAGCTCGCGCG ACGGTGATTTACGTGAAC
<i>xpa-1</i>	<i>ok698</i>	GACCGTTGAGCTTATTGCAG TAACTTGTTGTGGCCATGCG
<i>csb-1</i>	<i>ok2335</i>	GAAGACTGATCATCGGAGCG GGCTGGGGGATTCAAATTAT
<i>ercc-1</i>	<i>tm2073</i>	TTCGGGTCGTCTATCTAG TTTTTGCGACATCCCTGGCG
<i>png-1</i>	<i>cy9</i>	GTCGATAATTTTACCGAATTTTCCAC TATCTCCAAGTGACGTCAACCAC



**Table 3.3. A list of the *C. elegans* strains used in this study.**

Strain Name	Backcrossed?	Co-Injection Marker	Description
<b>RK65</b>	5x	N/A	<i>tm3690</i>
<b>RK66</b>	5x	N/A	<i>tm2595</i>
<b>RK67</b>	N/A	N/A	mutTDP-43 (M337V); RK65 ( <i>tm3690</i> )
<b>RK68</b>	N/A	N/A	mutTDP-43 (M337V); RK66 ( <i>tm2595</i> )
<b>RK69</b>	N/A	N/A	wtTDP-43; RK65 ( <i>tm3690</i> )
<b>RK70</b>	N/A	N/A	wtTDP-43; RK66 ( <i>tm2595</i> )
<b>RK71</b>	N/A	N/A	mutSOD (G85R); RK65 ( <i>tm3690</i> )
<b>RK72</b>	N/A	N/A	mutSOD (G85R); RK66 ( <i>tm2595</i> )
<b>RK73</b>	N/A	N/A	wtSOD; RK65 ( <i>tm3690</i> )
<b>RK74</b>	N/A	N/A	wtSOD; RK65 ( <i>tm3690</i> )
<b>RK75</b>	N/A	N/A	mutTDP-43 (M337V); <i>png-1 (cy9)</i>
<b>RK76</b>	N/A	N/A	mutTDP-43 (M337V); <i>xpa-1 (ok698)</i>
<b>RK77</b>	N/A	N/A	mutTDP-43 (M337V); <i>csb-1 (tm2073)</i>
<b>RK78</b>	N/A	N/A	mutTDP-43 (M337V); <i>ercc-1 (ok2335)</i>
<b>RK79(rkEx1)</b>	N/A	None	P <sub>RAD23::</sub> RAD23::GFP  (fosmid injected at  5ng/μL)
<b>RK80</b>	5x	N/A	<i>tm2909</i>
<b>RK81</b>	5x	N/A	<i>tm1574</i>
<b>RK82</b>	5x	N/A	<i>tm2915</i>
<b>RK84</b>	5x	N/A	<i>tm544</i>

<b>RK85</b>	5x	N/A	<i>tm3247</i>
<b>RK86</b>	N/A	N/A	mutTDP-43 (M337V); RK81 ( <i>tm1574</i> )
<b>RK87</b>	N/A	N/A	mutSOD (G85R); RK81 ( <i>tm1574</i> )
<b>RK88</b>	N/A	N/A	mutTDP-43 (M337V); RK82 ( <i>tm2915</i> )
<b>RK91</b>	N/A	N/A	mutTDP-43 (M337V); RK84 ( <i>tm544</i> )
<b>RK92</b>	N/A	N/A	mutTDP-43 (M337V); RK85 ( <i>tm3247</i> )
<b>OG695(drEx230)</b>	N/A	P <sub>unc-119</sub> ::GFP (injected at 100ng/μL)	mutTDP-43 (M337V); P <sub>unc-119</sub> ::RAD23::unc54 3'UTR – LINE1 (construct injected at 30ng/μL)
<b>OG696(drEx231)</b>	N/A	P <sub>unc-119</sub> ::GFP (injected at 100ng/μL)	mutTDP-43 (M337V); P <sub>unc-119</sub> ::RAD23:: unc54 3'UTR – LINE2 (construct injected at 30ng/μL)
<b>OG697(drEx232)</b>	N/A	P <sub>unc-119</sub> ::GFP (injected at 100ng/μL)	mutTDP-43 (M337V); P <sub>unc-119</sub> ::RAD23:: unc54 3'UTR – LINE3 (construct injected at 30ng/μL)
<b>OG692(drEx227)</b>	N/A	P <sub>unc-119</sub> ::GFP (injected at 100ng/μL)	mutTDP-43 (M337V); <i>rad23</i> ( <i>tm3690</i> ); P <sub>unc-119</sub> ::RAD23:: unc54 3'UTR – LINE1 (construct injected at 30ng/μL)
<b>OG693(drEx228)</b>	N/A	P <sub>unc-119</sub> ::GFP (injected at 100ng/μL)	mutTDP-43 (M337V); <i>rad23</i> ( <i>tm3690</i> ); P <sub>unc-119</sub> ::RAD23:: unc54 3'UTR – LINE2 (construct injected at 30ng/μL)
<b>OG694(drEx229)</b>	N/A	P <sub>unc-119</sub> ::GFP (injected at 100ng/μL)	mutTDP-43 (M337V); <i>rad23</i> ( <i>tm3690</i> ); P <sub>unc-119</sub> ::RAD23:: unc54 3'UTR – LINE3 (injected at 30ng/μL)

**Figure 3.1. Locomotor defects of *C. elegans* models of ALS and their modification by the loss of ERAD and UPS genes.**

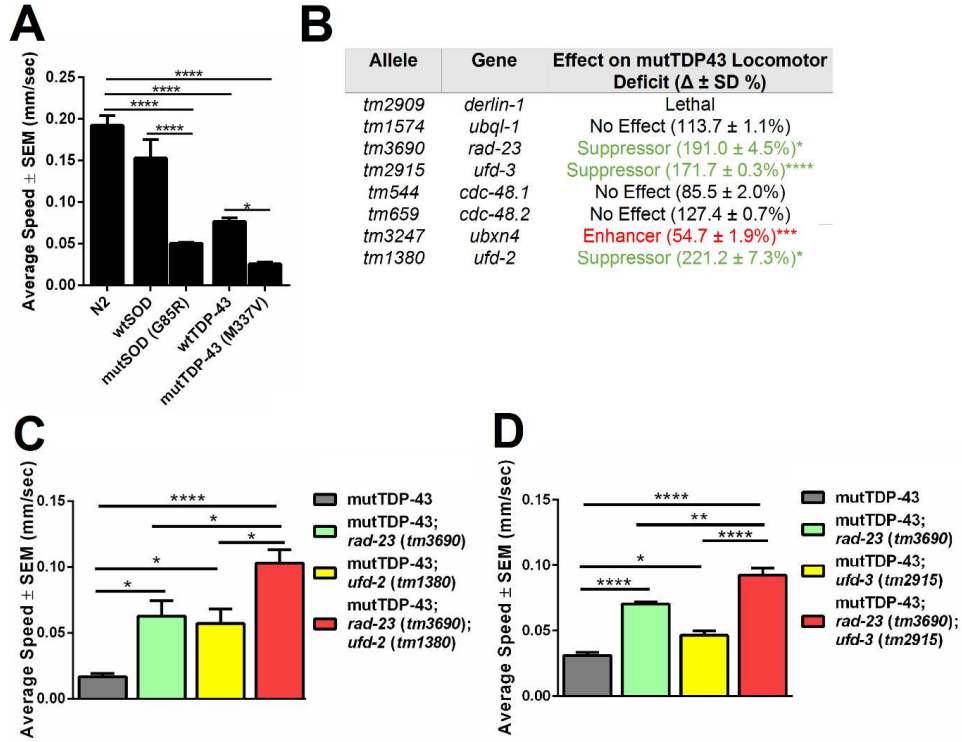
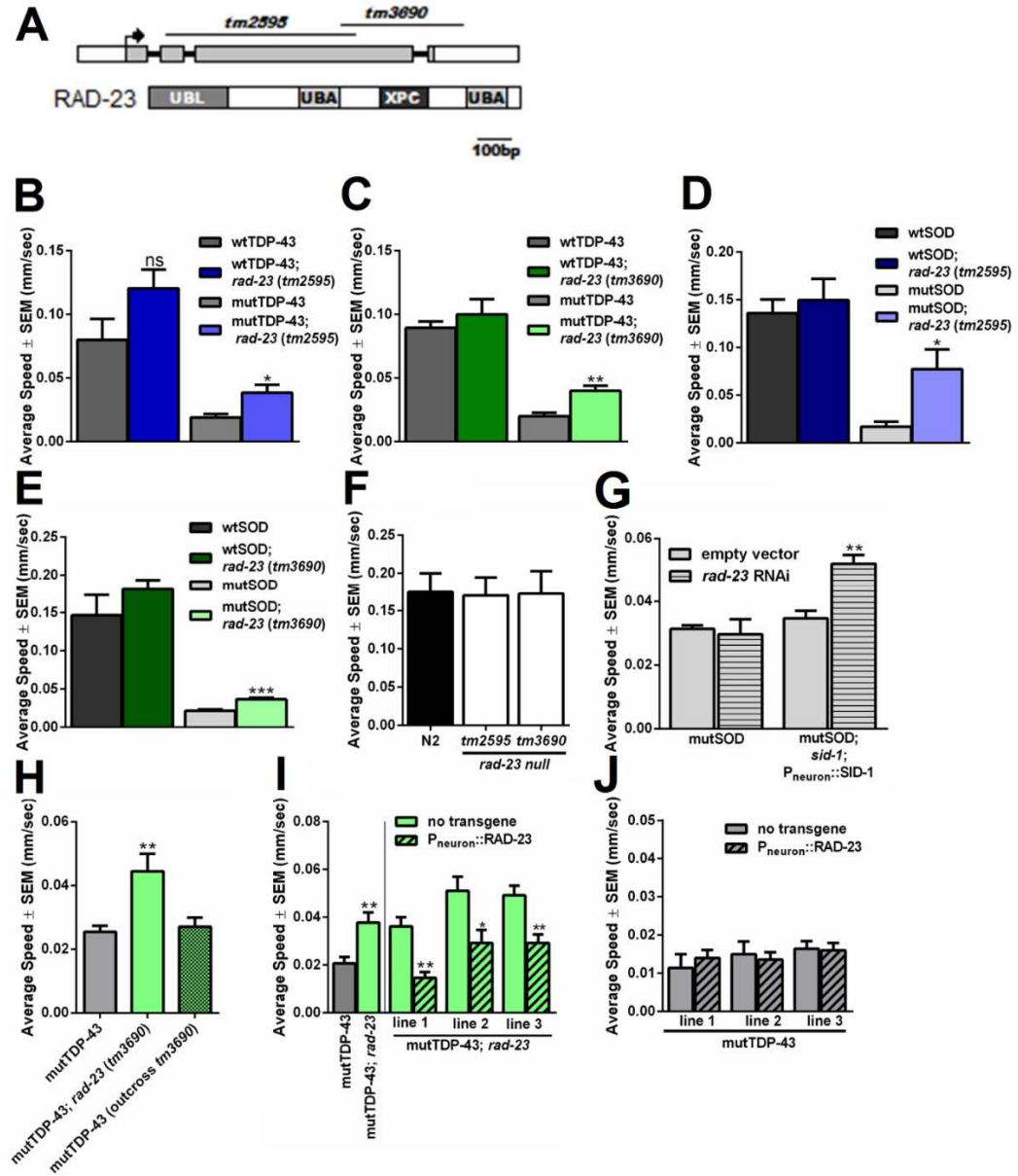


Figure 3.2. Loss of *rad-23* in *C. elegans* protects against models of ALS via an effect in the nervous system.



**Figure 3.3. Loss of *rad-23* in *C. elegans* protects against neurodegeneration following expression of *mutTDP-43* in vivo.**

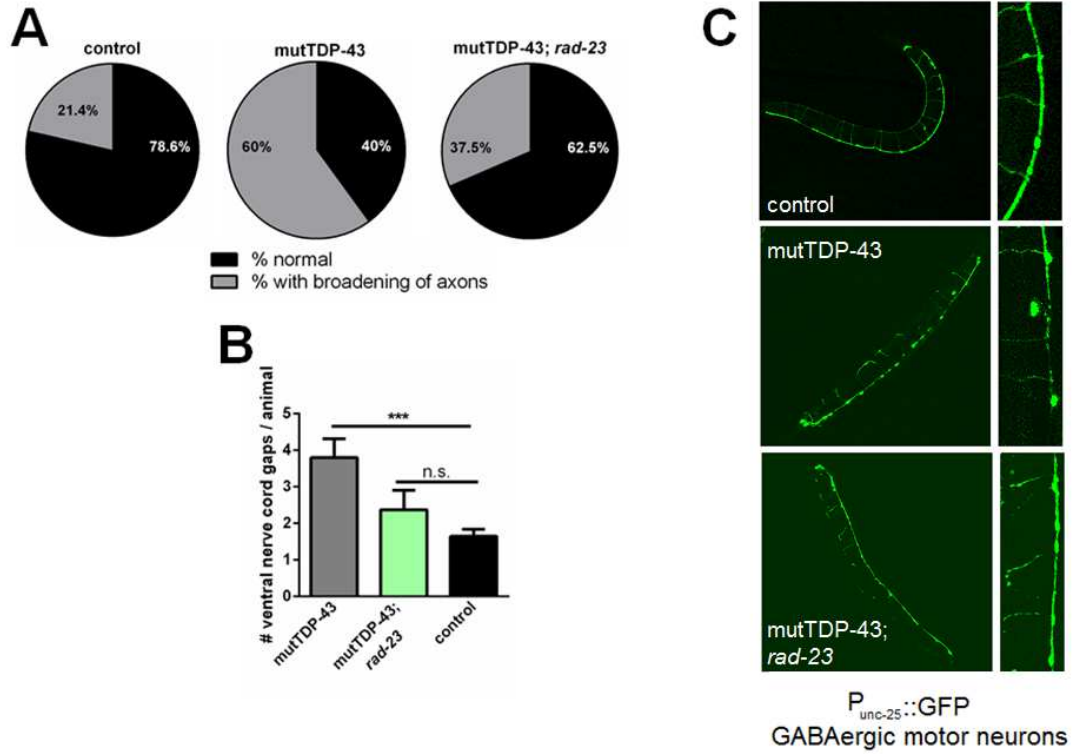
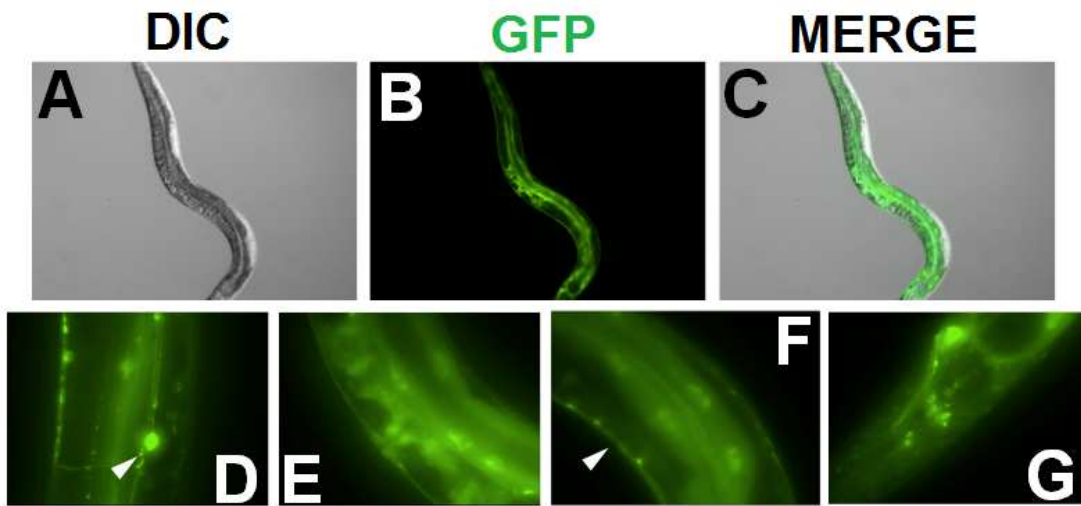


Figure 3.4. RAD-23 protein is expressed throughout the worm, including the worm nervous system.



**Figure 3.5. Loss of *RAD-23* in *C. elegans* protects against aging decline and proteotoxicity.**

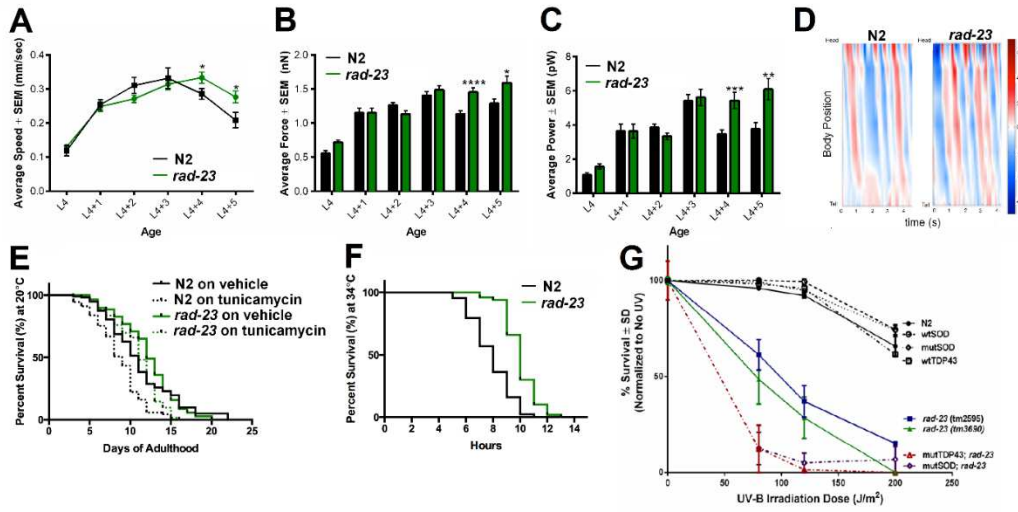
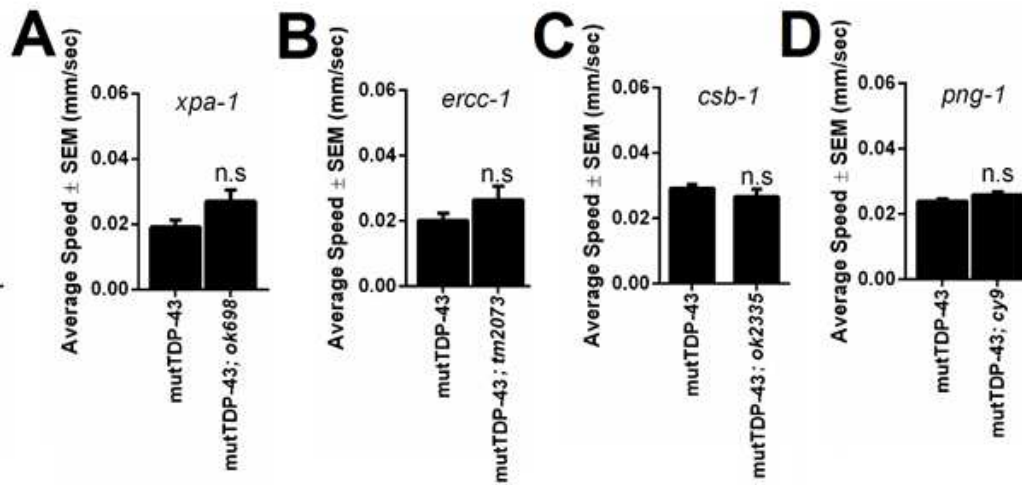
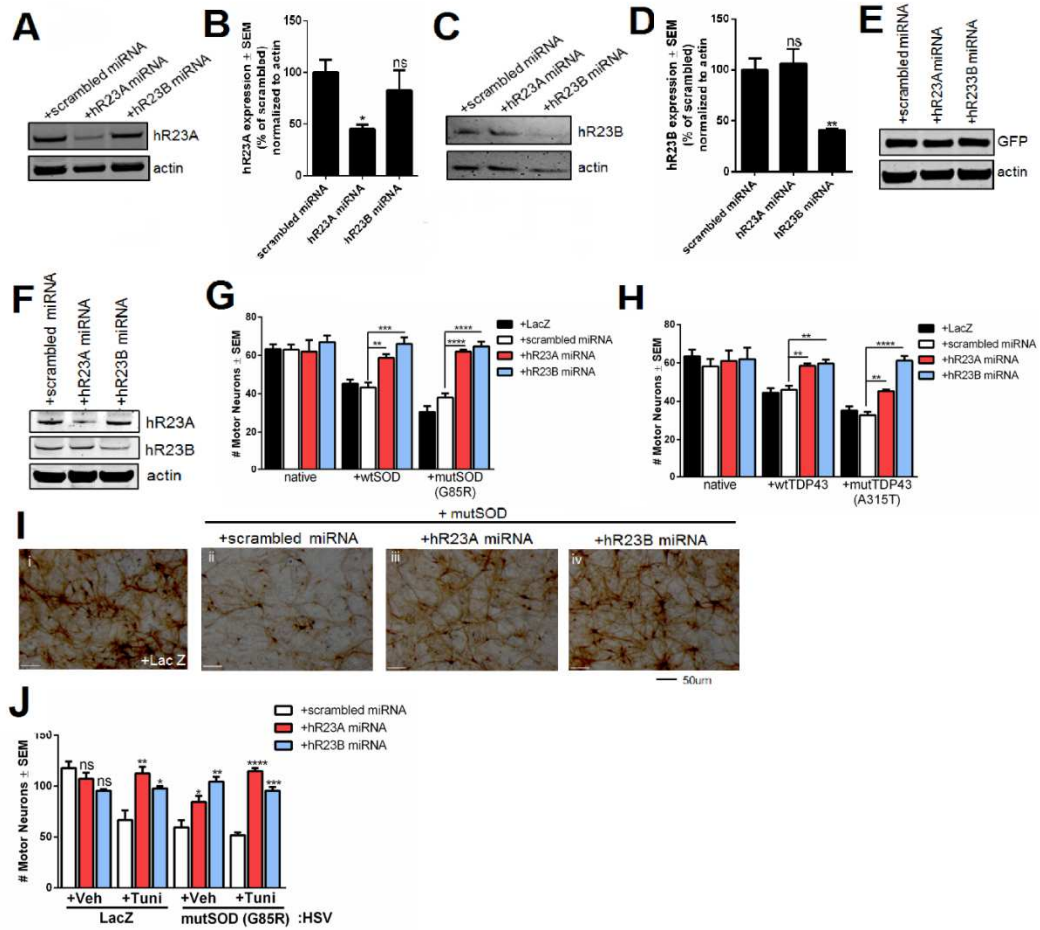


Figure 3.6. Loss of *rad-23* does not suppress the *C. elegans* *mutTDP-43* locomotor deficit via known pathways.





**Figure 3.7. Knockdown of RAD-23 orthologs in mammalian motor neurons protects against toxicity of mutSOD1 or mutTDP-43.**



**Figure 3.8. hR23A expression is increased in the spinal cord of mutSOD1 mice at P90 and P120.**

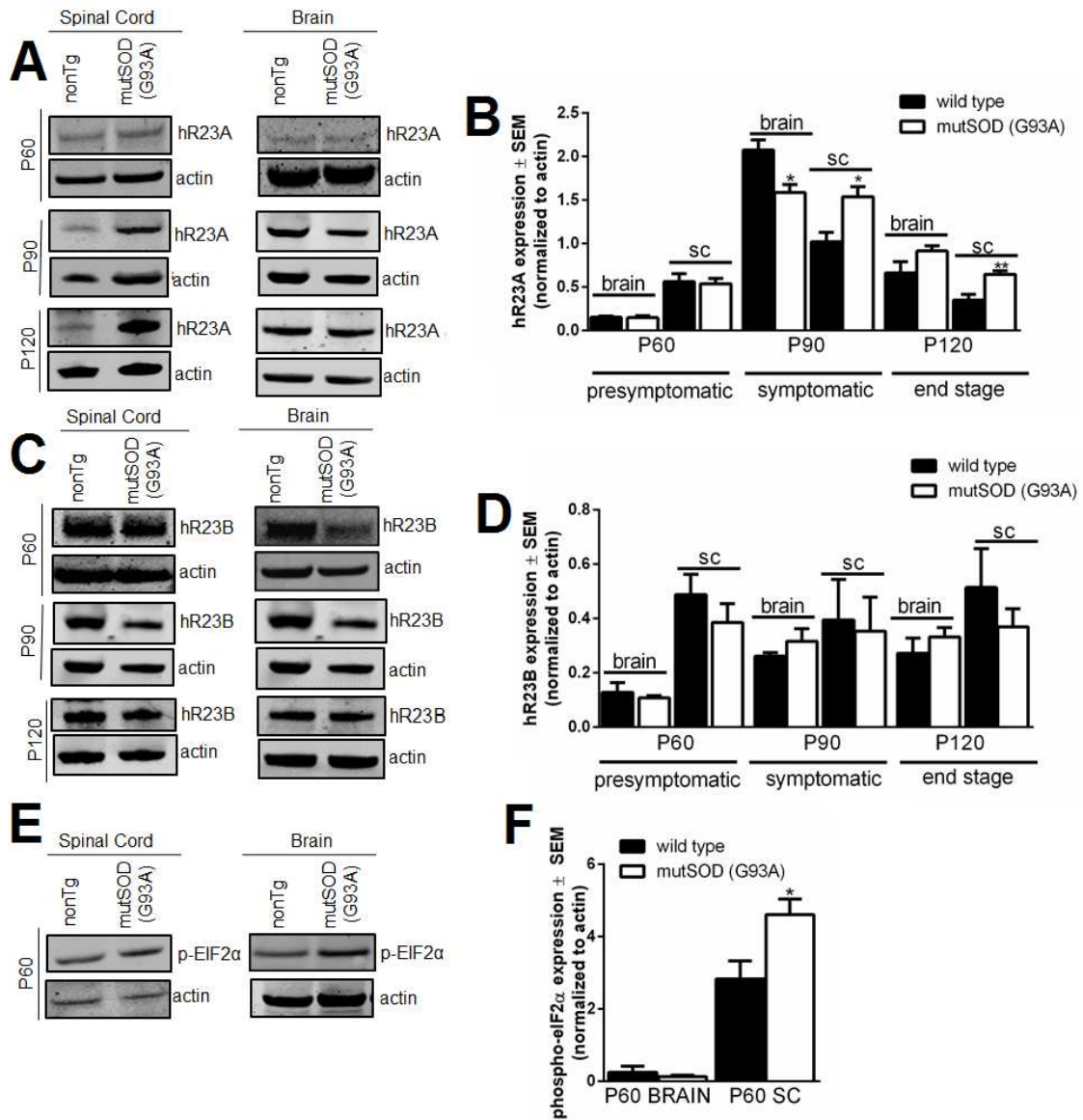


**Figure 3.9. Manipulations of RAD-23 expression change TDP-43 and SOD1 abundance and solubility.**

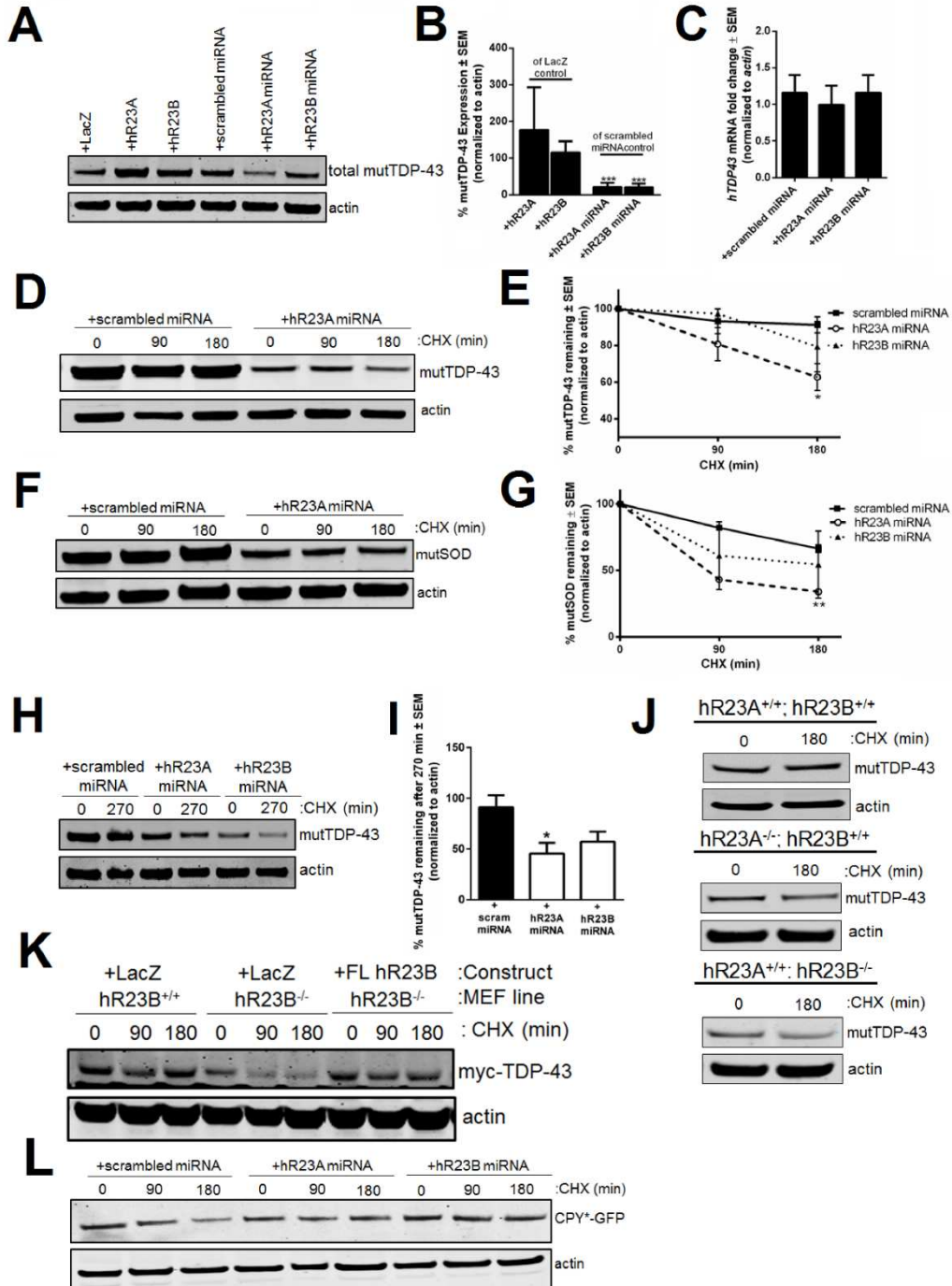


**Figure 3.10. Loss of RAD-23 accelerates turnover through the proteasome and autophagy by increasing ubiquitination.**

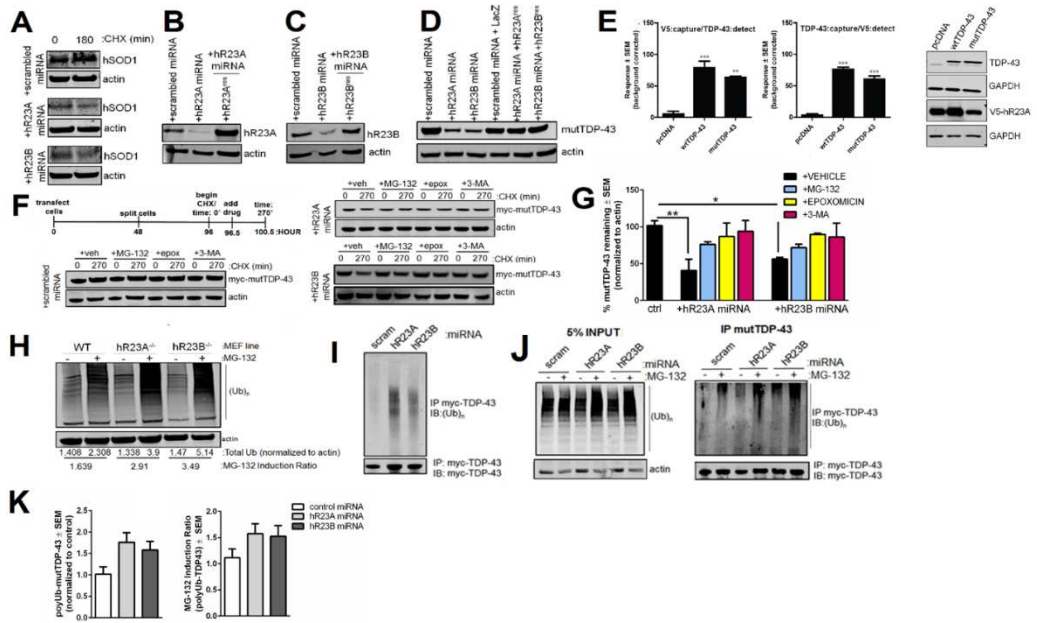


**Figure 3.11. Loss of *rad-23* reduces TDP-43 and SOD1 insolubility.**

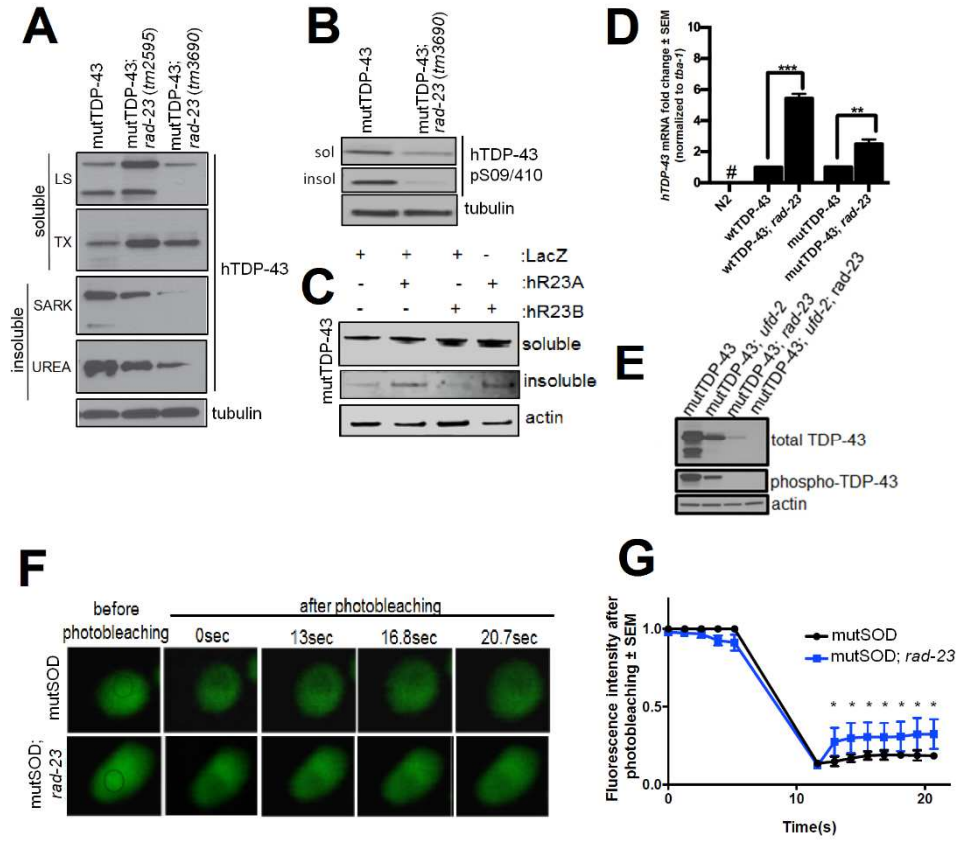
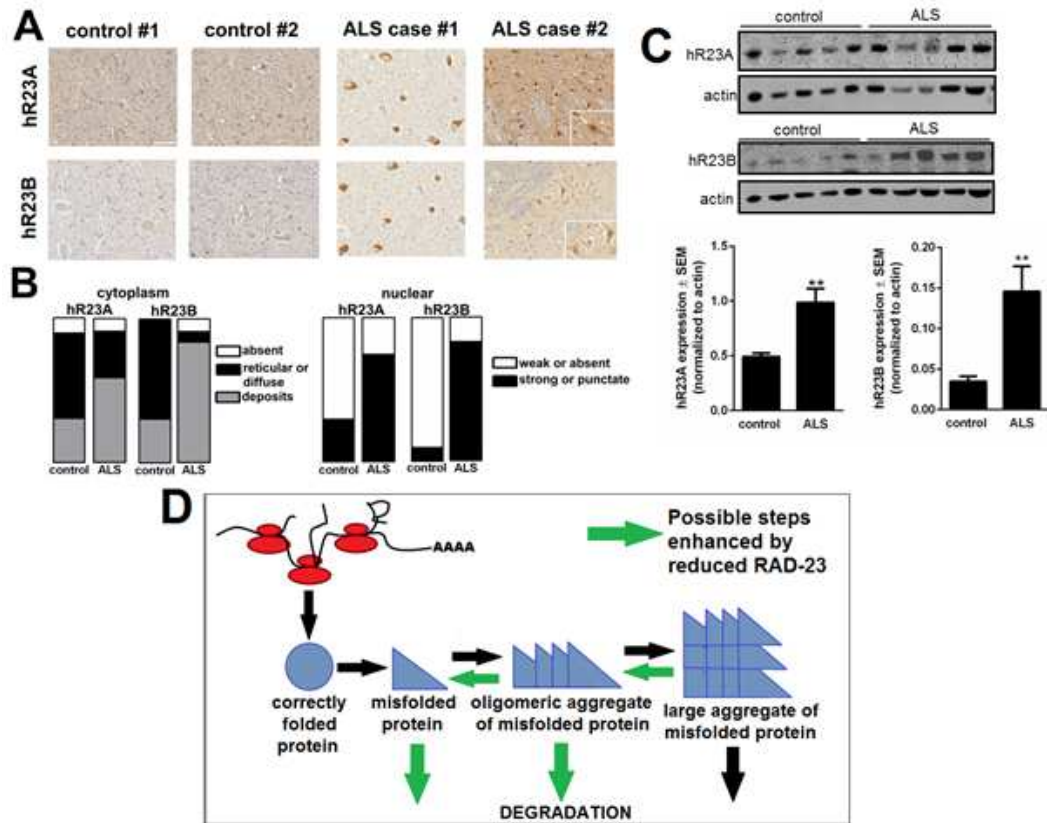


Figure 3.12. hR23A and hR23B are aberrantly expressed in human ALS tissue.



**Table 3.4. Description of human ALS cases used for staining and expression analysis.**

ALS Case	sALS or fALS?	Case Description	Age/Sex	Approximate Symptom Duration	Autopsy Interval	hR23A Cytoplasm Pattern	hR23A Nucleus Pattern	hR23B Cytoplasm Pattern	hR23B Nucleus Pattern
JH83	fALS	SOD1 N193K Onset: left leg	50/M	74 months	14.5 hours	Strong deposits	Strong staining	Strong deposits	Punctate staining
JH43	fALS	SOD1 A4V Onset: LE/left leg	55/M	21 months	Unknown	Reticular	Punctate staining	Weak deposits	Strong staining
JH74 <i>(note: ALS Case #2 in Figure 12)</i>	fALS	SOD1 A4V Bulbar onset	47/M	15 months	18.5 hours	Strong and weak deposits	Strong staining	Strong and weak deposits	Punctate staining
JH82	sALS	Onset: LE/left leg	66/M	43 months	13 hours	Absent	Strong staining	Weak deposits	Punctate staining
JH73	sALS	Onset: LE/left foot	70/F	36 months	8 hours	Strong deposits	Strong staining	Punctate and strong deposits	Strong staining
JH86	FTD+fALS (C9ORF72+)	Onset: legs/cognition	74/M	~84 months	32 hours	Strong deposits	Strong staining	Strong deposits	Weak staining
JH79	sALS	Bulbar onset	70/F	28 months	12 hours	Strong deposits	Strong staining	Strong deposits	Strong staining
JH22	fALS (C9ORF72+)	Onset: UE/left arm	66/M	22 months	6 hours	Punctate throughout	Punctate staining	Absent	Strong staining
JH49	sALS	Onset: UE/right hand	68/F	70 months	4 hours	Strong and weak deposits	Weak staining	Weak deposits	Punctate staining
JH88	FTD+fALS (C9ORF72+)	Bulbar onset	59/M	20 months	10 hours	Reticular	Weak staining	Strong and weak deposits	Weak staining
JH07 <i>(note: ALS Case #1 in Figure 12)</i>	sALS (C9ORF72+)	Bulbar onset	67/M	14 months	8 hours	Strong deposits	Weak staining	Strong deposits	Strong staining
JH80	sALS	Onset: UE (right)	56/F	50 months	21 hours	Strong deposits	Punctate staining	Strong and weak deposits	Punctate staining

**Table 3.5. Description of control cases used for staining and expression analysis.**

Control Case	Age at Death/Sex	Cause of Death	Autopsy Interval	hR23A Cytoplasm Pattern	hR23A Nucleus Pattern	hR23B Cytoplasm Pattern	hR23B Nucleus Pattern
23	77/M	Cardiac failure	6 hours	Diffuse	Light staining	Absent	Absent
26	49/M	Cancer and obesity	4 hours	Diffuse	Absent	Some reticular with weak deposits	Absent
31	67/M	Lung cancer	3.5 hours	Deposits	Absent	Weak deposits	Absent
37	57/M	Cardiac arrest due to ventricular fibrillation	14 hours	Deposits	Some light nuclear staining	Diffuse throughout and scattered	Absent
42	61/M	Brain tumor	6 hours	Scattered throughout cytoplasm	Light staining	Deposits	Light staining
44	80/F	Liver failure	5 hours	Some weak deposits	Light staining	Reticular	Absent
65	82/M	Unknown	4 hours	Reticular	Present	Diffuse and reticular	Absent
67	77/M	Unknown	4 hours	Reticular	Present	Deposits	Strong staining
78	58/F	Vasculitis, cerebral hemorrhage, hepatitis C	3 hours	Reticular	Absent	Reticular	Absent



**Table 3.6. RAD-23 has opposing roles on substrate stabilization.**

Substrate	RAD-23 Manipulation	Effect on Substrate	Platform	Reference
Arg-β-Gal	Overexpression	stabilizes	yeast	Ortolan <i>et al.</i> , 2000
Rad-4	Overexpression	stabilizes	yeast	Ortolan <i>et al.</i> , 2004
Ub-Pro-β-Gal	Overexpression	stabilizes	yeast	Ortolan <i>et al.</i> , 2000
Lactalbumin	Replacement	stabilizes	Ub-depleted reticulocyte extract	Raasi <i>et al.</i> , 2003
Ub <sub>5</sub> -DHFR	Replacement	stabilizes	HEK293T cells	Raasi <i>et al.</i> , 2003
BCA2	Overexpression	stabilizes	U2O2 and H1299 cells	Bacopulus <i>et al.</i> , 2012
p53	Overexpression	stabilizes	U2O2 cells	Brignone <i>et al.</i> , 2004
p53	Loss of function (hR23A and hR23B)	destabilizes	U2O2 cells	Brignone <i>et al.</i> , 2004
Ub-Pro-β-Gal	Loss of function	stabilizes	Δrad23 yeast	Lambertson <i>et al.</i> , 1999
Ub <sup>V78</sup> -V-β-Gal	Loss of function	stabilizes	Δrad23 yeast	Rao <i>et al.</i> , 2002 Kim <i>et al.</i> , 2004
Sic1	Replacement	destabilizes	Proteasomes purified from Δrad23 yeast	Verma <i>et al.</i> , 2004
Far1	Loss of function	stabilizes	Δrad23 yeast	Verma <i>et al.</i> , 2004
XPC	Loss of function (hR23A-null)	destabilizes	mouse embryonic fibroblasts	Ng <i>et al.</i> , 2003

## **CHAPTER 4: GENERAL CONCLUSIONS AND FUTURE DIRECTIONS**

In this thesis work, I have attempted to further understand how neurons, primarily within the context of the motor system, develop and later die in the case of neurodegenerative disease. In Chapter 2, I identify a novel interaction between SAP97 and CRIPT and present evidence that CRIPT is a component in a complex that mediates activity-dependent dendrite growth by GluA1-containing AMPA-R. In Chapter 3, I change the focus of my work to ALS and identify novel modifiers of ALS. I focus on RAD-23 and describe experiments which contribute towards an improved understanding of how reduced RAD23 mitigates the toxicity of ALS-linked proteins and their overall abundance. Below, I will describe the major implications for this work and discuss the remaining questions for future work.

### **ACTIVITY-DEPENDENT DEVELOPMENT**

Much research in the field of activity-dependent development has concentrated on the NMDA subtype of glutamate receptors, although previous work (Ingls et al., 2002; Jeong et al., 2006) indicates that NMDA-R-independent forms of activity-dependent development exist. The mechanism by which AMPA-R assembled with GluA1 promote dendrite growth and branching in the spinal cord is one key example of a form of plasticity that is NMDA-R independent. It is known that GluA1 uses SAP97 to exert its pro-dendrite growth effects (Zhang et al., 2008); however, until the work described in Chapter 2, the downstream effectors of SAP97 have remained unknown. We have now identified CRIPT as a key component in this process.

In the past, one challenge in identifying the functions of many membrane associated guanylate kinases (MAGUK) proteins, such as PSD-95 or SAP97, has been

their redundant functions in relation to synaptic plasticity (Schluter, 2006; Howard et al., 2010). This refers to the fact that members of the MAGUK family can compensate for loss of another MAGUK protein. This makes the form of NMDA-R-independent dendrite growth focused on in this thesis unique. For example, other MAGUK family members in the SAP97 conditional knockout do not compensate for the pro-growth effects of SAP97 on the dendrite tree (Zhang et al., 2008; Zhou et al., 2008). This suggests that this property of SAP97 is unique, and raises the possibility that proteins in the postsynaptic density involved in this process are unique as well. Furthermore, we know show that the pro-dendrite growth properties of CRIPT cannot be compensated for by other MAGUK family members because knockdown of CRIPT shortens and simplifies the dendritic tree of spinal cord neurons. In addition to being the first work to identify a downstream effector of SAP97, this work is also the first to identify a function for CRIPT since its description in the late 1990's. This suggests that SAP97, CRIPT, and presumably other proteins in this complex are unique from many other proteins found in the synaptic density.

What can be gained by understanding the components and mechanisms used by AMPA-R to guide the growth of the dendritic tree? Understanding how dendrite growth is promoted during early postnatal life can provide insight into how one may intervene later in life to promote recovery following CNS insult. Part of the evidence supporting this idea lies in the fact that, following spinal cord injury, repetitive activation of specific neuronal pathways can result in a significant improvement in motor behavior via the increase in AMPA-ergic transmission, resulting in the stabilization of dendrites and synapses (Engesser-Cesar, 2005; Spooren et al., 2008). If we can better understand the mechanism underlying this phenomenon, we might be able to restore the features unique to early postnatal life, allowing for dendrite growth in patients following injury.

Understanding the components in this process can also help us to further understand developmental disorders. Mutations in CRIPT have been correlated with primordial dwarfism (Shaheen et al., 2014). Mutations in SAP97 have also been correlated with schizophrenia (Uezato et al., 2012). Therefore, understanding functions for these proteins can help us to understand their importance in disease.

## **THE IDENTIFICATION OF OTHER MEDIATORS OF GLUA1-MEDIATED DENDRITE GROWTH**

In this work, we identified CRIPT as a mediator of GluA1- and SAP97-dependent dendrite growth. However, there are a number of issues that need to be resolved. Although knockdown of CRIPT *in vitro* and *in vivo* reduced the number of dendrite branches, overexpression of CRIPT had no effect. There are a number of explanations for this: (1) the number of SAP97 PDZ3-binding sites are saturated and, therefore, overexpressing CRIPT alone has no effect and (2) there are other components needed in the correct stoichiometry to allow for overexpression of CRIPT to promote dendrite growth.

In order to address the first possibility of saturated SAP97, one could overexpress SAP97 and CRIPT and ask whether or not there is a synthetic increase in dendrite branching. Furthermore, although we overexpressed palmitoylated (cell surface targeted) CRIPT, it is possible that it still needs an interaction with SAP97 or other mediators to have a pro-dendrite growth effect.

In order to address the possibility of other needed components of the GluA1/SAP97 complex, other SAP97 PDZ3 binding partners need to be identified. To do this, we created herpes simplex virus (HSV) expressing myc-tagged wild type and PDZ3

mutant SAP97 (see Appendix 1). These viruses were successfully infected into neuronal cultures and co-immunoprecipitated. We verified that we could immunoprecipitate SAP97 using the myc-tag as well. In the future, we hope to use these viruses to identify other specific SAP97 PDZ3-binding partners in a neuronal setting using Coomassie-stained gels and mass spectrometry. By understanding the other mediators that might play a part in GluA1-mediated dendrite growth, the mechanism might be more clearly elucidated. We ultimately hope to be able to identify other components of this pathway in an *in vivo* model. In Chapter 2, we showed that *cript* mutants in *C. elegans* have an abnormal dendrite tree compared to wild type counterparts *in vivo*. Because of the ease of culturing *C. elegans* and the ease at which many mutants are readily available, this represents another useful avenue for identifying other proteins in the GluA1/SAP97/CRIPT complex to promote the correct patterning of dendrite growth. For example, one could use an RNAi-feeding screen in *C. elegans* to look for genes that disrupt dendrite growth of the PVD neuron when knocked down.

#### **UNRESOLVED QUESTIONS REGARDING CRIPT'S ROLE IN DENDRITE GROWTH**

The work presented in Chapter 2 also has a number of limitations and there are a fair number of questions remaining to be answered. First and foremost, we still have not shown that CRIPT is actually downstream of GluA1, although we present strong evidence that CRIPT is downstream of SAP97. The key experiment needed to address this concern would be to overexpress GluA1 and observe an increase in dendrite growth. One could then determine if knockdown of CRIPT blocks the pro-dendrite growth actions of GluA1.

The next remaining question is if the pro-dendrite growth property of CRIPT is activity-dependent. We have found no evidence that the interaction between CRIPT and

SAP97 is influenced by synaptic activity (data not shown), although we have evidence that the interaction between GluA1 and SAP97 is influenced by synaptic activity (see Appendix 1). In Appendix 1, we show that increasing synaptic activity increases the amount of GluA1 bound to SAP97. Furthermore, blocking AMPA-R using CNQX decreases the amount of GluA1 bound to SAP97. However, in Chapter 2, we show that the knockdown of CRIPT does not block the observed increase in dendrite growth caused by increased synaptic activity stimulated by high potassium. Therefore, it appears that the activity dependence of the pro-dendrite growth actions of CRIPT are upstream and are possibly at the step of the interaction between GluA1 and SAP97. It would be important to know if the pool of SAP97 interacting with CRIPT is also bound to GluA1 to test this hypothesis. If this was true, then one would expect SAP97 bound to GluA1 to also be bound to CRIPT, whereas the pool of SAP97 unbound to CRIPT would also not be bound to GLuA1. It is also possible that other proteins are able to compensate for CRIPT in its absence following the stimulation of synaptic activity.

### **THE IMPORTANCE OF ERAD COMPONENTS IN ALS**

In Chapter 3, we show that the loss of various ERAD components are able to modify models of motor neuron disease (mutTDP-43 and mutSOD) in *C. elegans*. In the past decade, several genes have been identified as mutated in cases of fALS and frontotemporal dementia (FTD). As discussed earlier, many of these genes are in the ERAD pathway and include ubiquilin-2 (Deng et al., 2011) and VCP (González-Pérez et al., 2012). Evidence for the involvement of ALS in ERAD is also found in experimental data. Despite not being an ERAD substrate, ALS-linked mutant SOD1 has been found to enter the secretory pathway where it can interact with another ERAD component, DERLIN-1 (Nishitoh et al., 2008). It is through this interaction that mutant SOD1 is able

to inhibit the correct processing and degradation of other ERAD substrates. This suggests that ERAD might contribute to the symptoms and neurodegeneration found in ALS. It also suggests that ERAD can also be affected in ALS even if no mutation in an ERAD component is present.

ER stress is an essential mechanism that upregulates the amount of ubiquitination enzymes in an Ire1-mediated fashion to allow for the clearance of misfolded proteins by the proteasome and by ERAD itself (Hampton, 2003). Intuitively, this should lead to the clearance of ERAD substrates and other substrates by the proteasome. However, it has been reported that increasing the abundance of ubiquitination enzymes *in vitro* can stabilize ERAD substrates (Lenk et al., 2002). In opposition to this, ER stress pharmacologically evoked by tunicamycin has also been found to stabilize components of ERAD and increase the degradation of other ERAD substrates (Shen et al., 2007). These conflicting reports suggest that we do not yet have a complete understanding of the involvement of ER stress and ERAD during periods of cellular stress. We especially do not have a complete understanding as to why certain substrates are stabilized while others are degraded more readily.

When we began the work described in Chapter 3, we initially predicted that the loss of ERAD components would be harmful to models of proteotoxicity and/or motor neuron disease. However, we found that there were several ERAD components whose loss actually suppressed the toxicity associated with misfolded proteins known to cause ALS. This contradicts some previous work that showed that overexpression of two ERAD components, Hrd1 and EDEM, suppressed a model of late onset retinal degeneration in flies (Kang and Ryoo, 2009). Furthermore, reduced Hrd1 expression has been found in the brains of Alzheimer's disease patients and reduced Hrd1 levels have

been found to lead to amyloid precursor protein (APP) accumulation (Kaneko et al., 2010). Forced expression of Hrd1 was also found to enhance the degradation and suppress the toxicity of polyglutamine-expanded huntingtin (Yang et al., 2007). Overexpression of other ERAD component has also been found to reduce the toxicity of ALS-linked proteins. Overexpression of DERLIN-1 was previously found to ameliorate ER stress by reducing SOD-1 accumulation (Mori et al., 2011).

Meanwhile, our findings are in alignment with some studies showing that a deficiency in certain ERAD and ER stress response pathway components can be neuroprotective. For example, XBP1 deficiency was found to protect against mutSOD by increasing autophagy (Hetz et al., 2009). Furthermore, although overexpression of Hrd1 did increase the clearance of huntingtin, this was found to be independent of some ERAD components while requiring others (Yang et al., 2007). This would suggest that, although all ERAD components are in the same pathway, they do not all function in the same direction or on the same set of substrates.

In Chapter 3, we describe our work and summarize other findings which suggest that RAD-23 is one protein to act in this manner. RAD-23 can stabilize, promote, or have no effect on the turnover on different substrates, although the factors which determine this selectivity remain unknown. Our findings further suggest that an initial hypothesis that a loss of ERAD components would simply act to enhance disease models and exacerbate proteotoxicity is too simple. Finally, our findings suggest that there may be an overload of the contribution of ERAD and ER stress components in neurodegeneration. This may contribute to the toxicity associated with the misfolded proteins in disease. This would suggest that other ERAD components should be



investigated in future work to identify other modifiers of ALS-linked proteins. It is possible that other proteins may act in a similar manner as RAD-23.

## **TARGETING RAD-23 IN NEURODEGENERATIVE DISEASE**

In Chapter 3, we describe a novel role for RAD-23 in the stabilization of disease-causing proteins. We show that reduced RAD-23 protects against the phenotypes, neurodegeneration, and toxicity associated with ALS-linked mutant proteins *in vivo* and *in vitro*. This represents a novel insight into how to attenuate toxicity caused by mutant proteins associated with the disease. It is widely accepted that reducing the level of proteins associated with disease reduces their pathology in animals. This work is among the first to show that targeting stabilizers of these disease-linked proteins can prevent the toxicity of the mutant proteins. Furthermore, we found a mislocalization of RAD-23 in postmortem ALS tissue compared to controls suggesting that these stabilizers like RAD-23 appear to have their own pathology in disease. This suggests that both extrinsic and intrinsic factors of disease-linked proteins contribute to disease, specifically neurodegeneration.

One benefit of a targeted knockdown approach of RAD-23 in ALS is that we found that loss of either hR23A or hR23B could exert neuroprotective effects. Thus, although the RAD-23 proteins have critical functions in protein degradation and nucleotide excision repair, it is possible that hR23A or hR23B might compensate for one another in these critical functions. It is important to note, however, that non-overlapping functions for hR23A and hR23B do exist. Most notably, hR23B was previously found to have a stronger interaction with the proteasome (Chen and Madura, 2006). Still, the fact that both hR23A- and hR23B-null mice are viable suggests that reducing RAD-23 levels

might be a promising target in the treatment for ALS. This suggest that it might be possible to target hR23A or hR23B levels in disease without affecting the essential functions of RAD-23, although one might be concerned about conferring genomic instability if RAD-23 is entirely lost. It is worth noting, however, that although the loss of most nucleotide excision repair (NER) components causes a decrease in survival in yeast, *rad-23* mutants exhibit only a higher degree of UV sensitivity (Watkins et al., 1993). This would suggest that RAD-23 plays a more regulatory role in NER. This strengthens our argument that RAD-23 may be able to be safely manipulated in the treatment of ALS and neurodegenerative disease. However, in order to safely mitigate concerns regarding off-target effects when manipulating RAD-23 levels in disease, one would first have to answer the question: how much reduction in RAD-23 is sufficient to be protective against mutSOD1 or mutTDP-43 without having negative consequences on UV hypersensitivity?

All of this assumes that our work on RAD-23 can be actually translated to humans. Is this the case? We reported in Chapter 3 that there is a mislocalization of hR23A and hR23B proteins in the postmortem tissue of ALS patients when compared to controls. Although the significance of these changes remain to be seen, we believe that this suggests that this work on RAD-23 can be significant for human disease. Although initially surprised that reduced RAD-23 protected against toxicity associated with two ALS-linked proteins, RAD-23 has been identified previously in SNP studies using ALS patient data, although the significance of this finding has been unknown until now. For example, a previous eQTL linkage analysis correlated an intergenic SNP (rs17724552) with changes in RAD-23 expression ( $p < 1 \times 10^{-3}$ ) (Myers et al., 2007). More interestingly, that same SNP was associated with sporadic ALS in an Irish cohort compared to

controls (Cronin et al., 2008). Furthermore, in alignment with our finding that hR23A expression was increased in the spinal cord of mutSOD1 mice, hR23A mRNA expression was found to be increased in the gray matter of spinal cords of fALS patients compared to controls (Dagond et al., 2004). This is consistent with our findings that both hR23A and hR23B protein expression is significantly increased in human post mortem ALS spinal cord tissue compared to controls. Taken together, this suggests that this work is the first to identify RAD-23 as having a pathophysiological relevance to human ALS and, furthermore, the first to identify the mechanism by which RAD-23 may contribute to the disease.

This leads to another question. Can RAD-23 also be important in other neurodegenerative diseases outside of ALS? Recently, other work has identified RAD-23 as a stabilizer of ataxin-3. Polyglutamine repeat expansion in ataxin-3 causes neurodegenerations in the most common form of dominant ataxia, spinocerebellar ataxia type 3 (SCA3) (Blount et al., 2014). This suggests that this work might apply to other diseases outside of ALS, and may be applicable to other aggregation-prone proteins outside of neurodegeneration. It was shown that RAD-23 could bind ataxin-3 through ataxin-3's UbS2 domain and that RAD-23 presumably stabilized ataxin-3 through this interaction. Most relevant to this work, it was shown that reducing *rad-23* in flies suppressed degeneration by ataxin-3 in eyes. (Blount et al., 2014). This is very similar to the work we have done in Chapter 3 and suggests that what we have found may be applied to other non-ALS neurodegenerative diseases. This is consistent with the fact that RAD-23 mislocalization has been found in post-mortem tissue from patients exhibiting other forms of neurodegeneration, including Huntington's disease, Parkinson's disease, and other forms ataxia, including SCA3 (Bergink et al., 2006). Therefore, one

major question that this work has produced is: can loss of RAD-23 be beneficial in other forms of neurodegeneration or is it disease-specific? Future work using other models of proteotoxicity will need to be done to address this question.

## **HOW REDUCED RAD-23 ACCELERATES MUTANT PROTEIN TURNOVER AND MITIGATES TOXICITY**

In Chapter 3, we show that reduced RAD-23 levels protect against toxicity associated with proteins linked to ALS. This appears to be related to reducing the burden and abundance of the tested mutant proteins which are known to cause ALS. We also show that the accelerated turnover of mutTDP-43 by reducing RAD-23 is through both the ubiquitin-proteasome system and autophagy since drugs blocking these pathways block the effect of RAD-23 knockdown. This suggests that RAD-23 can prevent some of its substrates from being degraded by the proteasome and autophagy. Past work found that overexpression of the ubiquitin-like protein, PLIC-2 (ubiquilin-2), could inhibit G protein-coupled receptor endocytosis and this required its ubiquitin-like domain, a ligand for ubiquitin-interacting motifs (UIMs) (N'Diaye et al., 2008). In addition to this, more recent evidence has shown that RAD-23 can inhibit the degradation of ataxin-3 and this is mediated by the ubiquitin-binding site on ataxin-3 (Blount et al., 2014). All of this suggests that the ubiquitin-binding domain of RAD-23 might somehow be responsible for this inhibition of mutant protein clearance. Future work will be required to address this question. In this work, we were able to examine the ubiquitination status of mutTDP-43 in control and reduced RAD-23 conditions. In Chapter 3, we found that reduced RAD-23 increased the amount of poly-ubiquitination of mutTDP-43. In addition, reducing RAD-23 levels increased the flux of poly-ubiquitinated mutTDP-43 through the proteasome. It is also worth recalling that the other identified suppressors of mutTDP-43

in our candidate approach presented in Chapter 3 were ubiquitination components. This further suggests that ubiquitination may be a key step in determining the turnover and toxicity of proteins associated with ALS.

This most recent finding is consistent with past work showing that in an increase in the polyubiquitination status of a protein can lead to reduced aggregates and mitigate toxicity. For example, recent work showed that overexpression of parkin increased polyubiquitination in flies, but also reduced protein aggregation and increased the longevity of flies (Rana et al., 2013). It is also difficult to ignore that all of the suppressors found in our directed candidate screen in Chapter 3 are believed to have some interaction with CDC-48 (also known as p97 or VCP) and have some role on ubiquitination status. Interestingly, worms with mutations in *cdc-48.1* and *atx-3* (the worm ortholog of ataxin-3) previously showed a 50% extended lifespan through the insulin-like-growth-factor 1 (IGF-1) signaling pathway and the deubiquitination activity of wild type ATX-3 (Kuhlbrodt et al., 2011). Therefore, aside from accelerating the turnover of mutant proteins, it is possible that RAD-23 may edit the ubiquitination status of substrates to promote stress resistance and protection. Future work is warranted to understand if this is the case.

In Chapter 3, we also present evidence suggestive of a physical association between hR23A and mutTDP-43. It has been previously found that ubiquitin-binding proteins can interact with their substrates via the UBA domain (Chen et al., 2002). It is uncertain whether or not hR23A and mutTDP-43 interact via hR23A's UBA domain or whether or not this interaction may be through the ubiquitin chain. Therefore, future work is required to ask if hR23A inhibits the degradation and/or polyubiquitination of mutTDP-43 through a physical interaction or thorough a separate mechanism. This could be

accomplished by mapping the interaction between hR23A and mutTDP-43. One could then attempt to block this interaction to ask if blocking the interaction has the same result as knockdown of RAD-23.

Another key question remaining from this work is what species of mutTDP-43 RAD-23 is acting to stabilize. Although we show that reduced RAD-23 acts to decrease the steady state of ALS-linked proteins and accelerate their turnover, it is still unclear if RAD-23 is specifically acting on correctly folded mutTDP-43 or misfolded mutTDP-43. In addition, is RAD-23 acting on monomeric species or larger oligomeric species of aggregated protein? These questions will need to be addressed to further understand how RAD-23 is acting to inhibit the ubiquitination of mutTDP-43 and its clearance from the cell.

### **LOSS OF RAD-23 AS A PROTECTOR AGAINST PROTEOTOXICITY**

In Chapter 3, we present data that *rad-23* animals perform better than wild type when exposed to a variety of proteotoxic stressors, as well as aging. These results are compelling evidence that loss of *rad-23* might be protective against other late age-onset diseases related to proteotoxicity, versus being ALS-specific. However, a number of follow-up experiments remain.

For example, we show that *rad-23* animals have enhanced locomotor activity at 4 and 5 days post L4 in *C. elegans*. Unfortunately, we never tested whether or not this effect persisted at later ages. This would be a key experiment to do to determine whether or not loss of *rad-23* could protect against aging-related decline. This is especially important since we did not detect a significant extension of lifespan in *rad-23* animals.

Another weakness of this work is that it primarily focused on the contribution the UPR and ERAD. It is possible that other stress response pathways are responsible for mediating the mechanism by which loss of *rad-23* confers a resistance to proteotoxic stressors. In this light, a RNAi feeding strategy in *C. elegans* would also be useful in determining whether or not another pathway, such as the heat shock response (HSR) pathway, might be responsible. Another possible way to determine this would be to place *rad-23* animals on reporter backgrounds to measure activation of pathways such as ER stress, mitochondrial stress, or the heat shock response. The involvement of these pathways in *rad-23* animals could also be determined by measuring the mRNA levels of the pathway components using qPCR and comparing their expression to levels in wild type animals.

In Chapter 3, we also report a ~25% extension of survival for *C. elegans* that are deficient in *rad-23* compared to controls when exposed to high heat. Although this is a reasonable extension of survival, it is somewhat weak compared to other animals known to be resistant to similar stressors, such as *daf-2* animals (Bocchetto et al., 2012). This begs to question what underlying pathways might be mediating the effect of loss of *rad-23*. One way to determine this would be to utilize an RNAi-feeding strategy or genetic screen in *C. elegans*. One could look for genes that are capable of blocking the resistance to high heat in *rad-23* animals when knocked down or mutated. These suggested experiments would shed light on possible downstream effectors of RAD-23. In addition, one could ask if other NER genes, and thereby the NER pathway, are involved in mediating resistance to proteotoxicity in reduced RAD-23 settings.

## **A LINK BETWEEN NUCLEOTIDIE EXCISION REPAIR AND NEURODEGENERATIVE DISEASE**

Recently, there has been a number of links made between DNA damage and neurodegeneration (Madabhushi et al., 2014). More relevant to this work is the number of recent links that have been made between DNA damage and the protein quality control system. Work has investigated how DNA instability in the germ line might affect somatic tissues. Surprisingly, exogenous and endogenous triggers of DNA damage were found to induce a stress response in the somatic tissues of *C. elegans*. This response protected the animals from a number of stressors, including heat stress and oxidative stress. This was found to be mediated by the MAP/ERK pathway (Ermolaeva et al., 2013).

DNA damage has also been closely linked to ALS. FUS is an RNA-binding protein that is similar to TDP-43 in that cytoplasmic accumulations of FUS are also found in ALS. Interestingly, FUS RNA targets are enriched for genes in the DNA damage response pathway (Zhou et al., 2014). Furthermore, the induction of DNA damage in neurons was found to lead to the cytoplasmic accumulation of FUS (Deng et al., 2014).

Up until this point, DNA damage has been primarily studied within proliferating cells, especially in regards to cancer (Madabhushi et al., 2014). However, the work presented in this thesis suggests that DNA damage is grossly understudied within the nervous system. This is perhaps due to the fact that neurons are post-mitotic and thereby have a different requirement of the DNA damage repair pathways. Regardless, there are a number of neurodevelopmental diseases that feature mutations in DNA repair markers. This highlights the importance of DNA damage repair components within the nervous system (Madabhushi et al., 2014). In addition, as neurons age and cannot



be replaced, they inherently will accumulate DNA mutations. This may be why we observe an increase in RAD-23 expression in ALS tissue compared to controls. It would be insightful to determine if there is an increase in the DNA mutation rate within neurons in neurodegenerative disease settings compared to controls. The increase in RAD-23 expression in response to DNA damage in disease or aged individuals might also explain why RAD-23 can then take on a “gain of function” mechanism to prevent the clearance of misfolded proteins.

Future work is still needed to determine whether or not nucleotide excision repair or DNA damage contributes to the protection against toxicity observed in reduced RAD-23 conditions. Our findings in Chapter 3 are suggestive of an indirect relationship between protein quality control and DNA damage repair, although stronger evidence for this is still required in our work and in the literature in general. Thus far, we have not been able to identify any nucleotide excision repair factors that also suppress mutTDP-43 toxicity in *C. elegans*. However, the studies presented in this work are not an exhaustive search. In addition to this, future work is required to determine what stress response pathways are enhanced in loss of *rad-23* animals.

There is evidence that persistent transcription-blocking DNA damage can activate oxidative stress-responses and also downregulate insulin-like signaling (ILS) in mice (Fensgard et al., 2010). Previous work in the lab (Bocitto et al., 2012) found that reducing DAF-2 signaling (the ILS signaling pathway in *C. elegans*) could protect against mutSOD1 toxicity in *C. elegans*. Moreover, we observe in Chapter 3 that RAD-23 becomes nuclear in ALS postmortem tissue compared to controls. Recently, it was found that silencing the hR23A gene prevented the nuclear translocation of apoptosis-initiation-factor (AIF), which occurs during the initiation of cell death (Sudhakar and

Chow, 2014). It will be interesting to learn in future work whether or not NER or blocking the nuclear translocation of hR23A or hR23B observed in ALS-associated conditions contributes to the protection against toxicity by loss of RAD-23 in motor neurons.

## **FINAL REMARKS**

In sum, this work identifies new components and mechanisms that affect how our motor neurons develop and degenerate in disease. We hope that this new information can help to further inform the treatment of devastating and debilitating developmental and degenerative diseases. Aside from giving new insight into how these processes work, we also believe it reiterates the importance for further work in these fields. For example, a lot of recent work has begun to tease apart a possible relationship between DNA damage and neurodegeneration which may have been understudied thus far outside of the cancer field. In addition, this work provides new hope that we can uncover functions for orphan proteins like CRIPT, as well as new functions for proteins like RAD-23.

## **APPENDIX 1: OTHER COMPONENTS IN THE GLUA1/SAP97/CRIPT COMPLEX TO PROMOTE DENDRITE GROWTH**

### **SUMMARY**

In this Chapter 2 of this thesis, we report that CRIPT (cysteine-rich-interactor-of-PDZ-three) is necessary, but not sufficient to promote dendrite growth. We hypothesize that this effect is via the GluA1 subunit of AMPA receptors and its intracellular scaffolding protein, SAP97 (synapse-associated-protein-of-97 kDa molecular weight). One explanation for why we found that overexpression of CRIPT is insufficient to promote dendrite growth is that there are other components of this multi-protein complex necessary in the correct stoichiometry to promote dendrite growth. Therefore, we have developed a tool to identify these other binding partners that utilizes a neuronal infection and mass spectrometry approach. This tool can be employed to identify other PDZ3 binding partners of SAP97 that might help to promote dendrite growth.

### **INTRODUCTION**

During the first few weeks of postnatal life, synaptically-evoked activity helps to refine the connections and properties of the nervous system which were initially guided by a genetics program. One type of activity-dependent development is driven by NMDA-R and plasticity. A second type of activity-dependent development is driven solely by AMPA-R comprised of the GluA1 subunit and we have evidence that this is entirely independent of NMDA-R. We also believe that GluA1 exerts its effects using the scaffolding protein, SAP97.

This appendix presents new evidence that GluA1 and SAP97 physically interact in an activity-dependent manner and this complements past work showing that GluA1

uses SAP97 to translate synaptic activity into dendritic growth. We are also interested in identifying the downstream effectors of SAP97 used to promote dendrite growth via GluA1. We have found that SAP97's pro-dendrite growth properties relies on its PDZ3 domain. We have previously identified CRIPT (cysteine-rich-interactor of PDZ three) as one of the SAP97 binding partners that can promote dendrite growth in Chapter 2 of this work. However, we found that CRIPT was necessary, but not sufficient, to promote dendrite growth. Therefore, we hypothesized that there are other SAP97 PDZ3-binding partners needed to promote dendrite growth. Here, in Appendix 1, we describe the development of a tool that can be used to identify these other binding partners.

In sum, this work shows that GluA1 and SAP97 interact in an activity-dependent manner to promote dendrite growth. This further suggests that SAP97's binding partners are critical to promote dendrite growth. Furthermore, we have developed a new tool to help identify new SAP97 PDZ3-binding partners in neurons.

## **MATERIALS AND METHODS**

### **Cloning**

SAP97 (wild type and the PDZ3 mutant harboring the H469A and R470A mutations) was amplified from an expression plasmid and a myc-tag was added to the N-terminus utilizing the In Fusion cloning strategy (ClonTech). These constructs were then cloned into the pRPUC vector using the KpnI and EcoRI cloning sites. This plasmid was then used to construct a neuron-specific herpes simplex virus (HSV) for infection into neurons.

### **HEK293 Transfections**

HEK293 cells were maintained in DMEM (Invitrogen) containing 10% FBS (Sigma) and 1% Pen/Strep antibiotic (Sigma). When cells reached 75% confluency, cells were transfected with the PRPUC SAP97 expression constructs. Cells remained at 37°C for 48 hours to allow for expression before being lysed.

### **Activity-dependent co-immunoprecipitations**

For activity-dependent experiments, mixed spinal cord cultures were chronically treated with 5 $\mu$ M CNQX (72 hr) or 35mM KCl (48 hr) versus the vehicle (DMSO) control. After the indicated time period, cells were lysed in equal volumes 1% NP-40 lysis buffer (25 mM Tris HCl pH7.4, 150 mM NaCl, 1 mM EDTA, 1% NP40, 5% glycerol). Dynabeads (Invitrogen) were washed 3 times in 1x PBS supplemented with 0.1% Tween to pre-clear the beads before they were conjugated to SAP97 antibody (4 $\mu$ g, Thermo PA1-741; 30 min, room temperature). Cell lysates were then added and incubated for 1

hr at room temperature and then washed three times in 1% NP-40 lysis buffer. 5% of the starting material was saved for input. Samples were then boiled for 5 minutes in SDS sample buffer supplemented with 1% BME before being subjected to immunoblotting (mouse anti-SAP97 (Neuro Mab, UC Davis), rabbit anti GluR1 (EMD Millipore), and rabbit anti actin (Sigma) using SDS-Page.

### **Immunoprecipitation for mass spectrometry**

Cells were lysed in 1% Triton-X 100 lysis buffer and sonicated. Lysates were then spun down at 14,000 rpm for 10 minutes at 4°C to remove cellular debris. 5% of input was saved for input and verification of expression of the myc-tagged SAP97 constructs. Immunoprecipitation was done by standard DynaBeads (Invitrogen) protocol. Briefly, 50µL DynaBeads slurry mixture was washed three times in PBS containing 0.1% Tween-20 three times before being incubated with 4µg myc-tag (Cell Signaling) antibody for 30 minutes at room temperature. 95% of the lysate was then incubated with the antibody-bead mixture for 1 hour at room temperature. Lysate was removed and saved for checking immunoprecipitation efficacy. Beads were then washed three times in PBS and 40µL SDS-loading buffer with 1% BME was added. Beads were boiled for 5 minutes and 95°C before being processed for Western blot and Coomassie.

### **Coomassie and mass spectrometry**

5% of input and 5% of immunoprecipitation material was used for Western blot, and the rest was run on a 4-12% SDS-Page gel (Invitrogen). Gel was then stained using Coomassie R-250 dye (Bio-Rad) and the stained SDS-Page gel was washed per manufacturer protocol. Gel was developed and bands believed to be SAP97 were cut

out by Children's Hospital of Philadelphia (CHOP) Protein Core to confirm correct immunoprecipitation of SAP97.

## RESULTS

### **SAP97 and GluA1 interact in an activity-dependent manner**

Previous work has shown that SAP97 binds to the C-terminal amino acids of GluA1 through its PDZ2 domain. Until now, it was not clear how synaptic activity by GluA1-containing AMPA-R might drive dendrite growth. We hypothesized that the physical interaction between GluA1 and SAP97 might drive dendrite growth in an activity-dependent manner. To test this, mixed spinal cord cultures were chronically treated with either an AMPA-R antagonist, CNQX, for 72 hours or a vehicle (DMSO) for the same time period. SAP97 was then immunoprecipitated and samples were probed for SAP97 and GluA1. We found that roughly half the amount of GluA1 co-immunoprecipitated with SAP97 in the CNQX-cultures compared to vehicle (DMSO) treated cultures ( $*p < 0.05$ ) (Figure 1A). To test whether activity affected the interaction in a bi-directional manner, we used high potassium to stimulate the cultures. After 48 hours of chronic high potassium, stimulated or control (vehicle/DMSO) cultures were lysed and again endogenous SAP97 was immunoprecipitated. We found that there was roughly twice the amount of GluA1 that co-immunoprecipitated with SAP97 in stimulated cultures compared to control ( $*p < 0.05$ ) (Figure 1B). Taken together, this work suggests that synaptic activity influences the amount of interaction between GluA1 and SAP97 in a bi-directional manner.

### **Tool to identify SAP97 PDZ3-interactors**

In Chapter 2, we show that CRIPT interacts with the pro-dendrite growth PDZ3 domain of SAP97 and the PDZ3 domain of SAP97 is necessary for the pro-dendrite growth effects of SAP97. However, overexpression of CRIPT had no effect of dendrite



growth and data suggested that the interaction between SAP97 and CRIPT was not activity-dependent (data not shown). This is unlike the interaction between SAP97 and GluA1. This leads us to reason that other components of this complex besides CRIPT are required for forced expression of CRIPT to exert a pro-dendrite growth effect. There are ~25 likely SAP97 binding partners which may bind to the PDZ3 domain of SAP97, but it is unknown whether these interactions would occur in neurons or mediate dendrite growth. Therefore, to pursue other proteins in this complex, we wanted to create a tool that could identify new SAP97 PDZ3-binding partners in neurons. To do this, we created a neurotropic herpes simplex virus (HSV) expressing myc-tagged wild type (wt) and mutant (mut) SAP97 (PDZ3mut) that could be infected into neurons in either a wild type or loss of SAP97 background. This version of SAP97 could be immunoprecipitated successfully. A Coomassie-stained gel of the immunoprecipitate identified possible binding partners in HEK293 cells (Figure 2). This suggests that this tool could be used in neurons and a proteomics approach could be employed to identify SAP97 binding partners in neurons, as well as specific PDZ3 binding partners.

## DISCUSSION

This work hopes to gain further insight into how SAP97, GluA1, and CRIPT mediate dendrite growth.

Up until this point, the mechanism of how GluA1 and SAP97 mediate dendrite growth has remained unclear and this work is the first to show that the interaction between these two proteins is mediated by activity. Previous work in the lab has shown that the interaction between GluA1 and SAP97 is necessary for SAP97 to correctly traffic to the cell surface (Zhou et al., 2008; Zhang et al., 2008). Furthermore, the interaction between SAP97 and GluA1 is necessary for SAP97's pro-dendrite growth effects (Zhang et al., 2008; unpublished observations). This work would suggest that excitatory activity at synapses strengthens the interaction between GluA1 and SAP97, allowing for more SAP97 to traffic to the cell surface and promote dendrite growth. There are a number of ways to test this hypothesis including asking whether or not blocking AMPA-R activity using CNQX or stimulating activity with high potassium brings less or more SAP97 respectively to the cell surface via surface biotinylation studies. Therefore, further experimentation is needed to come to this final conclusion.

Next, we hoped to identify new SAP97 binding partners that might also be part of the GluA1/SAP97/CRIPT pro-dendrite growth complex. Given the number of likely SAP97 binding partners, we wanted a higher throughput approach to achieve this. Therefore, we were also successful in creating a tool for future work to uncover other downstream effectors in the proposed "GluA1/SAP97/CRIPT" complex to promote dendrite growth.

Taken together, these new tools and insights can help us to understand not only the components that drive AMPA-R activity-dependent development, but also the molecular mechanisms.

## FIGURE LEGENDS

**Figure A1.1. Association of GluA1 with SAP97 is activity-dependent.** (A) Spinal cord cultures were exposed to the AMPA-R antagonist CNQX for 72 hours and then lysates were immunoprecipitated (IP'ed) for SAP97 and immunoblotted for GluA1 or SAP97. Less GluA1 was present in the SAP97 immunoprecipitated in CNQX-treated neurons in comparison with vehicle treated neurons. Input levels of GluA1, SAP97 and actin were similar among the groups. Below Western blot images is the quantification of immunoblots denoted as fold-change over vehicle; paired ratio t-test:  $*p < 0.05$  according to Student's *t-test*. (B) Spinal cord cultures were exposed to high potassium ("High K+") for three days and then lysates were IP'ed for SAP97 and immunoblotted for GluA1 or SAP97. A longer and a shorter exposure for signal acquisition was obtained and shown. More GluA1 was present in the SAP97 immunoprecipitated in High K+ treated neurons in comparison with vehicle treated neurons. Input levels of GluA1, SAP97 and actin were similar among the groups. Below Western blot images is the quantification of immunoblots denoted as fold-change over vehicle; paired ratio t-test:  $*p < 0.05$  according to Student's *t-test*.

**Figure A1.2. Successful tool development to identify new SAP97 PDZ3 domain binding partners in neurons.** (A) Representative Coomassie of myc-tagged immunoprecipitations following infection with herpes simplex virus (HSV) expressing LacZ [1], myc-tagged wild type (wt) SAP97 [2], or myc-tagged mutant PDZ3 mutant SAP97 (PDZ3mut) [3]. We cut out the bands we identified on the Coomassie gel and confirmed that they were SAP97 using mass spectrometry. (B) Representative Western blot (immunoblot for myc) of HEK293 cells infected with herpes simplex virus (HSV) expressing LacZ, wild type (wt) SAP97, or mutSAP97 (PDZ3mut). Representative

Coomassie of lysates following myc immunoprecipitation. #SAP97 band; \*protein co-immunoprecipitated with myc-tagged wild type (wt) or mutSAP97 (PDZ3mut); \*\*protein co-immunoprecipitated selectively with myc-tagged wild type (wt) SAP97, but not the PDZ3 mutant SAP97.

Figure A1.1. Association of GluA1 with SAP97 is activity-dependent.

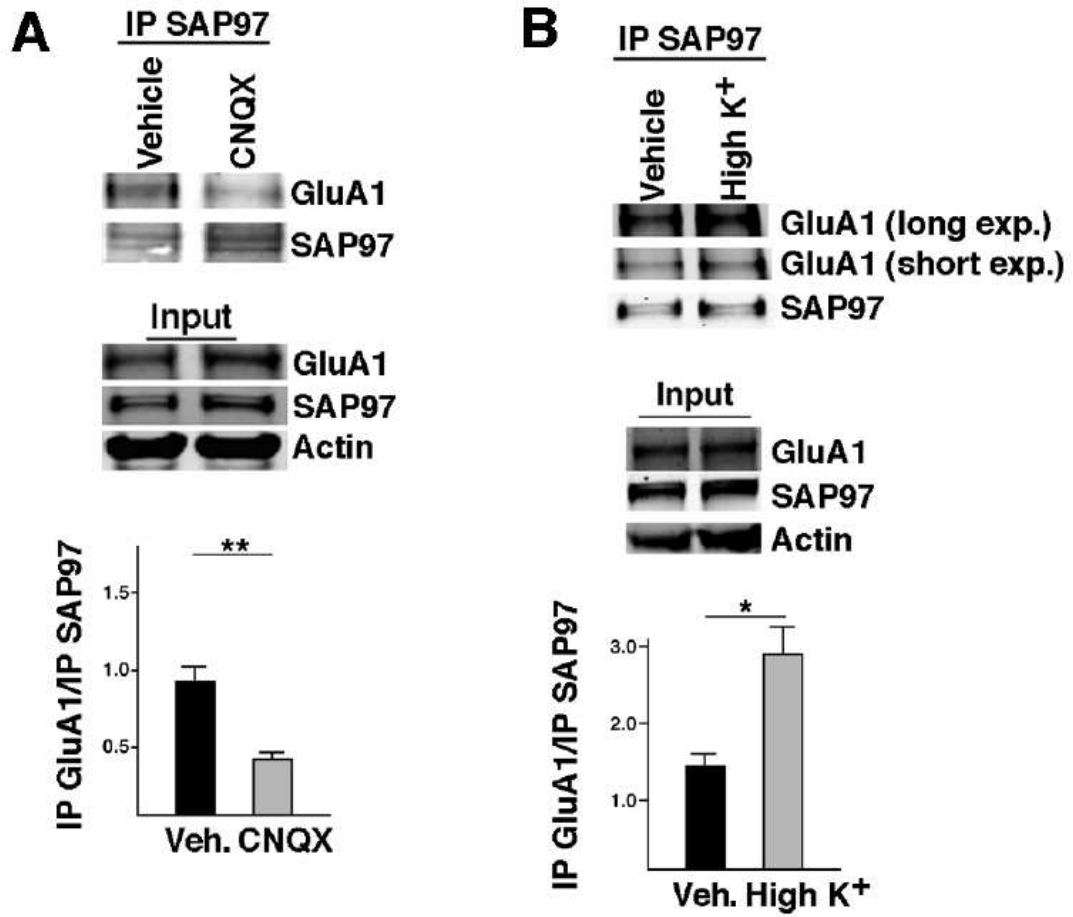
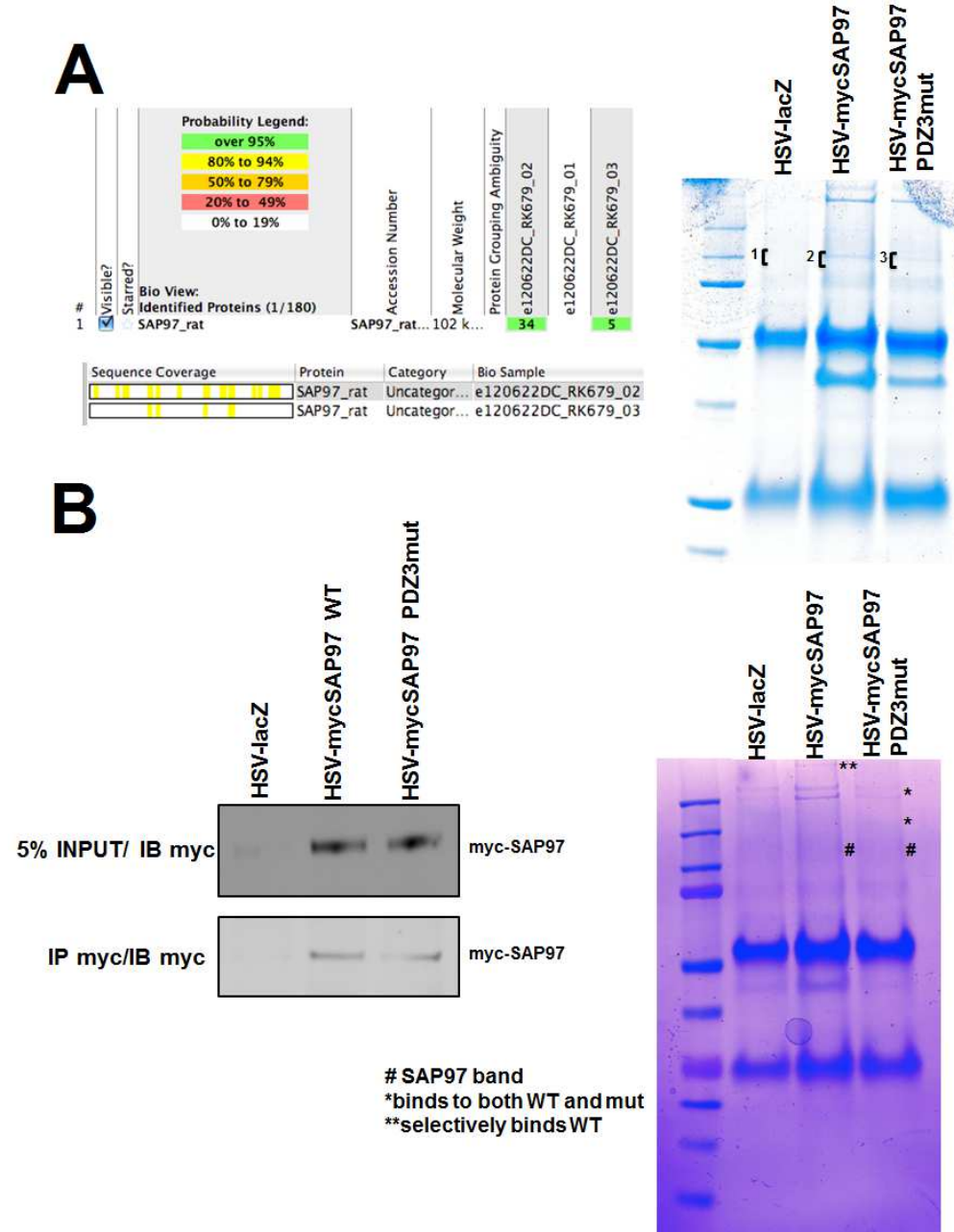


**Figure A1.2. Successful tool development to identify new SAP97 PDZ3 domain binding partners in neurons.**



## APPENDIX 2: OTHER MODIFIERS OF MOTOR NEURON DISEASE MODELS

### SUMMARY

Amyotrophic Lateral Sclerosis (ALS) is a multifactorial adult-onset disease that attacks the upper motor neurons of the cortex and lower motor neurons of the spinal cord. Observed pathology includes (but is not limited to): (1) changes in protein quality control; (2) heightened unfolded protein response (UPR) and endoplasmic reticulum (ER) stress; and (3) changes in metabolism. Therefore, we utilized the small nematode, *Caenorhabditis elegans* (*C. elegans*), and mixed spinal cord cultures to investigate what (if any) modifiers of ALS-related proteins might exist in these pathways outside of the main focus of this dissertation (endoplasmic reticulum-associated degradation, or ERAD).

### INTRODUCTION

This appendix presents work done to identify other modifiers of motor neuron disease models in *C. elegans* and in mixed spinal cord culture.

First, because RAD-23 may exert its effects on mutTDP-43 through altering mutTDP-43's ubiquitination status, we are interested in exploring the status of ubiquitination in models of motor neuron disease, as well in in *rad-23* mutants. In this work, we show that there is an accumulation of normally destroyed ubiquitinated GFP in the wild type TDP-43 (wtTDP-43) and mutant (M337V) TDP-43 (mutTDP-43) models of ALS in *C. elegans*. This was predicted because past evidence suggests that the accumulation of misfolded proteins prevents the ubiquitin-proteasome system from degrading normally processed substrates. We examine the effect that reduced *rad-23*



and *ufd-3*, two suppressors found in our genetic screen described in Chapter 3, have on this accumulation of ubiquitinated GFP (UbV-GFP). Interestingly, knockdown of *rad-23* or *ufd-3* by RNAi had opposing effects, further validating our belief that the involvement of ERAD components in models of motor neuron disease is much more complex than initially anticipated.

This leads to our next finding presented in Appendix 2 which aimed to ask if constitutive ER stress could protect against models of motor neuron disease. *C. elegans* were engineered to express a constitutively spliced form of XBP1 (“XBP1s”) in their nervous system both as a single copy and multiple copies (“extrachromosomal array”). We found that, as opposed to protecting against ER stress, constitutively spliced XBP1 actually enhanced toxicity caused by pharmacologically evoked ER stress using tunicamycin. This prevented us from being able to ask if this form of constitutively spliced XBP1 could protect against models of motor neuron disease in *C. elegans*.

We also report in Chapter 3 that reduced RAD-23 protects *C. elegans* from mutTDP-43 toxicity in a cell-autonomous manner. It is important to note that not all of the modifiers of mutTDP-43 and mutSOD toxicity in *C. elegans* acted in this manner. For example, we also present evidence here that *ubq1-1* enhances mutSOD toxicity in *C. elegans* via a possible non-cell-autonomous manner. In relation to the work completed on RAD-23 in Chapter 3, we report that pharmacological stabilization of a RAD-23 substrate, p53, is able to protect against mutSOD1 toxicity in mixed spinal cord cultures.

Finally, we also examined the effect of constitutively “on” HIF1 $\alpha$  in the mutSOD model of motor neuron disease. HIF1 $\alpha$  belongs to a class of transcription factors that are readily destroyed but become stabilized in certain environments, such as those where

there is a deprivation of oxygen. Up until recently, the hypoxia response pathway has not been well studied in the context of ALS. In addition, there have been conflicting results concerning the expression of HIF1 $\alpha$  and its targets in ALS mouse models (Sato et al., 2012). For example, some studies have found that there is an increase in HIF1 $\alpha$  and its targets in the transgenic SOD1 ALS mouse model (Sato et al., 2012). Meanwhile, other studies have suggested that there may be a lack of induction of HIF1 $\alpha$  targets, specifically VEGF, which contributes to motor neuron degeneration (Cleveland and Rothstein, 2001). We report that a constitutively “on” version of HIF1 $\alpha$  protects against the locomotor deficit associated with mutSOD in *C. elegans* supporting the idea that there may instead be a lack of activation of HIF1 $\alpha$  targets or HIF1 $\alpha$  itself.

## **MATERIALS AND METHODS**

### **Caenorhabditis elegans (*C. elegans*) strains and maintenance**

$P_{sur-5}::UbV$ -GFP animals were made as described previously and were a gift from Thorsten Hoppe (Segref et al., 2011).

### **Quantification of GFP Fluorescence Signal in *C. elegans***

Animals were synchronized to the L4 stage by egg dropping from gravid hermaphrodites. 25 young adult (L4 + 1 day old) animals were placed in 50 $\mu$ L of M9 buffer in a 96-well plate. 3 wells (75 animals total) were each measured and averaged per condition. Fluorescence intensity was then measured using a 96-well fluorescent plate scanner.

### **Locomotor assays**

*C. elegans* locomotor assays were performed as a swimming assay done in a drop of M9 on the surface of an agar plate. For each assay, 15 to 25 worms were allowed to lay eggs for 4 hours. Once larvae reached the L4 stage, locomotor behavior was blindly recorded on a video camera attached to a Zeiss Stemi SV11 dissecting scope and tracked using the Parallel Worm Tracker program (<http://wormsense.stanford.edu/tracker>; Miriam Goodman; Stanford University, Palo Alto, CA). Behavior was also recorded at a young adult stage (24 hours after L4). For each experiment, five trials containing 7-10 animals per group were completed, and at least three independent experiments were performed for each locomotor assay on different days. To analyze the swimming behavior, animal tracks were analyzed on MATLAB (MathWorks) to determine the average speed (millimeters (mm) per second). All experiments were performed blind to genotype. Each locomotor assay was performed at

least three independent times on different days. One representative experiment is shown.

### **Motor neuron survival assays with tenovin-1**

Mixed spinal cord neuron cultures were prepared as described previously (Jeong et al., 2006; Mojsilovic-Petrovic et al., 2006). Briefly, an astrocyte feeder layer was prepared from the cortex of newborn Sprague Dawley rat pups (postnatal day 2 (P2)) and grown to ~80% confluency. Subsequently, dissociated embryonic day 15 (E15) spinal cord neurons were added. One to two days later, AraC (5mM) (catalog #C6645; Sigma) was added for 24 hours to arrest astrocyte proliferation. Cultures were maintained in glia-conditioned medium supplemented with the following trophic factors (1.0ng/mL each): human neurotrophin-3, human neurotrophin-4, human brain-derived neurotrophic factor, and rat ciliary neurotrophic factor (Alomone Labs). Half of the culture medium was replaced on a biweekly basis.

For motor neuron toxicity assays with tenovin-1, cultures were pre-treated with 1.6µM tenovin-1 at DIV13. The next day, HSV-mutSOD1 (G85R) virus was added to the media at 1µL per mL. Fresh drug was added when the media was changed three times per week. At DIV19, cultures were fixed in freshly prepared 4% PFA and stained with SMI-32 antibody (Convance). Slides were then developed using standard HRP protocol. Motor neurons were then counted blindly. Briefly, motor neurons were counted in three fields of view per slide and the average was taken. The experiment was repeated two independent times and the representative experiment is shown.

### **RNAi knockdown in *C. elegans***

Each RNAi (RNA Interference) colony was grown overnight in Luria broth containing ampicillin (50 µg/mL), and 200uL was seeded onto NGM plates containing isopropylthiogalactoside (1mM) to induce dsRNA expression. The RNAi clone for *rad-23* was generated as described previously in the Ahringer library (Fraser et al., 2000). For locomotor experiments, L4 animals were placed on RNAi plates overnight. On the next day, young adult animals were transferred to a fresh RNAi plate and allowed to lay eggs for 4-6 hours. Progeny were subsequently tested at the young adult (L4 + 1 day) stage for locomotor activity. All assays were performed blind to genotype. Average of three independent experiments is shown.

### **Tunicamycin lifespan assay**

For the tunicamycin lifespan assay, worms were allowed to lay eggs on NGM plates for 4-6 hours. At the young adult stage (L4+1 day), 100 worms were placed on either a NGM plate supplemented with either vehicle (DMSO) or tunicamycin (Sigma T7765; 5µg/mL). NGM plates were all seeded with OP50 and the final concentration of DMSO in the plates did not exceed 0.2%. Worms were transferred to a fresh plate every day and scored for survival by response to light touch. Bagging worms or worms with a vulva explosion phenotype were excluded from the analysis. All assays were completed blind to genotype.

## RESULTS

### **Overexpression of mutTDP-43 in the nervous system causes a non-cell autonomous increase in ubiquitinated GFP**

To investigate the imbalance of protein quality control in a model of motor neuron disease, we placed transgenic mutTDP-43 animals on the background of worms expressing ubiquitinated GFP under control of the ubiquitous *sur-5* promoter. Under wild type conditions at young ages, this GFP molecule is degraded due to the presence of the ubiquitin tag. However, when we placed this on the wtTDP-43 or mutTDP-43 background, we observed a significant increase in the accumulation of GFP ( $p < 0.05$ ) in non-neuronal tissues, although exogenous human TDP-43 expression is limited to the nervous system due to the *snb-1* promoter (Figure 1A-B). These results suggest there is an accumulation of normally degraded ubiquitinated substrates in the presence of overexpressed mutTDP-43 which is non-cell autonomous. This is resonant with an emerging theme of imbalanced protein quality control of the proteome in neurodegeneration.

### **Loss of *ufd-3*, but not *rad-23*, reduces UbV-GFP in the mutTDP-43 background**

We asked if any of the suppressors or enhancers identified in the directed genetic screen presented in Chapter 3 might also modify the burden of non-degraded UbV-GFP. We observed that only knockdown of *ufd-3* suppressed the accumulation of UbV-GFP in the mutTDP-43 background (Figure 2A-B).

### **Constitutive activation of ER stress enhances toxicity to tunicamycin**

Given the recent hypothesis that there may be too much activation of ER stress in neurodegeneration, we wanted to ask if constitutive activation of the ER stress pathway by the effector XBP1 (constitutively spliced XBP1, “XBP1s”) could modify models of motor neuron disease. We created *C. elegans* that overexpressed or expressed a single copy of “XBP1s” under the control of a nervous specific promoter ( $P_{UNC-119}$ ). We then asked if this protected animals against ER stress pharmacologically induced by the drug, tunicamycin. We found that ~40% of wild type animals were dead after one week on tunicamycin-containing NGM (nematode growth medium) plates, compared to roughly ~90% of the animals that either overexpressed or expressed only a single copy of “XBP1s” (Figure 3A). Furthermore, the animals with a constitutively spliced “XBP1s” also showed lower average speeds compared to control animals in a 30 second forced swimming assay, although this change was not significant ( $p > 0.05$ ) (Figure 3B).

### **Stabilization of p53 protects motor neurons against death caused by mutSOD1**

RAD-23 has been shown to have conflicting the roles on the turnover of a number of proteins. In Chapter 3, we present evidence that RAD-23 inhibits the turnover of ALS-linked proteins and thereby exacerbate their toxicity. p53 has been linked to neurodegenerative disease in a number of settings (Lanni et al., 2012) and is one RAD-23 substrate (Brignone et al., 2003). Furthermore, loss of *ufd-2* identified in our directed genetic screen for suppressors of mutTDP-43 also has a role in p53 stabilization (Jiou Wang, personal communication). Therefore, we wanted to ask if the stabilization of p53 could also suppress the toxicity of mutated proteins in neurodegeneration. To do this, we pre-treated cultures with tenovin-1, a known p53 stabilizing drug, and asked if it suppressed toxicity caused but mutSOD. We found that treatment of tenovin-1 had no

effect on motor neuron survival at low to medium concentrations, but was toxic at higher concentrations (data not shown). We therefore used a medium concentration of tenovin-1 (1.6 $\mu$ M) to ask if it protected against toxicity of mutSOD in motor neuron survival. We found that mutSOD1 reduced motor neuron survival was reduced by ~50%, however mutSOD toxicity was reduced by ~45% ( $p < 0.0001$ ) in cultures that were treated with tenovin-1 (Figure 4).

### **Some suppressors and enhancers operate in a non-cell autonomous manner**

Because *rad-23* and *ubql-1* are similar genes with opposite effects on the mutSOD phenotype, we wanted to further investigate how loss of *ubql-1* might enhance the mutSOD locomotor deficit. To do this, we took advantage again of the resistance of the *C. elegans* nervous system to RNAi. When we fed *ubql-1* RNAi to mutSOD worms, we found an enhancement of the locomotor deficit ( $p < 0.05$ ) (Figure 5A). However, G85R; *sid-1*;  $P_{unc-119}::SID-1$  animals fed *ubql-1* RNAi for two generations showed no effect on the locomotor deficit ( $p > 0.05$ ) (Figure 5B). These results suggest that *ubql-1* might enhance the mutSOD1 locomotor deficit in a non-cell autonomous manner, although we found in Chapter 3 of this work that loss of *rad-23* operated a cell autonomous manner within the nervous system

### **Constitutively “on” HIF1 $\alpha$ suppresses the mutSOD locomotor deficit**

Although *C. elegans* with ubiquitously expressed “on” HIF1 $\alpha$  showed a locomotor deficit compared to wild type animals in a forced swimming assay ( $p < 0.05$ ) (Figure 6A), we observed that animals with “on” HIF1 $\alpha$  only in the nervous system suppressed the mutSOD locomotor deficit two fold ( $p < 0.05$ ) (Figure 6B).



## FIGURE LEGENDS

**Figure A2.1. Overexpression of wild type (wt-) and mutant (mut-) TDP-43 (M337V) in the nervous system causes an accumulation of normally degraded ubiquitinated substrates in a non-cell autonomous manner.** mutTDP-43 worms were placed on the background of the ubiquitous *sur-5* promoter expressing a ubiquitinated GFP (UbV-GFP). (A) Representative images of the UbV-GFP lines in wild type, wtTDP43, and mutTDP-43 animals at the young adult stage. Arrowheads point out accumulation of GFP primarily in the intestine and pharynx. (B) Mean GFP fluorescence of 25 animals per well (n=3) containing 50 $\mu$ L of M9 buffer. \* $p < 0.05$  according to Student's *t*-test. ("M337V": mutTDP-43)

**Figure A2.2. Knockdown of *ufd-3*, but not *rad-23*, in *C. elegans* reduces ubiquitinated GFP abundance.** (A) Representative images of young adult (L4+1day) *C. elegans* fed indicated RNAi for the previous two generations. (B) Mean GFP fluorescence of 25 animals per well containing 50 $\mu$ L of M9 buffer.

**Figure A2.3. Expression of constitutively spliced XBP1 in the nervous system enhances toxicity of ER stress.** (A) *C. elegans* containing an extrachromosomal array or single copy of P<sub>unc-119</sub>::XBP1s::mCherry show enhanced toxicity to tunicamycin. Lifespan assay of *C. elegans* placed on NGM plates containing 5 $\mu$ g/mL tunicamycin beginning at 1 day of adulthood. (B) Average speed of young adult (L4+1 day) animals in a 30 second forced swimming assay in M9. *C. elegans* containing an extrachromosomal array or a single copy of P<sub>unc-119</sub>::XBP1s::mCherry show reduced average speeds, although this is not significant.

**Figure A2.4. Stabilization of p53 by treatment with tenovin-1 protects motor neurons from toxicity caused by mutSOD1 (G85R).** (A-D) Representative images of motor neurons stained with SMI-32 following indicated treatment. (E) % of motor neurons (of control) remaining following indicated treatment. One-way ANOVA revealed group differences ( $F_{(3,12)}=9.867$ ;  $p = 0.0015$ ). There is a significant ( $p < 0.0001$ ; Tukey's *post hoc* test) protection of motor neurons from mutSOD toxicity in the tenovin-1 treatment group.

**Figure A2.5. Only ubiquitous knockdown of *ubq1-1* enhances the mutSOD locomotor deficit.** (A) Feeding *ubq1-1* RNAi to mutSOD1 animals suppresses the locomotor deficit ( $p = 0.005$  according to Student's *t-test*). (B) Feeding *ubq1-1* RNAi to mutSOD1 animals where the RNAi effect is limited to the nervous system has no effect on the locomotor deficit.

**Figure A2.6. Constitutively 'on' HIF1 $\alpha$  in the nervous system alone protects against mutSOD toxicity in *C. elegans*.** (A) Average speed of *C. elegans* (wild type, constitutively 'on' HIF1 $\alpha$  in all tissues, constitutively 'off' HIF1 $\alpha$  in all tissues) in a 30 second forced swimming assay in M9 buffer. Animals with constitutively 'on' HIF1 $\alpha$  in all tissues show decreased average speed compared to wild type animals. (B) Constitutively 'on' HIF1 $\alpha$  in the nervous system alone protects against mutSOD toxicity in *C. elegans* as measured by the average speed in 30 second forced swim assay.  $*p < 0.05$  according to Student's *t-test*.

**Figure A2.1. Overexpression of wild type (wt-) and mutant (mut-) TDP-43 (M337V) in the nervous system causes an accumulation of normally degraded ubiquitinated substrates in a non-cell autonomous manner.**

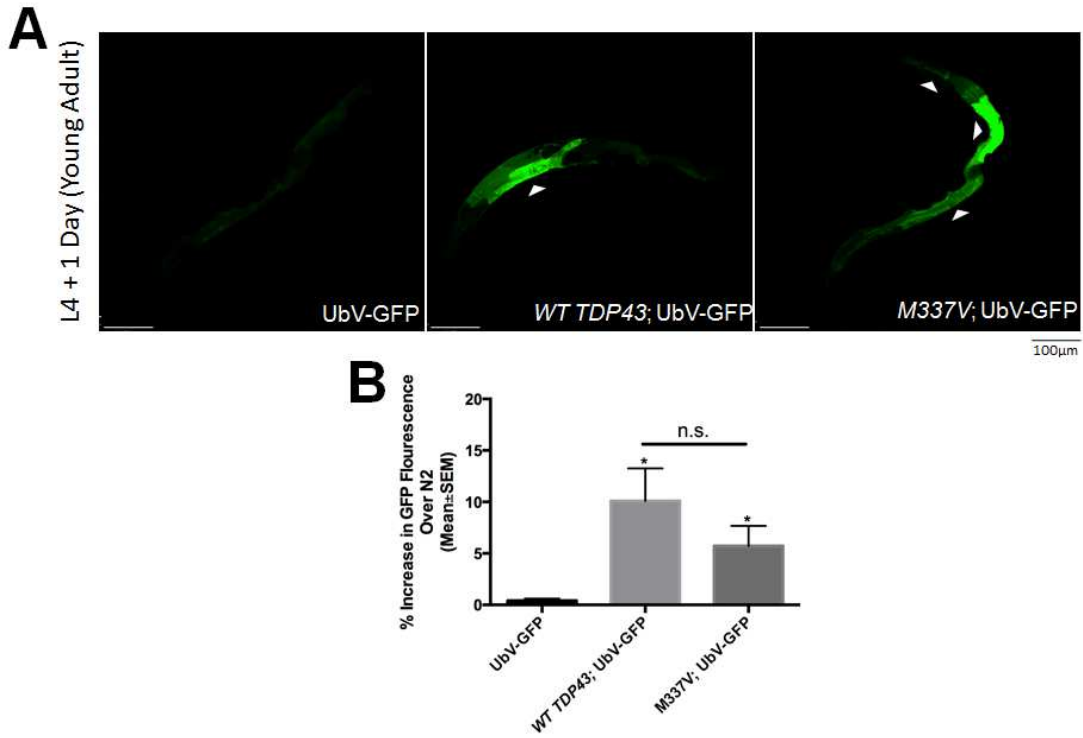
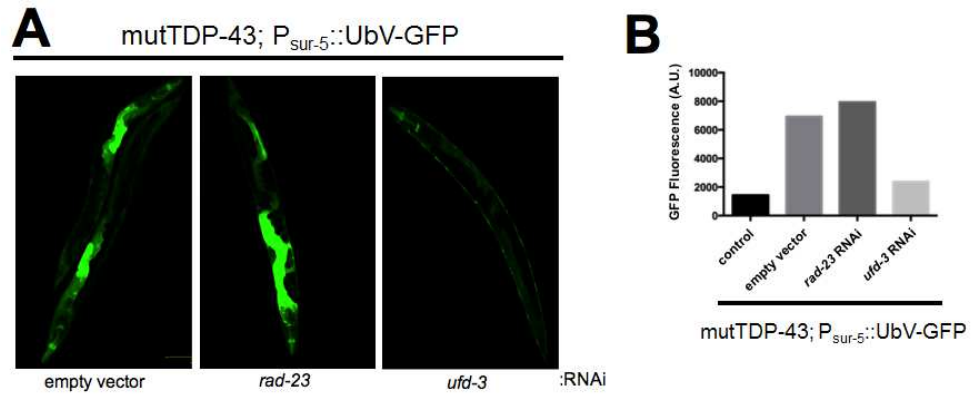
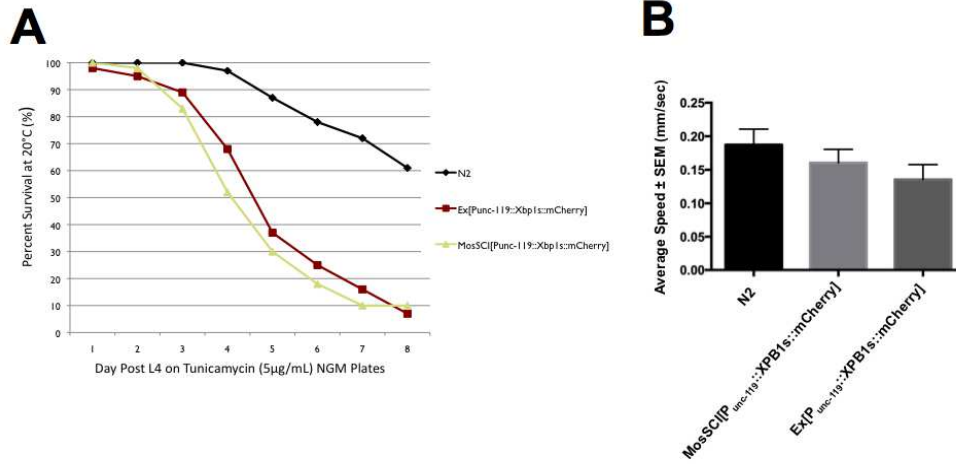


Figure A2.2. Knockdown of *ufd-3*, but not *rad-23*, in *C. elegans* reduces ubiquitinated GFP abundance in mutTDP-43 background.



**Figure A2.3. Expression of constitutively spliced XBP1 in the nervous system enhances toxicity of ER stress.**



**Figure A2.4. Stabilization of p53 by treatment with tenovin-1 protects motor neurons from toxicity caused by mutSOD1 (G85R).**

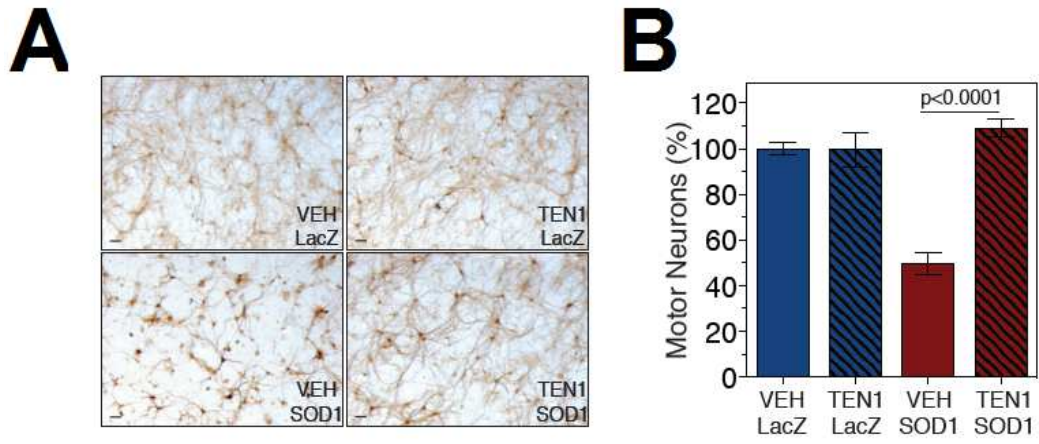


Figure A2.5. Only ubiquitous knockdown of *ubq1-1* enhances the *mutSOD* locomotor deficit.

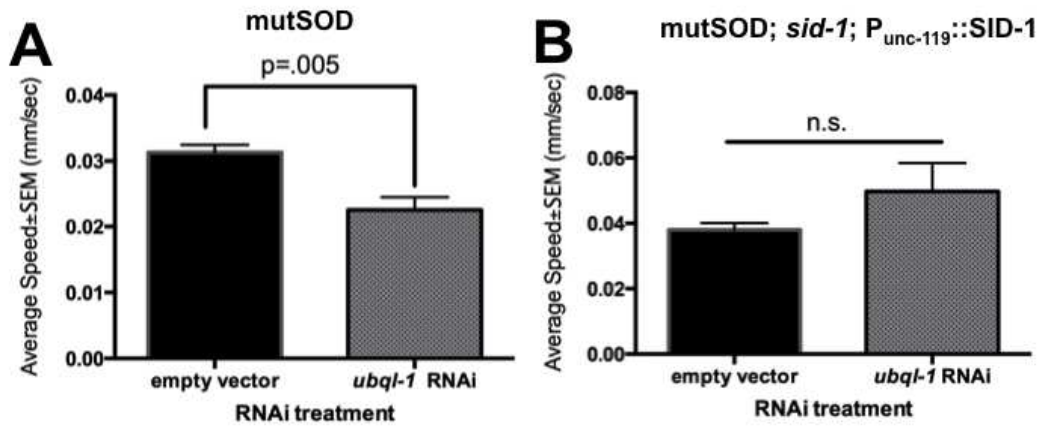
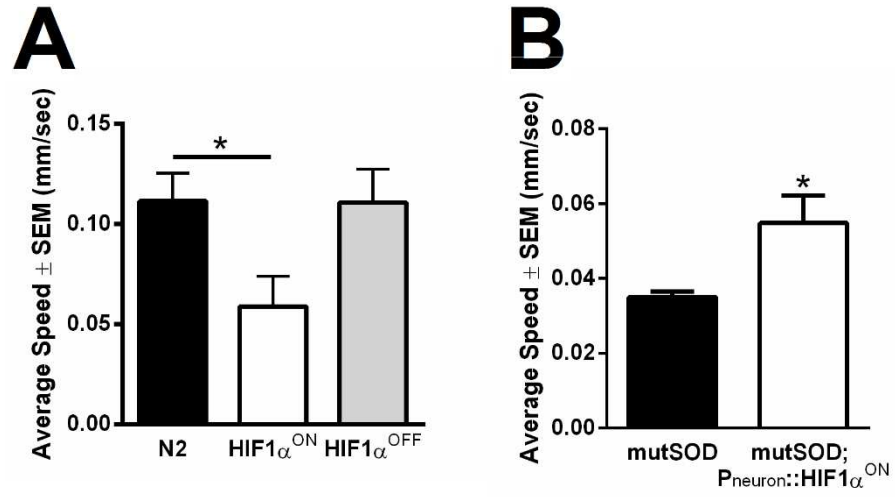


Figure A2.6. Constitutively 'on' HIF1 $\alpha$  in the nervous system alone protects against mutSOD toxicity in *C. elegans*.





## BIBLIOGRAPHY

Abisambra JF, Jinwal UK, Blair LJ, O'Leary JC, Li Q, Brady S, Wang L, Guidi CE, Zhang B, Nordhues BA, et al. (2013) Tau accumulation activates the unfolded protein response by impairing endoplasmic reticulum-associated degradation. *J Neurosci* 33:9498-9507.

Arnold ES, Ling SC, Huelga SC, et al. (2013) ALS-linked TDP-43 mutations produce aberrant RNA splicing and adult-onset motor neuron disease without aggregation or loss of nuclear TDP-43. *Proc Natl Acad Sci* 110:736-745.

Atkin JD, Atkin MA, Farg BJ, Turner D, Tomas JA, Lysaght J, Nunan J, Rembach A, Nagley P, Beart PM, Cheema SS, Home MK (2006) Induction of the unfolded protein response in familial amyotrophic lateral sclerosis and association of protein-disulfide isomerase with superoxide dismutase 1. *J Biol Chem* 281:30152-30165.

Atkin JD, Farg MA, Walker AK, McLean C, Tomas D, Horne MK (2008) Endoplasmic reticulum stress and induction of the unfolded protein response in human sporadic amyotrophic lateral sclerosis. *Neurobiol Dis* 30: 400-7.

Austin JA, Wright GS, Watanabe S, Grossman JF, Antonyuk SV, Yamanaka K, Hasnain SS (2014) Disease causing mutants of TDP-43 nucleic acid binding domains are resistant to aggregation and have increased stability and half-life. *Proc Natl Acad Sci USA* 111: 4309-14.

Avendano-Vasquez SE, Dhir A, Bembich S, Buratti E, Proudfoot N, Baralle FE (2012) Autoregulation of TDP-43 mRNA levels involves interplay between transcription, splicing, and alternative polyA site selection. *Genes Dev* 26: 1679-84.

Bacopulus S, Amemiya Y, Yang W, Zubovits J, Burger A, Yaffe M, Seth AK (2012) Effects of partner proteins on BCA2 RING ligase activity. *BMC Cancer* 8: 12-63.

Baralle M, Buratti E, Baralle FE (2013) The role of TDP-43 in the pathogenesis of ALS and FTL. *Biochem Soc Trans* 41:1536-1540.

Barmada SJ, Serio A, Arjun A, Bilican B, Daub A, Ando DM, Tsvetkov A, Pleiss M, Li X, Peisach D, Shaw C, Chandan S, Finkbeiner S (2014) Autophagy induction enhances TDP43 turnover and survival in neuronal ALS models. *Nat Chem Biol* 10:67-85.

Beckman JS, Carson M, Smith CD, Koppenhol WH (1993) ALS, SOD, and peroxynitrite. *Nature* 364:584.

Bergink S, Severijnen LA, Wilgers N, Sugasawa K, Yousaf H, Kros JM, van Swieten J, Oostra BA, Vermeulen W, Willemsen R (2006) The DNA repair-ubiquitin-associated HR23 proteins are constituents of neuronal inclusions in specific neurodegenerative disorders without hampering DNA repair. *Neurobiology of Disease* 23:708-716.

Bergink S, Toussaint W, Luijsterburg MS, Dinant C, Alekseev S, Hoeijmakers JH, Dantuma NP, Houtsmuller AB, Vermeulen W (2012) Recognition of DNA damage by XPC coincides with disruption of the XPC-RAD23 complex. *J Cell Bio* 196:681-8.

Bertolaet BL, Clarke DJ, Wolff M, Watson MH, Henze M, Divita G, Reed SI (2001) UBA domains of DNA damage-inducible proteins interact with ubiquitin. *Nat Struct Biol* 8:417-422.

Blount JR, Tsou WL, Ristic G, Burr AA, Ouyang M, Galante H, Scaglione KM, Todi SV (2014) Ubiquitin-binding site 2 of ataxin-3 prevents its proteasomal degradation by interacting with Rad23. *Nature Communications* 5:4638.

Bocitto M, Lamitina T, Kalb RG (2012) Daf-2 signaling modifies mutant SOD1 toxicity in *C. elegans*. *PLoS One* 7:e33494.

Bohm S, Lamberti G, Fernandez-Saiz V, Stapf C, Buchberger A (2011) Cellular functions of Ufd2 and Ufd3 in proteasomal protein degradation depend on Cdc48 binding. *Mol Cell Bio* 31:1528-39.

Brenner S (1974) The genetics of *Caenorhabditis elegans*. *Genetics* 1:71-94.

Brignone C, Bradley KE, Kisselev AF, Grossman SR (2004) A post-ubiquitination role for MDM2 and hHR23A in the p53 degradation pathway. *Oncogene* 23:4121-4129.

Brujin LI, Houseweart MK, Kato S, Anderson KL, Anderson SD, Ohama E, Reaume AG, Scott RW, Cleveland DW (1998) Aggregation and motor neuron toxicity of an ALS-linked SOD1 mutant independent from wild-type SOD1. *Science* 281:1851-1854.

Butts DA, Kanold PO, Shatz CJ (2007) A burst-based "Hebbian" learning rule at retinogeniculate synapses links retinal waves to activity-dependent refinement. *PLoS Biology* 5:e61.

Calixto A, Chelur D, Topalidou I, Chen X, Chalfie M (2010) Enhanced neuronal RNAi in *C. elegans* using SID-1. *Nat Methods* 7:554-559.

Casticas M, Allcorn S, Mobbs P (2001) Early activation of Ca<sup>2+</sup>-permeable AMPA receptors reduces neurite outgrowth in embryonic chick retinal neurons. *J Neurobiol* 49:200-211.

Caudron F, Barral Y (2013) A super-assembly of Whi3 encodes memory of deceptive encounters by single cells during yeast courtship. *Cell* 155:1244-1257.

Chen L, Shinde U, Ortolan TG, Madura K (2001) Ubiquitin-associated (UBA) domains in Rad23 bind ubiquitin and promote inhibition of multi-ubiquitin chain assembly. *EMBO Rep* 10:933-938.

Chen L, Madura K (2002) Rad23 promotes the targeting of proteolytic substrates to the proteasome. *Mol Cell Biol* 22:4902-4913.

Chen L, Madura K. (2006) Evidence for distinct functions for human DNA repair factors hHR23A and hHR23B. *FEBS Letters* 580:3401-3408.

Chen SX, Tari PK, She K, Haas K (2010) Neurexin-neurologin cell adhesion complexes contribute to synaptotropic dendritogenesis via growth stabilization mechanisms in vivo. *Neuron* 67:967-983.

Cleveland DW, Rothstein JD (2001) From Charcot to Lou Gehrig: deciphering selective motor neuron death in ALS. *Nat Rev Neurosci* 2:806-819.

Cronin S, Berger S, Ding J, Schymick JC, Washecka N, Hernandez DG, Greenway MJ, Bradley DG, Traynor BJ, Hardiman O (2008) A genome-wide association study of sporadic ALS in a homogenous Irish population. *Hum Mol Genet* 17:768-774.

Cronin S, Hardiman O, Traynor BJ (2007) Ethnic variation in the incidence of ALS: a systematic review. *Neurology* 68:1002-1007.

Dangond F, Hwang D, Camelo S, Pasinelli P, Frosch MP, Stephanopoulos G, Stephanopoulos G, Brown RH, Gullans SR (2004) Molecular signature of late-stage human ALS revealed by expression profiling of postmortem spinal cord gray matter. *Physiol Genomics* 16:229-239.

Dantuma NP, Heinen C, Hoogstraten D (2009) The ubiquitin receptor RAD-23: at the crossroads of nuclear excision repair and proteasomal degradation. *DNA Repair* 8:449-460.

Deng HX, Chen W, Hong ST, et al. (2011) Mutations in UBQLN2 cause dominant X-linked juvenile and adult-onset ALS and ALS/dementia. *Nature* 477:211-217.

Deng HX, Hentati A, Tainer JA, Iqbal Z, Cayabyab A, Hung WY, Getzoff ED, Hu P, Herzfeldt B, Roos RP, et al. (1993) Amyotrophic lateral sclerosis and structural defects in Cu, Zn superoxide dismutase. *Science* 261: 1047-1051.

Deng Q, Holler CJ, Taylor G, Hudson KF, Watkins W, Gearing M, Ito D, Murray ME, Dickson DW, Seyfried NT, Kukar T (2014) FUS is phosphorylated by DNA-PK and accumulates in the cytoplasm after DNA damage. *J Neurosci* 34:7802-7813.

Dip R, Camenisch U, Naegeli H (2004) Mechanisms of DNA damage recognition and strand discrimination in human nucleotide excision repair. *DNA Repair* 3:1409-1423.

Elias GM, Funke L, Stein V, Grant SG, Bredt DS, Nicoll RA (2007) Synapse-specific and developmentally regulated targeting of AMPA receptors by a family of MAGUK scaffolding proteins. *Neuron* 52:307-320.

Engesser-Cesar C, Anderson AJ, Basso DM, Edgerton VR, Cotman CW (2005) Voluntary wheel running improves recovery from a moderate spinal cord injury. *Journal of Neurotrauma* 22:157-171.

Ermolaeva MA, Segref A, Dakhovnik A, Ou HL, Schneider JI, Utermöhlen O, Hoppe T, Schumacher B (2013) DNA damage in germ cells induces an innate immune response that triggers systemic stress resistance. *Nature* 501:416-420.

Fawzi NL, Yap EH, Okabe Y, Kohlstedt KL, Brown SP, Head-Gordon T (2008) Contrasting disease and nondisease protein aggregation by molecular simulation. *Acc Chem Res* 41:1037-1047.

Fensgard O, Kassahun H, Bombik I, Rognes T, Lindvall JM, Nilsen H (2010) A two-tiered compensatory response to loss of DNA repair modulates aging and stress response pathways. *Aging* 2:133-158.

Ferraiuolo L, Higginbottom A, Heath PR, Barber S, Greenald D, Kirby J, Shaw PJ (2011) Dysregulation of astrocyte-motoneuron cross-talk in mutant superoxide dismutase 1-related amyotrophic lateral sclerosis. *Brain* 134:2627-2641.

Ferraiuolo L, Kirby J, Grierson AJ, Sendtner M, Shaw PJ (2011) Molecular pathways of motor neuron injury in amyotrophic lateral sclerosis. *Nat Rev Neurol* 7:616-630.

Fischer LR, Li Y, Asress SA, Jones DP, Glass JD (2012) Absence of SOD1 leads to oxidative stress in peripheral nerve and causes a progressive distal motor axonopathy. *Exp Neurol* 233:163-171.

Fishbain S, Prakash S, Herrig A, Elsasser S, Matouscheck A (2011) Rad23 escapes degradation because it lacks a proteasome initiation region. *Nature Communications* 8:192.

Flood DG, Reaume AG, Gruner JA, Hoffman EK, Hirsch JD, Lin YG, Dorgman KS, Scott RW (1999) Hindlimb motor neurons require Cu/Zn superoxide dismutase for maintenance of neuromuscular junctions. *Am J Pathol* 155:663-67.

Ford DL, Monteiro MJ (2007) Studies of the role of ubiquitination in the interaction of the ubiquilin with the loop and carboxyl terminal regions of presenilin-2. *Biochem* 46:8827-8837.

Forman MS, Trojanowski JQ, Lee VMY (2004) Neurodegenerative diseases: a decade of discoveries paves the way for therapeutic breakthroughs. *Nature Medicine* 10:1055-1063.

Funakoshi M, Sasaki T, Nishimoto T, Kobayashi H (2002) Budding yeast Dsk2p is a polyubiquitin-binding protein that can interact with the proteasome. *Proc Natl Acad Sci USA* 99:745-750.

González-Pérez P, Cirulli ET, Drory VE, Dabby R, Nisipeanu P, Carasso RL, Sadeh M, Fox A, Festoff BW, Sapp PC, McKenna-Yasek D, Golstein DB, Brown RH, Blumen SC (2012) Novel mutation in VCP gene causes atypical amyotrophic lateral sclerosis. *Neurology* 79:2201-2208.

Haas K, Li J, Cline HT (2006) AMPA receptors regulate experience-dependent dendritic arbor growth in the intact brain. *Proc Natl Acad Sci* 103:12127-12131.

Habibi-Babadi N, Su A, de Carvalho CE, Colavita A (2010) The N-glycanase png-1 acts to limit axon branching during organ formation in *Caenorhabditis elegans*. *J Neurosci* 30:1766-1776.

Halfmann R, Jarosz DF, Jones SK, Chang A, Lancaster AK, Lindquist S (2012) Prions are a common mechanism for phenotypic inheritance in wild yeasts. *Nature* 482:363-368.

Hampton RY (2003) IRE1: a role in UPREgulation of ER degradation. *Dev Cell* 4:144-146.

Hebb DO (1949) *The Organization of Behavior*. John Wiley & Sons, Inc. New York.

Heinen C, Acs K, Hoogstraten D, Dantuma NP (2011) C-terminal UBA domains protect ubiquitin receptors by preventing initiation of protein degradation. *Nature Communications* 8:191.

Hetz C, Thielen P, Matsus S, Nassif M, Court F, Kiffin R, Martinez G, Cuervo AM, Brown RH, Gllimcher LH (2009) XBP-1 deficiency in the nervous system protects against amyotrophic lateral sclerosis by increasing autophagy. *Genes Dev* 23:2294-2306.

Holmes DL, Lancaster AK, Lindquist S, Halfmann R (2013) Heritable remodeling of yeast multicellularity by an environmentally responsive prion. *Cell* 153:153-165.

Hou F, Sun L, Zheng SH, Skaug B, Jiang QX, Chen ZJ (2011) MAVS forms functional prion-like aggregates to active and propagate antiviral innate immune response. *Cell* 146:448-461.

Howard MA, Elias GM, Elias LA, Swat W, Nicoll RA (2010) The role of SAP97 in synaptic glutamate receptor dynamics. *Proc Natl Acad Sci USA* 107:3805-3810.

Hubel DH, Wiesel TN, LeVay S (1977) Plasticity of ocular dominance columns in monkey triate cortex. *Phil Trans R Sec Lond* 278:377-409.

Hughes EG, Peng X, Gleichman AJ, Lai M, Zhou L, Tsou R, Parsons TD, Lynch DR, Dalmau J, Balice-Gordon RJ. (2010) Cellular and synaptic mechanisms of anti-NMDA receptor encephalitis. *J. Neurosci.* 30: 5866-5875.



Hughes EG, Elmariah SB, Balice-Gordon RJ. (2010) Astrocyte secreted proteins selectively increase hippocampal GABAergic axon length, branching, and synaptogenesis. *Mol. Cell Neurosci.* 43: 136-145.

Hume RI, Purves D (1981) Geometry of neonatal neurons and the regulation of synapse of elimination. *Nature* 293:469-471.

Igaz LM, Kwong LK, Lee EB, Chen-Plotkin A, Swanson E, Unger T, Malunda J, Xu Y, Winton MJ, Trojanowski JQ, and Lee VM (2011) Dysregulation of the ALS-associated gene TDP-43 leads to neuronal death and degeneration in mice. *J Clin Invest* 121:726-738.

Ilieva EV, Ayala V, Jové M, Dalfó E, Cacabelos D, Povedano M, Bellmunt MJ, Ferrer I, Pamplona R, Portero-Otin M (2007) Oxidative and endoplasmic reticulum stress interplay in sporadic amyotrophic lateral sclerosis. *Brain* 130:3111-3123.

Ilieva H, Polymenidou M, Cleveland DW (2009) Non-cell autonomous toxicity in neurodegenerative disorders: ALS and beyond. *J Cell Biol* 187:761-772.

Inglis FM, Crockett R, Korada S, Abraham WC, Hollmann M, Kalb RG (2002) The AMPA receptor subunit GluR1 regulates dendritic architecture of motor neurons. *J Neurosci* 22:8042-8051.

Ito Y, Yamada M, Tanaka H, Aida K, Tsuruma K, Shimazawa M, Hozumi I, Inuzuka T, Takahashi H, Hara H (2009) Involvement of CHOP, an ER stress apoptotic mediator, in both human sporadic ALS and ALS model mice. *Neurobiol Dis* 36:470-476.

Jaarsma D, Haasdijk ED, Grashorn JA, Hawkins R, van Duijn W, Verspaget HW, London J, Holstege JC (2000) Human Cu/Zn superoxide dismutase (SOD1)

overexpression in mice causes mitochondrial vacuolization, axonal degeneration, and premature motoneuron death and accelerates motorneuron disease in mice expressing a familial amyotrophic lateral sclerosis mutant SOD1. *Neurobiol Dis* 7:623-643.

Jaarsma D, van der Pluijm I, de Waard MC, Haasdijk ED, Brandt R, Vermeij M, Rijkse Y, van Steeg H, Hoeijmakers JH, van der Horst GT (2011) Age-related neuronal degeneration: complementary roles of nucleotide excision repair and transcription-coupled repair in preventing neuropathology. *PLoS Genet* 7:e1002405.

Jablonski AM, Kalb RG (2013) GluA1 promotes the activity-dependent development of motor circuitry in the developing spinal cord. *Ann N Y Acad Sci* 1279:54-59.

Jakowec MW, Len Y, Kalb RG (1995) In situ hybridization analysis of AMPA receptor subunit gene expression in the developing rat spinal cord. *Neuroscience* 67:909-920.

Jakowec MW, Fox AJ, Martin LJ, Kalb RG (1995) Quantitative and qualitative changes in AMPA receptor expression during spinal cord development. *Neuroscience* 67:893-907.

Jeong GB, Wener M, Gazula VR, Itoh T, Roberts M, David S, Pfister B, Cohen A, Neve RL, Hollmann M, Kalb RG (2006) Bi-directional control of motor neuron dendrite remodeling by the calcium permeability of AMPA receptors. *Mol Cell Neurosci* 37:299-314.

Johnson ES, Ma PC, Ota IM, Varshavsky A (1995) A proteolytic pathway that recognizes ubiquitin as a degradation signal. *J Biol Chem* 270:17442-56.

Johnson JO, Mandrioli J, Benatar M, et al. (2010) Exome sequencing reveals VCP mutations as a cause of familial ALS. *Neuron* 68:857-864. .

Kabashi E, Valdmanis PN, Dion P, et al. (2008) TARDBP mutations in individuals with sporadic and familial amyotrophic lateral sclerosis. *Nat Genet* 40:574-574.

Kalb RG, Zhang L, Zhou W (2013) The molecular basis of experience-dependent motor system development. *Adv Exp Med Biol* 782:23-38.

Kaneko M, Koike H, Saito R, Kitamura Y, Okuma Y, Nomura Y (2010) Loss of HRD1-mediated protein degradation causes amyloid precursor protein accumulation and myloid-beta generation. *J Neurosci* 30:392-3932.

Kang MJ, Ryoo HD (2009) Suppression of retinal degeneration in *Drosophila* by stimulation of ER-associated degradation. *PNAS* 106:17043-17048.

Katz LC, Shatz CJ (1996) Synaptic activity and the construction of cortical circuits. *Science* 274:1133-1138.

Kim CH, Takamiya K, Petralia RS, Sattler R, Yu S, Zhou W, Kalb R, Wenthold R, Huganir R (2005) Persistent hippocampal CA1 LTP in mice lacking the C-terminal PDZ ligand of GluR1. *Nature Neuroscience* 8:985-987.

Kikuchi H, Almer G, Yamashita C, Guegan C, Nagai M, Zuoshang X, Sosunov AA, McKhann GM, Przedborski S (2006) Spinal cord endoplasmic reticulum stress associated with a microsomal accumulation of mutant superoxide dismutase-1 in an ALS model. *Proc Natl Acad Sci USA* 103:6025-6030.

Kim HJ, Raphael AR, LaDow ES, McGurk L, Weber RA, Trojanowski JQ, Lee VM, Finkbeiner S, Gitler AD, Bonini NM. (2014) Therapeutic modulation of eIF2 $\alpha$  phosphorylation rescues TDP-43 toxicity in amyotrophic lateral sclerosis disease models. *Nature Genetics* 46:152-160.

Kim I, Mi, K, Rao H (2004) Multiple interactions of rad23 suggest a mechanism for ubiquitylated substrate delivery important in proteolysis. *Mol Biol Cell* 15:3357-3365.

Kim I, Ahn J, Liu C, Tanabe K, Apodaca J, Suzuki T, Rao H (2006) The Png1-Rad23 complex regulates glycoprotein turnover. *J Cell Biol* 172:211-219.

Kim SH, Shi Y, Hanson KA, Williams LM, Sakasai R, Bowler MJ, Tibbetts RS (2009) Potentiation of amyotrophic lateral sclerosis (ALS)-associated TDP-43 aggregation by the proteasome-targeting factor, ubiquilin 1. *Journal of Biological Chemistry* 284:8083-8092.

Kraemer BC, Schuck T, Wheeler JM, Robinson LC, Trojanowski JQ, Lee VMY, Schellenberg GD (2010) Loss of murine TDP-43 disrupts motor function and plays an essential role in embryogenesis. *Acta Neuropathol* 119:409-419.

Krajacic P, Shen X, Purohit PK, Arratia P, Lamitina T (2012) Biomechanical profiling of *Caenorhabditis elegans*. *Genetics* 191:1015-1021.

Krivosheya D, Tapia L, Levinson JN, Huang K, Kang Y, Hines R, Ting AK, Craig AM, Mei L, Bamji SX, El-Husseini A. (2008) ErbB4-neuregulin signaling modulates synapse development and dendritic arborization through distinct mechanisms. *J. Biol. Chem.* 283:32944-32956.

Kruman II, Pedersen WA, Springer JE, Mattson MP (1999) ALS-linked Cu-ZN-SOD mutation increases vulnerability of motor neurons to excitotoxicity by a mechanism involving increased oxidative stress and perturbed calcium homeostasis. *Exp Neurol* 160:28-39.

Kuhlbrodt K, Janiesch PC, Kevel K, Segref A, Barikbin R, Hoppe T (2011) The Machado-Joseph disease deubiquitylase ATX-3 couples longevity and proteostasis. *Nat Cell Biol* 13:273-281.

Lamberson D, Chen L, Madura K (1999) Pleiotropic defects caused by loss of the proteasome-interacting factors Rad23 and Rpn10 of *Saccharomyces cerevisiae*. *Genetics* 153:69-79.

Lans H, Marteiijn JA, Schumacher B, Hoeijmakers JH, Jansen G, Vemeulen W (2010) Involvement of global genome repair, transcription coupled repair, and chromatin remodeling in UV DNA damage response changes during development. *PLoS Genet* 6:e1000941.

Lans H, Lindvall JM, Thijssen K, Karambelas AE, Cupac D, Fensgard O, Jansen G, Hoeijmakers JH, Nilsen H, Vermeulen W (2013) DNA damage leads to progressive replicative decline but extends the life span of long-lived mutant animals. *Cell Death Differ* 20:1709-1718.

Lans H, Vermeulen W (2011) Nucleotide excision repair in *Caenorhabditis elegans*. *Mol Bio Int* 2011:542795.

Lanni C, Racchi M, Memo M, Govoni S, Uberti D (2012) p53 at the crossroads between cancer and neurodegeneration. *Free Radic Biol Med* 52:1727-1733.

Le May N, Egly JM, Coin F (2010) True lies: the double life of the nucleotide excision repair factors in transcription and DNA repair. *J Nucleic Acids* 25:616342.

Lenk U, Yu H, Walter J, Gelman MS, Hartmann E, Kopito RR, Sommer T (2002) A role for mammalian Ubc6 homologues in ER-associated protein degradation. *J Cell Sci* 115:3007-3014.

Liachko NF, Guthrie CR, Kraemer BC (2010) Phosphorylation promotes neurotoxicity in a *Caenorhabditis elegans* model of TDP-43 proteinopathy. *J Neurosci* 30:16208-16219.

Lilley BN, Ploegh HL (2004) A membrane protein required for dislocation of misfolded proteins from the ER. *Nature* 429:834-840.

Lim MA, Selak MA, Xiang Z, Kraeinc D, Neve RL, Kraemer BC, Watts JL, Kalb RG (2012) Reduced activity of AMP-activated protein kinase protects against genetic models of motor neuron disease. *J Neurosci* 32:1123-1141.

Ling SC, Albuquerque CP, Han JS, Lagier-Tourenne C, Tokunaga S, Zhou H, Cleveland DW (2010) ALS-associated mutations in TDP-43 increase its stability and promote TDP-43 complexes with FUS/TLS. *Proc Natl Acad Sci USA* 107:13318-13323.

Ling SC, Polymenidou M, Cleveland DW (2013) Converging mechanisms in ALS and FTD: disrupted RNA and protein homeostasis. *Neuron* 79:416-438.

Liu OW, Shen K (2011) The transmembrane LRR protein DMA-1 promotes dendrite branching and growth in *C. elegans*. *Nature Neuroscience* 15:57-63.

Lommel L, Ortolan T, Chen L, Madura K, Sweder KS (2002). Proteolysis of a nucleotide excision repair protein by the 26 S proteasome. *Curr Genet* 42:9-20.

Lu K, Psakhye I, Jentsch S (2014) Autophagic clearance of polyQ proteins mediated by ubiquitin-Atg8 adaptors o the conserved CUET protein family. *Cell* 158:549-63.

Luthi A, Wikstrom MA, Palmer MJ, Matthews P, Benke TA, Isaac JT, Collingridge GL (2004) Bi-directional modulation of AMPA receptor unitary conductance by synaptic activity. *BMC Neurosci* 5:44.

Madabhushi R, Pan L, Tsai LH (2014) DNA damage and its links to neurodegeneration. *Neuron* 83:266-282.

Marchetto MC, Muotri AR, Mu Y, Smith AM, Cezar HH, Gage FH (2008) Non-cell-autonomous effect of human SOD1 G37R astrocytes on motor neurons derived from human embryonic stem cells. *Cell Stem Cell* 3:649-657.

Marteijn JA, Lans H, Vermeulen W, Hoeijmakers JH (2014) Understanding nucleotide excision repair and its roles in cancer and ageing. *Nat Rev Mol Cell Biol* 15:465-481.

Matus S, Lisbona F, Torres M, Leon C, Theirlen P, Hetz C (2013) The stress rheostat: an interplay between the unfolded protein response (UPR) and autophagy in neurodegeneration. *Current Molecular Medicine* 8:152-172.

Matus S, Nassif M, Glimcher LH, Hetz C (2009) XBP-1 deficiency in the nervous system reveals a homeostatic switch to activate autophagy. *Autophagy* 5:1226-1228.

Miller RG, Mitchell JD, Lyon M, Moore DH (2007) Riluzole for amyotrophic lateral sclerosis (ALS)/motor neuron disease (MND). *Cochrane Database Syst Rev* 1:CD001447.

Mooney R, Penn AA, Gallego R, Shatz CJ (1996) Thalamic relay of spontaneous retinal activity prior to vision. *Neuron* 17:863-874.

Mojsilovic-Petrovic J, Jeong GB, Crocker A, Arneja A, David S, Russell DS, Kalb RG (2006) Protecting motor neurons from toxic insult by antagonism of adenosine A2a and Trk receptors. *J Neurosci* 26:9250-63.

Mori A, Yamashita S, Uchino K, Suga Y, Ikeda Y, Takamatsu K, Ishizaki M, Koide T, Kimura E, Mita S, Maeda Y, Hirano T, Uchino M (2011) Derlin-1 overexpression ameliorates mutant SOD-1 induced endoplasmic reticulum stress by reducing mutant SOD1 accumulation. *Neurochem Int* 58:344-352.

Musaro A (2013) Understanding ALS: new therapeutic approaches. *The FEBS Journal* 280:4315-4322.

Myers AJ, Gibbs JR, Webster JA, et al. (2007) A survey of genetic human cortical gene expression. *Nat Genet* 39:1494-9.

Nagata T, Ilieva H, Murakami T, Shiote M, Narai H, Ohta Y, Hayashi T, Shoji M, Abe K (2007) Increased ER stress during motor neuron degeneration in transgenic mouse model of amyotrophic lateral sclerosis. *Neurol Res* 29:767-71.

N'Diaye EN, Hanyaloglu AC, Kajihara KK, Puthenveedu MA, Wu P, von Zastrow M, Brown EJ (200) The ubiquitin-like protein PLIC-2 is a negative regulator of G protein-coupled receptor endocytosis. *Molecular Biology of the Cell* 19: 1252-1260.

Nakatsukasa K, Brodsky JL (2008). The recognition and retrotranslocation of misfolded proteins from the endoplasmic reticulum. *Traffic* 9:861-870.

Neumann M, Kwong LK, Lee EB, Kremmer E, Flatley A, Xu Y, Forman MS, Troost D, Kretzschmar HA, Trojanowski JQ, Lee VM (2009) Phosphorylation of S409/410 of TDP-



43 is a consistent feature in all sporadic and familial forms of TDP-43 proteinopathies. *Acta Neuropathol* 117:137-149.

Neumann M, Sampathu DM, Kwong LK, et al. (2006) Ubiquitinated TDP-43 in frontotemporal lobar degeneration and amyotrophic lateral sclerosis. *Science* 314:130-133.

Ng JM, Veremeulen W, van der Horst GTJ, Bergink S, Sugawara K, Vrieling H, Hoeijmakers JHJ (2003) A novel regulation mechanism of DNA repair by damage-induced and RAD-23-dependent stabilization of xeroderma pigmentosum group C protein. *Genes Dev* 17:1640-1645.

Ni X, Martin-Caraballo M (2010) Differential effect of glutamate receptor blockade on dendritic outgrowth in chicken lumbar motoneurons. *Neuropharmacology* 58:593-604.

Niethammer M, Valtschanoff JG, Kapoor TM, Allison DW, Weinberg RJ, Craig AM, Sheng M (1998) CRIPT, a novel postsynaptic protein that binds to the third PDZ domain of PSD-95/SAP90. *Neuron* 4:693-707.

Nishitoh N, Kadowaki H, Nagai A, Maruyama T, Yokota T, Fukutomi H, Noguchi T, Matsuzawa A, Takeda K, Ichijo H (2008) ALS-linked mutant SOD1 induces ER stress- and ASK-1 dependent motor neuron death by targeting Derlin-1. *Genes Dev* 22:1451-1464.

Olzmann JA, Kopita RR, Christianson JC (2013) The mammalian endoplasmic reticulum-associated degradation system. *Cold Spring Harb Perspect Biol* 5:a013185.

Okuda Y, Nishi R, Ng JM, Vermeulen W, van der Horst GT, Mori T, Hoeijmakers JH, Hanaoka F, Sugawara K (2004) Relative levels of the two mammalian RAD-23

homologs determine composition and stabilization of xeroderma pigmentosum group C protein complex. *DNA Repair (Amst.)*3:1285-1295.

Ortolan TG, Chen L, Tongaonkar P, Madura K (2004) Rad23 stabilizes Rad4 from degradation by the Ub/proteasome pathway. *Nucleic Acids Res* 32:6490-6500.

Ortolan TG, Tongaonkar P, Lambertson D, Chen L, Madura K (2000) The Rad23 DNA repair protein is a negative regulator of substrate-linked multi-ubiquitin chain assembly. *Nature Cell Biol* 2:601-608.

Oswald S (1989) *Principles of Cellular, Molecular, and Developmental Neuroscience*. Springer-Verlag New York.

Park SH, Kukushkin Y, Gupta R, Chen T, Konagai A, Hipp MS, Hayer-Hartl M, Hartl FU (2013) PolyQ proteins interfere with nuclear degradation of cytosolic proteins by sequestering the Sis1P chaperone. *Cell* 154:134-145.

Passafaro M, Sala C, Niethammer M, Sheng M (1999) Microtubule binding by CRIPT and its potential role in the synaptic clustering of PSD-95. *Nat Neurosci* (12):1069-1069.

Peng YR, He S, Marie H, Zeng SY, Ma J, Tan ZJ, Lee SY, Malenka RC, Yu X (2009) Coordinated changes in dendritic arborization and synaptic strength during neural circuit development. *Neuron* 61:71-84.

Polymenidou M, Lagier-Tourenne C, Hutt KR, Huelga SC, Moran J, Liang TY, Ling SC, Sun E, Wancewicz E, Mazur C, Kordasiewicz H, Sedaghat Y, Donohue JP, Shiue L, Bennett CF, Yeo GW, Cleveland DW (2011) Long pre-mRNA depletion and RNA missplicing contribute to neuronal vulnerability from loss of TDP-43. *Nature Neuroscience* 14:459-468.

Pozo J, Godo Y (2010) Unraveling mechanisms of homeostatic synaptic plasticity. *Neuron* 66:337-351.

Prakash S, Sung P, Prakash L (1993) DNA repair genes and proteins of *Saccharomyces cerevisiae*. *Annu Rev Genet* 27:33-70.

Raasi S, Pickart CM (2003) Rad23 ubiquitin-associated domains (UBA) inhibit 26 S proteasome-catalyzed proteolysis by sequestering lysine 48-linked polyubiquitin chains. *J Biol Chem* 278:1-9.

Rao H, Sastry A (2002) Recognition of specific ubiquitin conjugates is important for proteolytic functions of the ubiquitin-associated domain proteins Dsk2 and Rad23. *J Biol Chem* 277:11691-5.

Rana A, Rera M, Walker DW (2013) Parkin overexpression during aging reduces proteotoxicity, alters mitochondrial dynamics, and extends lifespan. *Proc Natl Acad Sci USA* 110:8638-8643.

Ratovitski T, Corson LB, Strain J, Wong P, Cleveland DW, Culotta VC, Borchelt DR (1999) Variation in the biochemical/biophysical properties of mutant superoxide dismutase 1 enzymes and the rate of disease progression in familial amyotrophic lateral sclerosis kindreds. *Hum Mol Genet* 8:1451-1460.

Reddi AR, Culotta VC (2013) SOD1 integrates signals from oxygen and glucose to repress respiration. *Cell* 152:224-235.

Ringholz GM, Appel SH, Bradshaw M, Cooke NA, Mosnik DM, Schulz PE (2005) Prevalence and patterns of cognitive impairment in sporadic ALS. *Neurology* 65:586-590.

Rosen DR, Siddique T, Patterson D, Figlewicz DA, Sapp P, Hentati A, Donaldson D, Goto J, O'Regan JP, Deng HX, et al. (1993) Mutations in Cu/Zn superoxide dismutase gene are associated with familial amyotrophic lateral sclerosis. *Nature* 362:59-62.

Rothstein JD (2009) Current hypotheses for the underlying biology of amyotrophic lateral sclerosis. *Ann Neurol* 65(S1):S3-S9.

Rumpf S, Jentsch S (2006) Functional division of substrate processing cofactors of the ubiquitin-selective Cdc48 chaperone. *Mol Cell* 21:261-269.

Sato K, Morimoto N, Kurata T, Mimoto T, Miyazaki K, Ikeda Y, Abe K (2012) Impaired response of hypoxic sensor protein HIF-1 $\alpha$  and its downstream proteins in the spinal motor neurons of ALS model mice. *Brain Res* 14:55-62.

Saxena S, Cabuy E, Caroni P (2009) A role for motoneuron subtype-selective ER stress in disease manifestations of FALS mice. *Nat Neurosci* 12:627-636.

Schauber S, Chen L, Tongaonkar P, Vega I, Lambertson D, Potts W, Madura K (1998) RAD-23 links DNA repair to the ubiquitin/proteasome pathway. *Nature* 391:715--718.

Schluter OM, Xu W, Malenka RC (2006) Alternative N-terminal domains of PSD-95 and SAP97 govern activity-dependent regulation of synaptic AMPA receptor function. *Neuron* 51:99-111.

Scotter EL, Vance C, Nishimura AL, Lee YB, Chen HJ, Urwin H, Sardone V, Mitchell JC, Rogelj B, Rubinsztein DC, Shae CE (2014) Differential roles of the ubiquitin proteasome system (UPS) and autophagy in the clearance of aggregated TDP-43 species. *J Cell Sci* 127:1263-1278.

Seeburg PH, Burnashev N, Kohr G, Kuner T, Sprengel R, Monyer H (1995) The NMDA receptor channel: molecular design of a coincidence detector. *Recent Progress in Hormone Research* 50:19-34.

Segref A, Torres S, Hoppe T (2011) A screenable in vivo assay to study proteostasis networks in *Caenorhabditis elegans*. *Genetics* 187:1235-1240.

Sepe S, Payan-Gomez C, Milanese C, Hoeijmakers JH, Mastroberardino PG (2013) Nucleotide excision repair in chronic neurodegenerative diseases. *DNA Repair (Amst)* 12:568-577.

Shaheen R, Fageih E, Ansari S, Abdel-Salam G, Al-Hassnan ZN, Al-Shidi T, Alomar R, Sogaty S, Alkuraya FS (2014) Genomic analysis of primordial dwarfism reveals novel disease genes. *Genome Res* 24:291-299.

Shatz CJ (1996) Emergence of order in visual system development. *Proc Natl Acad Sci USA* 93:602-608.

Shaywitz AJ, Greenberg ME (1999) CREB: a stimulus-induced transcription factor activated by a diverse array of extracellular signals. *Ann Rev of Biochemistry* 68:821-861.

Shen Y, Ballar P, Apostolou A, Doong H, Fang S (2007) ER stress differentially regulates the stabilities of ERAD ubiquitin ligases and their substrates. *Biochem Biophys Res Commun* 352:919-924.

Smith CJ, Watson JD, Spencer WC, O'Brien T, Cha B, Albeg A, Treinin M, Miller DM 3rd (2010) Time-lapse imaging and cell-specific expression profiling reveal dynamic

branching and molecular determinants of a multi-dendritic nociceptor in *C. elegans*. *Dev Bio* 345:18-33.

Smith CJ, O'Brien T, Chatzigeorgiou M, Spencer WC, Feingold-Link E, Husson SJ, Hori S, Mitani S, Gottschalk A, Schafer WR, Miller DM 3rd (2013) Sensory neuron fates are distinguished by a transcriptional switch that regulates dendrite branch stabilization. *Neuron* 79:266-280.

Spooren AI, Janssen-Potten YJ, Snoek GJ, Ijzerman MJ, Kerckhofs E, Seelen HA (2008) Rehabilitation outcome of upper extremity skilled performance in persons with cervical spinal cord injuries. *J Rehabil Med.* 40:647-644.

Sreedharan J, Blair IP, Tripathi VB, et al. (2008) TDP-43 mutations in familial and sporadic amyotrophic lateral sclerosis. *Science* 319:1668-1672.

Stegenga SL, Kalb RG (2001) Developmental regulation of N-methyl-D-aspartate- and kainate-type glutamate receptor expression in the rat spinal cord. *Neuroscience* 105:499-507.

Subramaniam JR, Lyons WE, Liu J, Bartnikas TB, Rothstein J, Price DL, Cleveland DW, Gitlin JD, Wong PC (2002) Mutant SOD1 causes motor neuron disease independent of copper chaperone-mediated copper loading. *Nature Neuroscience* 5:301-307.

Sudhakar JN, Chow KC (2014) Human RAD23 homolog A is required for the nuclear translocation of apoptosis-inducing factor during induction of cell death. *Biol Cell*:Epub ahead of print.

Swarup V, Julien JP (2011) ALS pathogenesis: recent insights from genetics and mouse models. *Prog Neuropsychopharmacol Biol Psychiatry* 35:363-369.

Sznitman R, Gupta M, Hager GD, Arratia PE, Sznitman J (2010) Multi-environment model estimation for motility analysis of *Caenorhabditis elegans*. *PLoS One* 5:e11631.

Thompson ML, Chen P, Yan X, Kim H, Borom AR, Roberts NB, Caldwell KA, Caldwell GA (2014) TorsinA rescues ER-associated stress and locomotive defects in *C. elegans* models of ALS. *Dis Model Mech* 7:233-243.

Tong J, Huang C, Bi F, Wu Q, Huang B, Liu X, Li F, Zhou H, Zia XG (2013) Expression of ALS-linked TDP-43 mutant in astrocytes causes non-cell-autonomous motor neuron death in rats. *EMBO J* 32:1917-1926.

Travers KJ, Patil CK, Wodicka L, Lockhart DL, Weissman JS, Walter P (2000) Functional and genomic analyses reveal an essential coordination between the unfolded protein response and ER-associated degradation. *Cell* 101: 249-258.

Tyedmers J, Mogk A, Bukau B (2010) Cellular strategies for controlling protein aggregation. *Nat Rev Mol Cell Bio* 11:777-788.

Uezato A, Kimura-Sato J, Yamamoto N, Iijima Y, Kunugi H, Nishikawa T (2012) Further evidence for a male-selective genetic association of synapse-associated protein 97 (SAP97) gene with schizophrenia. *Behav Brain Funct.* 8:2.

Urbanka M, Swiech L, Jaworski J (2012) Developmental plasticity of the dendritic compartment: focus on the cytoskeleton. *Adv Exp Med Biol* 970:265-284.

Urushitani M, Ezzi SA, Matsuo A, Tooyama I, Julien JP (2008) The endoplasmic reticulum-Golgi pathway is a target for translocation and aggregation of mutant superoxide dismutase linked to ALS. *The FASEB Journal* 22:2476-2487.

Vaccaro A, Patten SA, Aggad D, Julien C, Maios C, Kabashi E, Drapeau P, Parker JA (2013) Pharmacological reduction of ER stress protects against TDP-43 neuronal toxicity in vivo. *Neurobio of Dis* 55:64-75.

van Deerlin VM, Leverenz JB, Bekris LB, et al. (2008) TARDP mutations in amyotrophic lateral sclerosis with TDP-43 neuropathology: a genetic and histopathological analysis. *Lancet Neurol* 7:409-416.

van Laar T, van der Eb, AJ, Terleth C (2002) A role for RAD-23 proteins in 26S proteasome-dependent protein degradation? *Mut Res* 499:53-61.

Varadan R, Assfalg M, Raasi S, Pickart C, Fushman D (2005) Structural determinants for selective recognition of a Lys48-linked polyubiquitin chain by a UBA domain. *Mol Cell* 18:687-698.

Vaughn JE (1989) Fine structure of synaptogenesis in the vertebrate central nervous system. *Synapse* 3:255-285.

Vembar SS, Brodsky JL (2008) One step at a time: endoplasmic reticulum-associated degradation. *Nat Rev Mol Cell Biol* 9:944-57.

Verbeeck C, Deng Q, Dejesus-Hernandez M, Taylor G, Ceballos-Diaz C, Kocerha J, Golde T, Das P, Rademakers R, Dickson DW, Kukar T (2012) Expression of Fused in sarcoma mutations in mice recapitulates the neuropathology of FUS proteinopathies and provides insight into disease pathogenesis. *Mol Neurodegener* 10:1326-1353.



Verma R, Oania R, Graumann J, Deshaies RJ (2004) Multiubiquitin chain receptors define a layer of substrate selectivity in the ubiquitin-proteasome system. *Cell* 118:99-110.

Walker AK, Soo KY, Sundaramoorthy V, Parakh S, Ma Y, Farg MA, Wallace RH, Crouch PJ, Turner BJ, Horne MK, Atkin JD (2013) ALS-associated TDP-43 induced endoplasmic reticulum stress, which drives cytoplasmic TDP-43 accumulation and stress granule formation. *PLoS One* 8:e81170.

Wang J, Farr GW, Hall DH, Li F, Furtak K, Dreier L, Horwich AL (2009) An ALS-linked mutant SOD1 produces a locomotor defect associated with aggregation and synapse dysfunction when expressed in neurons of *Caenorhabditis elegans*. *PLoS Genet* 5:e1000350.

Wang L, Popko B, Roos RP (2011) The unfolded protein response in familial amyotrophic lateral sclerosis. *Hum Mol Genet* 20:1008-15.

Watkins JF, Sung P, Prakash L, Prakash S (1993) The *Saccharomyces cerevisiae* DNA repair gene RAD23 encodes a nuclear protein containing a ubiquitin-like domain required for biological function. *Mol Cell Biol* 12:7757-7765.

Way JC, Chalfie M (1989) The *mec-3* gene of *Caenorhabditis elegans* requires its own product for maintained expression and is expressed in three neuronal cell types. *Genes Dev* 3:1823-1833.

Wei JP, Srinivasan C, Han H, Valentine JS, Gralla EB (2001) Evidence for a novel role of copper-zinc superoxide dismutase in zinc metabolism. *J Biol Chem* 276:44798-44803.

Welchman RL, Gordon C, Mayer RJ (2005) Ubiquitin and ubiquitin-like proteins as multifunctional signals. *Nat Rev Mol Cell Bio* 6:599-609.

Wilkinson CR, Seeger M, Hartmann-Petersen R, Stone M, Wallace M, Semple C, Gordon C (2001) Proteins containing the UBA domain are able to bind to multi-ubiquitin chains. *Nat Cell Biol* 3:939-943.

Yamada H, Abe T, Satoh A, Okazaki N, Tago S, Kobayashi K, Yoshida Y, Oda Y, Watanabe M, Tomizawa K, Matsui H (2013) Stabilization of actin bundles by a dynamin 1/cortactin ring complex is necessary for growth cone filopodia. *J Neurosci* 33:4514-4526.

Yang H, Zhong X, Ballar P, Luo S, Shen Y, Rubinsztein DC, Monteiro MJ, Fang S (2007) Ubiquitin ligase Hrd1 enhances the degradation and suppresses the toxicity of polyglutamine-expanded huntingtin. *Exp Cell Res* 313:538-550.

Ye Y, Shibata Y, Yun C, Ron D, Rapoport TA (2004) A membrane protein complex mediates retro-translocon from the ER lumen to the cytosol. *Nature* 429:841-847.

Zhang Y, Rohde LH, Wu H (2009) Involvement of nucleotide excision and mismatch repair mechanisms in double strand break repair. *Current Genomics* 10:250-258.

Zhang L, Schessl J, Werner M, Bonnemann C, Xiong G, Mojsilovic-Petrovic J, Zhou W, Cohen A, Seeburg P, Misawa H, Javaram A, Personius K, Hollmann M, Sprengel R, Kalb RG (2008) Role of GluR1 in activity-dependent motor system development. *J Neurosci* 28:9953-9968.

Zhou W, Zhang L, Guoxiang X, Mojsilovic-Petrovic K, Takamaya K, et al. (2008) GluR1 controls dendrite growth through its binding partner, SAP97. *J Neurosci* 28:10220-10233.

Zhou Y, Liu S, Ozturk, A, Hicks GG (2014) FUS-regulated RNA metabolism and DNA damage repair: implications for amyotrophic lateral sclerosis and frontotemporal dementia pathogenesis. *Rare Dis* 2:e29515.